Heat pump for industrial drying processes

Designing an experimental test setup

ME55035: ME-EFPT MSc Thesis

Zoë van der Jagt

Delft University of Technology

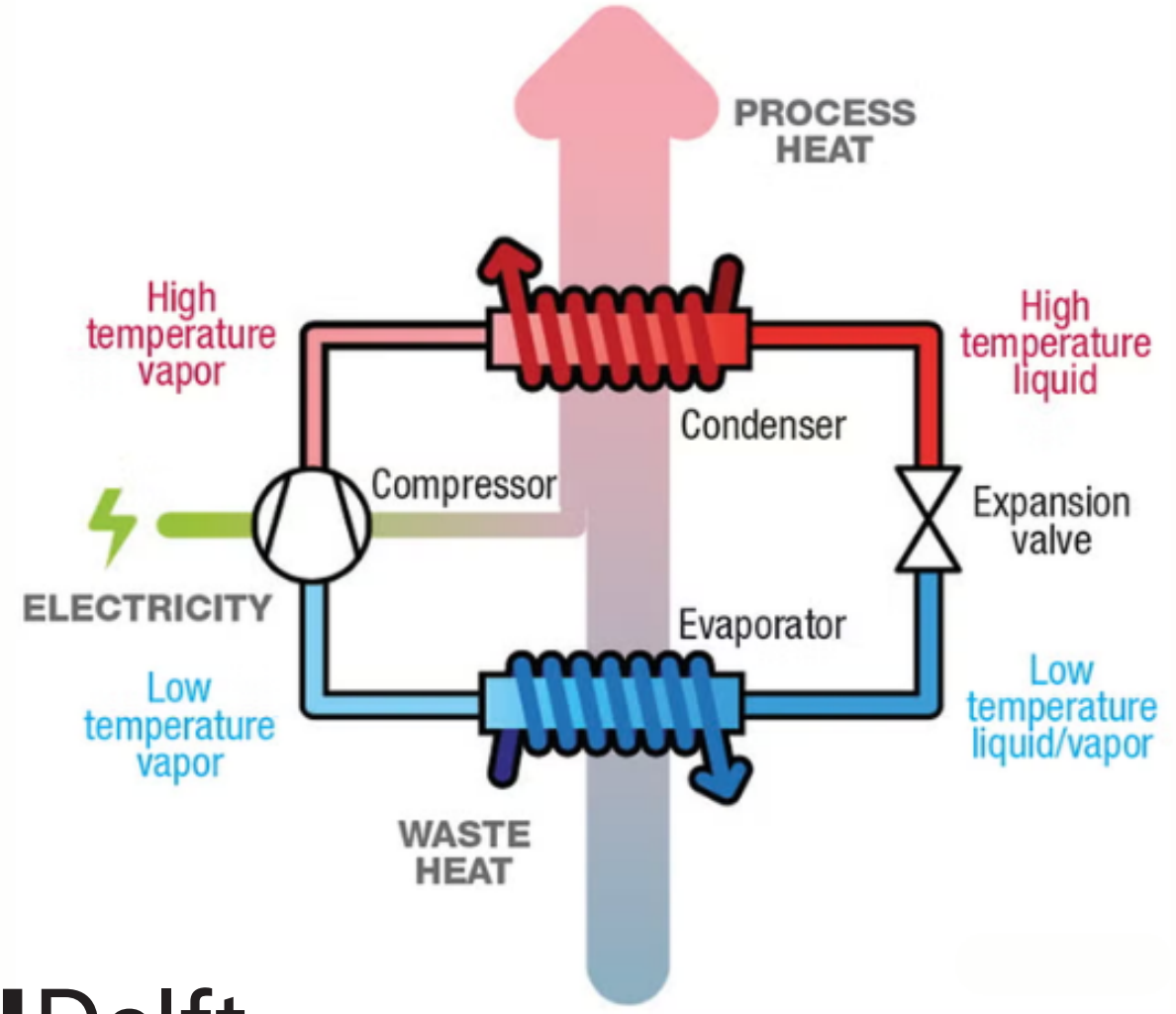

TU Delft

Heat pump for industrial drying processes

Designing an experimental test setup

by

Zoë van der Jagt

to obtain the degree of Master of Science
at the Delft University of Technology,
to be defended publicly on Wednesday December 17, 2025 at 1:00 PM.

Student number:	4888685	
Project duration:	December, 2024 – December, 2025	
Thesis committee:	Prof. dr. ir. S. A. Klein,	TU Delft, supervisor
	Dr. ir. J. W. R. Peeters,	TU Delft, supervisor
	Prof. dr. R. Pecnik,	TU Delft, supervisor
	Dr. E. Zanetti,	TU Delft

Cover: de Boer et al (2020). Strengthening industrial heat pump innovation: Decarbonizing industrial heat.

An electronic version of this thesis is available at http://repository.tudelft.nl/.

TU Delft

Preface

With great pleasure I present my master's thesis, the final project of my Mechanical Engineering degree at the TU Delft. In this work, I focused on designing an experimental setup of a heat pump dryer, a challenging yet fascinating project that allowed me to express my interest and passion for heat and energy. This thesis marks the highlight of my academic journey and reflects the knowledge, skills, and insights I have gained throughout this period.

The past year has been an intense, but also a very educational period. I have not only learned a lot about heat pumps and dryers, but also about the process of research itself and the importance of trusting my own abilities.

The research presented here would not have been possible without the support and guidance of many people. First, I would like to thank my supervisors, Sikke Klein, Jurriaan Peeters en Rene Pecnik, for not only giving me the opportunity to be involved in this interesting project, but also for all their guidance. Your knowledge, support and patience have helped me immensely to bring this project to a successful conclusion.

Furthermore, I would like to thank my family and friends for all their support and encouragement. You always been there to motivate me and help me push through the more challenging moments. Looking back on the past years, I am proud of what I have achieved and truly grateful for everything I have learned along the way.

Zoë van der Jagt
Delft, December 2025

Abstract

This report presents the process of developing an experimental test setup of a laboratory-scale convective industrial heat pump dryer. The setup is designed to test various zeotropic mixtures as refrigerant. Previous research has shown that the use of zeotropic mixtures as refrigerant in a heat pump dryer can increase the efficiency. This is used as the foundation for the present study, as it provides optimized cycles for various zeotropic mixtures.

A literature study is performed on dryers and heat pump technology, to form a foundation for further research in the field of industrial heat pump dryers. Regarding dryers, various drying techniques as well as the underlying psychrometric principles were reviewed to establish a clear understanding of moisture removal processes and their relevance to convective heat pump dryers. Additionally, the review of heat pump technology covered both the overall heat pump cycle and each of its individual components. For the heat exchangers and compressors, different types were examined, along with an assessment of which options are most suitable under specific operating conditions. In addition, various developments related to refrigerants were examined. This is followed by the collection of design requirements based on the cycles from the earlier study. Subsequently, a test setup is designed in which the refrigerant mixtures 87.5$\%_{mol}$ CO_2-Isopentane and 90$\%_{mol}$ CO_2-Isobutane can be evaluated.

The design process begins with the selection of a compressor, based on the design requirements and the laboratory constraints. A reciprocating compressor was chosen. The cycle is then recalculated using the updated compressor specifications. Next, the heat exchangers are designed. A model is used to determine the required surface areas, heat transfer coefficients, and pressure drops of finned tube heat exchangers. Based on these results, final designs are established for both the gas cooler and evaporator. The dryer is then designed as the final major component. A nozzle is selected and the droplet evaporation time is calculated.

Once all main components are designed and selected, a sensitivity analysis is performed to evaluate how the system responds to variations in several key parameters. This includes changes in the inlet air conditions, the outlet conditions of the dryer, the effect of air velocity on the system performance and the impact of changing the refrigerant mixture. Finally, all components are integrated into the final design. Additional essential elements are included, and specific attention is given to safety, instrumentation, and the refrigerant replacement procedure.

The results of this research can contribute to validating the potential efficiency improvements of heat pump dryers when using zeotropic mixtures as refrigerants.

Contents

List of Figures

List of Tables

Nomenclature

Abbreviations

Abbreviation	Definition
COP	Coefficient of Performance
GWP	Global Warming Potential
HEX	Heat exchanger
HPD	Heat Pump Dryer
LMTD	Logarithmic Mean Temperature Difference
MER	Moisture Extraction Rate
ODP	Ozone Depletion Potential
PFAS	Per- and Polyfluoroalkyl Substances
PR	Pressure Ratio
SMER	Specific moisture extraction rate
VHC	Volumetric Heating Capacity

Symbols

Symbol	Definition	Unit
A	Area	m^2
E	Exergy	kJ
d	Diameter	m
G	Mass velocity	$\mathrm{kg\,m^{-2}s^{-1}}$
h	Specific enthalpy	$\mathrm{kJ\,kg^{-1}}$
H	Enthalpy	kJ
k	Conductivity	$\mathrm{W\,m^{-1}K^{-1}}$
L	Length	m
m	Mass	kg
M	Molecular weight	$\mathrm{kg\,kmol^{-1}}$
P	Pressure	kPa
$\dot{Q}$	Heat flow	kW
R	Resistance	$\mathrm{K\,W^{-1}}$
RH	Relative humidity	-
S	Spacing	m
T	Temperature	K
U	Overall heat transfer coefficient	$\mathrm{W\,m^{-2}\,K^{-1}}$
u	Velocity	$\mathrm{m\,s^{-1}}$
V	Volume	m^3
v	Specific volume	$\mathrm{m^3kg^{-1}}$
$\dot{W}$	Work flow	kW
x	Mole fraction	-
Y	Mass fraction	-
z	Amount of tubes	-
Δ	Difference	-
η	Efficiency	-
ρ	Density	$\mathrm{kg\,m^{-3}}$
σ	Entropy production	$\mathrm{kJ\,K^{-1}}$

Symbol	Definition	Unit
ϕ	Relative humidity	-
ω	Specific humidity	$\mathrm{kg\,kg^{-1}}$
φ	Strength coefficient	-
δ	Thickness	m

Subscript	Definition
a	Air
dp	Dew point
e	Environment
fg	Latent
g	Glide
i	State
is	Isentropic
r	Fin
ref	Refrigerant
sat	Saturation
t	Tube
v	Vapour
wb	Wet bulb

1

Introduction

Drying is an important process in the industry [1]. It serves various purposes. In the processing of food and agriculture products, for example, drying can improve shelf life and quality. It is also used to produce powders or pellets, such as in the pharmaceutical industry. However, drying has a large share in total energy consumption. According to the International Energy Agency (IEA), 37% of the global energy in 2022 was being used by the industry sector [2]. Drying is one of the most energy intensive operations in the industry and can account for up to 15% of the total industrial energy usage [3]. In many of the industrial drying processes, a substantial amount of energy is wasted [4].

The Net Zero Emissions by 2050 Scenario (NZE Scenario) is a pathway created for the global energy sector to ensure the CO_2 emissions are net zero in 2050 [2]. This scenario is in line with the Paris Agreement [5]. To ensure the industry is in line with the NZE Scenario it is important that the energy consumption is reduced, which results in a reduction of CO_2 emissions. In 2022, emissions from the industry sector were responsible for a quarter of the global energy system CO_2 emissions [2].

The addition of heat pump technology to a dryer system can ensure lower energy losses compared to a conventional dryer, since waste heat can be recycled [6]. A heat pump dryer is a drying system used in different industries such as the paper, food and textile industry. An overview of this cycle is presented in Figure 1.1. The heat pump reuses energy coming from the humid air leaving the dryer, for heating the inlet air of the dryer. The advantages of adding heat pump technology to dryers is the energy saving potential and the ability to accurately control the temperature and air humidity in the dryer [7].

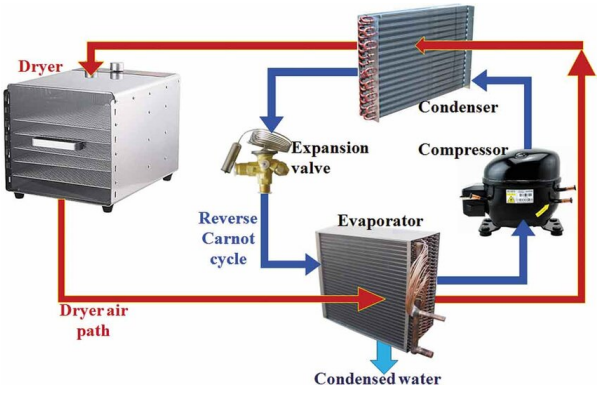

Figure 1.1: Schematic overview of a heat pump dryer. [8]

Recent studies have shown that the performance of a heat pump dryer can be increased with the use of different zeotropic mixtures as refrigerants [9] [10]. But it is not clear what a setup exactly must look like to confirm these expectations by using various refrigerant options. To verify the results experiments should be performed. This requires an experimental test setup. Developing an experimental test setup

enables the comparison of existing models and expectations, which can lead to improvements in the efficiency of heat pump dryers. Ultimately, this can be applied in industry, reducing CO_2 emissions and offering benefits from both an economic and sustainability perspective. Therefore, the goal of this study is to design an experimental test setup for a convective heat pump dryer. Based on this, the following research question has been formulated: *How can an experimental test setup be designed to evaluate the (thermodynamic) performance of a laboratory-scale convective industrial heat pump dryer with zeotropic mixtures?* To be able to answer the research question, the following sub-questions are identified:

- *What is the impact of zeotropic mixtures on the performance of the heat pump dryer at different operating conditions?* This is the motivation for building a test setup. With the test setup the following questions can be investigated: how do different operational conditions affect the (thermodynamic) performance of the heat pump dryer? What is the dynamic performance of the heat pump dryer?
- *What does the design of a test setup look like that is representative of industrial applications?* The following questions will be answered here: What will the temperature levels be? What zeotropic mixtures are being used in the test setup? What is the size of the experimental setup in kW?
- *Which types of heat exchangers and compressors are the most suitable for a scaled-down test setup in a lab of an industrial dryer?* Different types of heat exchangers and compressors will be analysed. Which types are used in the industrial applications? And which are used in representative experimental setups?
- *What zeotropic mixtures of refrigerant can be applied in the laboratory setup?* Important aspect to consider here are: toxicity, flammability, greenhouse warming potential, mixing behaviour of the components and easiness to change/modify mixtures.

This report consists of seven chapters, including a literature review examining dryers and heat pumps, the methodology used for the design, followed by the results and conclusion.

Chapter 2 covers the fundamental principles of dryers, including industrial drying applications and psychrometry. Psychrometry is the study of the properties of air and water vapour mixtures, which is crucial for understanding drying processes. An analysis of psychrometric charts will also be presented in this chapter.

Chapter 3 focuses on heat pump technology. It provides an in depth discussion of all the separate components of a heat pump: heat exchanger, compressor, pressure reduction part and refrigerants. In addition to this, a general analysis of a total heat pump cycle is given together with key design considerations.

Chapter 4 provides the research methodology, that is used to design the experimental setup of a heat pump dryer. First, the approach of the design process will be discussed, along with the assumptions taken from the previous research on which this process is based. In addition, the design procedure of the heat exchangers is described in detail.

Chapter 5 provides a in-depth discussion of the design of the main components. This includes the selection of the compressor and the design of the heat exchangers and dryer. In chapter 6, a sensitivity analysis is carried out to evaluate the robustness of the design. Various conditions are investigated to determine their influence on system performance, such as the coefficient of performance of the cycle.

All these components are then combined into a final design in chapter 7. This section also covers the additional elements required for the final design, including safety considerations and the procedure for replacing the refrigerants. Finally, chapter 8 presents the conclusions regarding the development of the heat pump dryer test setup. This includes answering the main research question and sub questions. Recommendations for future research as well as potential pathways for further optimisation of the design are provided.

2

Dryers

A dryer is a piece of equipment which can extract moisture from various types of items. It is being used in different industries; food processing, pharmaceuticals, agriculture, pulp and paper, textile, and metal fabrication. The drying process has several advantages [11]. It can protect a product against growth of bacteria and mould, but also against rust and corrosion. Additionally it can help to improve and maintain positive properties of materials, prepare the material for further processing and transportation, and reduce the weight of the product.

Dryers can be divided in three different types: direct (conductive heating), indirect (convective heating) and radiant dryers [12]. Since this study will be focussed on the design of convective drying process, this will be the main discussed type of dryer.

2.1. Industrial drying applications

The biggest amount of energy used for industrial drying, which is 33% in total, is used in the paper industry [13]. The second largest user of industrial drying is the food and agriculture field with 12% [13]. In this section, the most common dryers in these industries will be discussed.

2.1.1. The paper industry

The most commonly used method in the paper industry is multi-cylinder drying, which holds an 85-90% share [14]. An overview of this dominant paper drying technology can be seen in Figure 2.1.

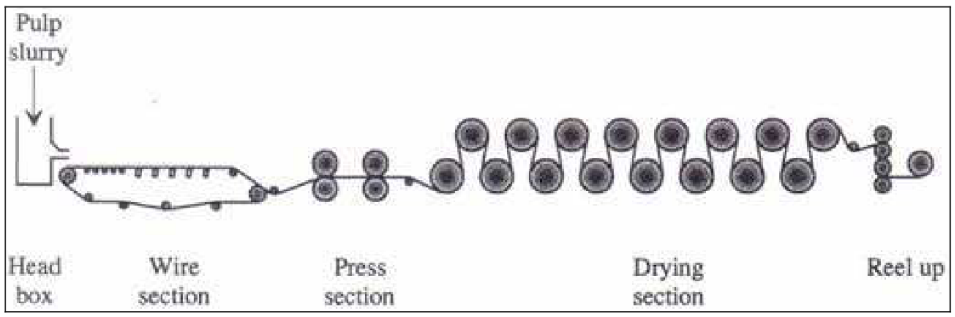

Figure 2.1: Schematic overview of a paper machine, using a multi-cylinder dryer. [15]

The multi-cylinder dryer section, indicated as dryer section in Figure 2.1, consists of hollow cylinders, which are used to transfer heat to the the paper sheets. The temperature of the cylinders is raised on its inside by the use of steam. Since the cylinders transfer the heat of the stream to the paper, the main mechanism of heat transfer is conduction. The temperature of the air used to remove moisture from paper is approximately $95\,^{\circ}\mathrm{C}$ [16].

2.1.2. The food and agriculture industry

In the food industry, several dryer types are developed due to different requirements per food type. Many of these dryers use heated air convection, approximately 85% of all the dryers in the food and agriculture industry [14]. This drying technique involves drying by contact between a process stream and a hot gas stream. This can be achieved in three different ways: letting all the product entrain by the gas stream, a part of the product or a small but not negligible part [12].

Within these different types of dryers there are four types of flow: countercurrent, parallel, mixed and cross flow. The highest temperature of the products is achieved with a countercurrent flow. With a parallel flow, the feed is exposed to the highest temperature. The operational efficiency of the dryer is not strongly influenced by the type of flow, since the largest part of the drying process is taking place with the solid having the adiabatic saturation temperature. Usually, the inlet temperature of the air for convective drying overall is between 100 and $800\,^{\circ}\mathrm{C}$, and the temperature of the outlet air between 50 and $150\,^{\circ}\mathrm{C}$ [12]. Many organic chemicals are dried at a temperature below $200\,^{\circ}\mathrm{C}$.

The type of drying mainly used for solid food is convective hot air drying [17]. A type of dryer that is used for this food is a conveyor band dryer, which can be seen in Figure 2.2. As the name suggests, the main components of this dryer are conveyor belts. The wet material is fed into one side of the dryer, after which it is transferred to the other side via the belts. In the meantime, hot air is forced through the bed of moving product upward or downward. The product is dried uniform by keeping the thickness of the bed at 25-$250\,\mathrm{mm}$ and by higher airflow rates [14].

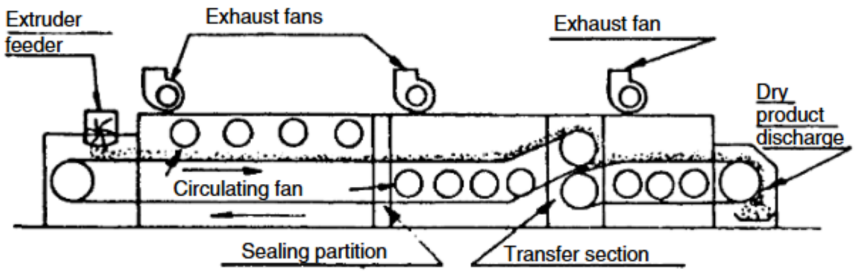

Figure 2.2: Schematic view of a two-stage conveyor band dryer. [14]

Another dryer that is being used often to produce powdered food products is a spray dryer [14]. In spray dryers fluids are being dehydrated. This fluid is being brought into a drying chamber with the use of an atomization and dispersion device, which generates small droplets. This process can be seen in Figure 2.3. An air-heating and blowing system will make sure the feed stream dries.

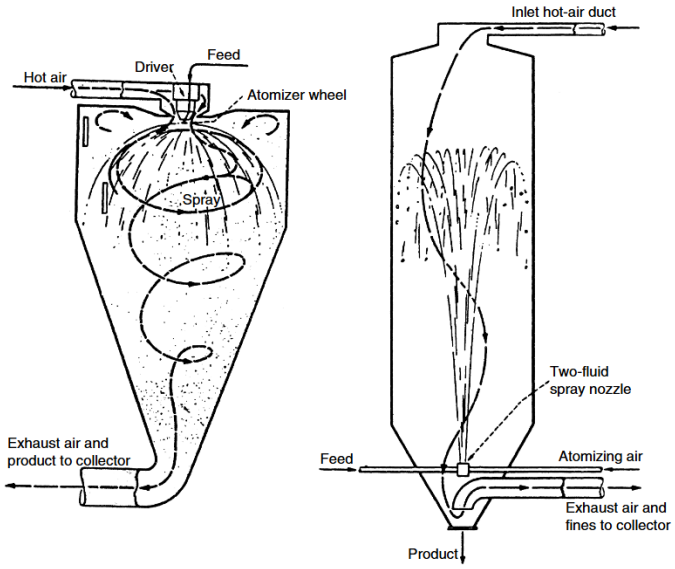

Figure 2.3: Schematic views of two configurations of a spray dryer. [14]

The temperature of the air in the spray dryer should remain at least $20\,^{\circ}\mathrm{C}$ below the melting point of the product. When drying organic powders, the air temperature of the spray dryer cannot exceed $200\,^{\circ}\mathrm{C}$ [12]. This is a rule of thumb used for quality and safety reasons.

2.2. Psychrometry

In the previous section different drying techniques were introduced. In this section, the thermodynamics of the drying processes will be discussed. The efficiency of the drying process strongly depends on the temperature and humidity of the air in the dryer. Psychrometry is the study of systems involving mixtures of dry air and water vapour, and therefore is important while analysing a dryer.

2.2.1. Fundamental properties of moist air

Moist air is a mixture of dry air and water vapour. In this mixture, the dry air is being treated as a pure component [18]. Clearly stating the definitions of the properties of moist air will help describe its behaviour during the drying process.

For dry air, the thermodynamic state is determined by two quantities: temperature and pressure. This temperature is called the dry-bulb temperature, and can be measured by placing a standard thermometer directly into the mixture of air. For moist air an additional variable is added: the amount of water that is present in the air. To determine this amount, the wet-bulb temperature is required. This can be obtained by enclosing the bulb of a thermometer by a wet cotton before placing it into the mixture of air and water. The wet-bulb temperature of the mixture will be lower than the dry-bulb temperature of the mixture, due to evaporation.

Another important property of moist air is the dew point temperature. This is the temperature at which the moist air becomes saturated, which leads to condensation. The dew point temperature depends on the pressure and the water content of the air. This water content of the air can be indicated as the humidity ratio, which is defined as the ratio of the mass of water vapour to the mass of dry air. Sometimes this ratio is also referred to as the specific humidity, and results in the following equation

$$\omega = \frac{m_v}{m_a} = 0.622 \left(\frac{p_v}{p - p_v} \right) \tag{2.1}$$

Where m_v is the mass of the water vapour and m_a the mass of dry air, both in kg. p_v and p are the partial pressure of the water vapour and the total pressure of the mixture, respectively. This will result in the specific humidity in kg_{vapour}/kg_{air}.

Subsequently, the mass fraction Y can be determined using the specific humidity. This fraction represents the total mass of vapour divided by the total mass of the air mixture, and can be calculated using the following expression:

$$Y = \frac{w}{1+w} \tag{2.2}$$

Another way of describing moist air is with the use of relative humidity [18]. This is the ratio of actual moisture content to the maximum possible moisture content in the air at a given temperature, which can be written as

$$RH = \frac{p_v}{p_g\left(T\right)} = \frac{\omega p}{\left(0.622+\omega\right)p_g\left(T\right)} \tag{2.3}$$

where p_v is the partial pressure of the vapour and p_g the saturation pressure of water at the mixture temperature in Pa. The relative humidity can also be written in terms of specific humidity, where p is the total pressure of the mixture.

Additionally, the values of the mixture enthalpy, entropy and internal energy of the moist air can be found. This can be found by adding the contribution of each separate component with the corresponding conditions of the mixture. So for example the mixture enthalpy per unit mass of dry air can be determined with:

$$\frac{H}{m_a} = h_a + \frac{m_v}{m_a}h_v = h_a + \omega h_v \tag{2.4}$$

with H the mixture enthalpy, and h_a and h_v the enthalpies of dry air and water vapour respectively.

Van 't Land gives an equation to connect most of these moist air properties together [12].

$$\frac{p_g^* - p_g}{T_g - T_w} = \frac{RTc_p\rho\left(Le\right)^{2/3}}{\Delta H} \tag{2.5}$$

Le is here the Lewis number, that is the quotient of Sc and Pr. For an air-water system this is typically 0.95. c_p and ρ are the specific heat capacity and density, taken at temperature T. p_g^* is the saturated water vapour pressure at the temperature T_w and p_g the pressure of the gas flow. This relation between the moist air properties can also be seen in psychrometric charts in subsection 2.2.2.

For calculations in a dryer, the mass fraction of water vapour in an air stream is required. This can be calculated with the following equation [19]:

$$m_{1,e} = \frac{x_{1,e}}{x_{1,e} + \frac{M_{air}}{M_{H_2O}}\left(1-x_{1,e}\right)} \tag{2.6}$$

In this equation $x_{1,e}$ the mole fraction of water vapour in the air and M_{air} and M_{H_2O} are the molecular weight of of air and water in $\mathrm{kg\,kmol^{-1}}$, respectively. $x_{1,e}$ can be determined with the following relation:

$$x_{1,e} = \frac{P_{1,e}}{P} \tag{2.7}$$

where $P_{1,e}$ is the pressure of the water vapour in the air stream and P is the pressure of the air stream in Pa. The pressure of the water vapour in the air stream can be determined by multiplying the saturation pressure at the temperature of the air $P_{sat}\left(T_e\right)$ in Pa by the relative humidity:

$$P_{1,e} = RH \cdot P_{sat}\left(T_e\right) \tag{2.8}$$

2.2.2. Psychrometric charts

Psychrometric charts give several important properties of moist air. The most well known psychrometric chart is the Mollier diagram, which is used to give a visual interpretation of thermodynamic processes and can be found in Figure 2.4.

A general drying process is drawn on the graph in purple. In state 1, the air has a dry bulb temperature of $15\,^{\circ}\mathrm{C}$ and a relative humidity of 0.9. With the use of the Mollier diagram, the dew point temperature (T_{dp}) and the wet bulb temperature (T_{wb}) can be determined. First, the air will be heated to state 2, which is at a dry bulb temperature of $33\,^{\circ}\mathrm{C}$. Water will evaporate from the product and increases the humidity of the air to state 3. This is the outlet air from the dryer. When a heat pump is being added to the dryer, the heat pump connects state 3 back to state 1.

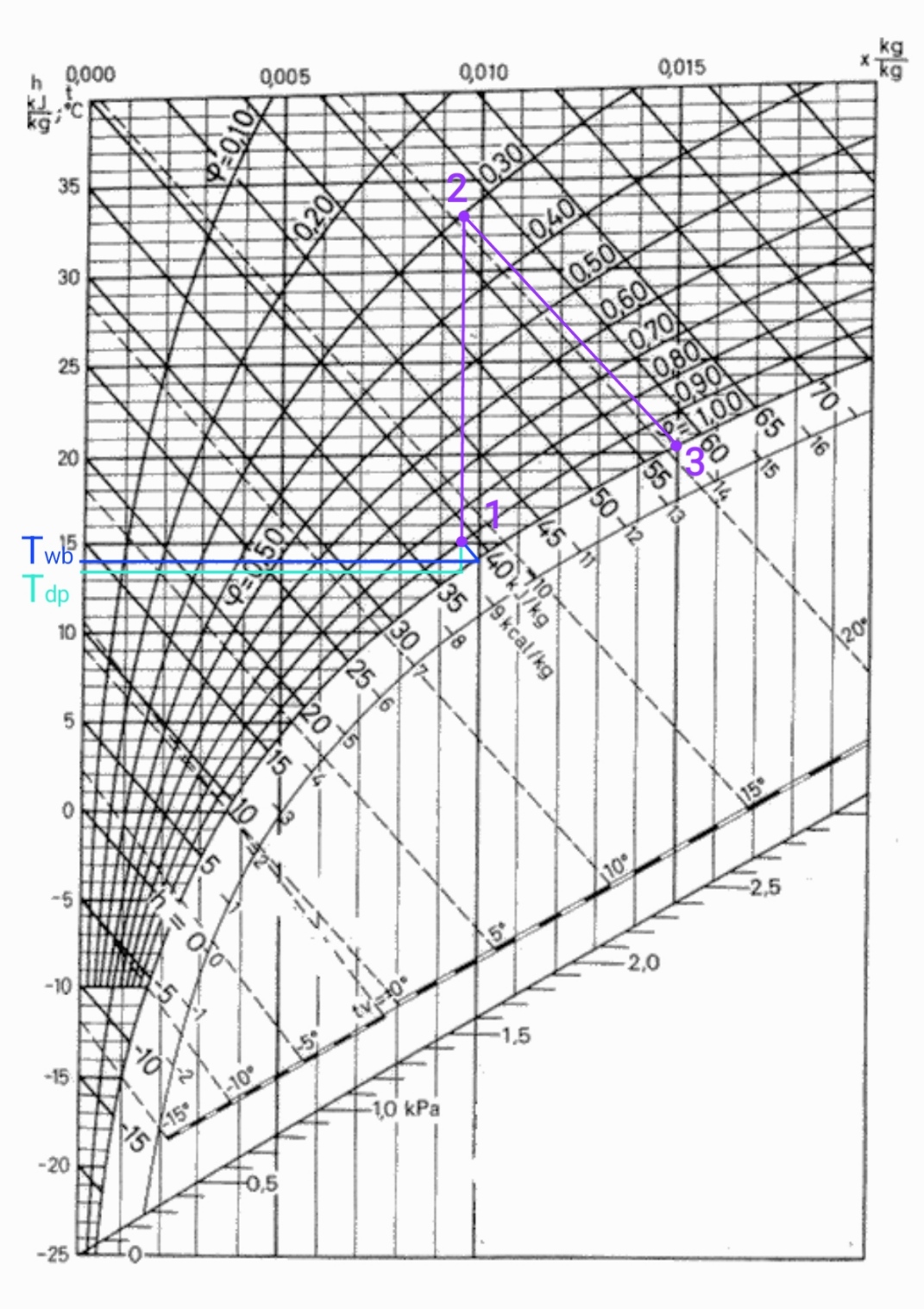

Figure 2.4: Mollier diagram with a general drying process. With on the vertical axis t as the dry bulb temperature in $^{\circ}\mathrm{C}$ and h as the specific enthalpy in $\mathrm{kJ/kg}$. On the horizontal axis the absolute humidity is given in $\mathrm{kg/kg}$. The relative humidity in the graph is given as φ. [20]

3

Heat pump cycle

The fundamental aspects of heat pump cycles need to be understood to be able to design a test setup for a heat pump drying system. This chapter begins with an overview of the heat pump cycle, followed by the optimisation of heat pump cycles and a detailed discussion of the separate parts of the heat pump cycle: heat exchanger, compressor and pressure reduction valve. This includes their working principles, different types and the selection criteria for each type. The chapter concludes with a section on the working fluid of a heat pump: the refrigerant.

3.1. Basic heat pump cycle

A heat pump is a system designed for increasing the temperature level of the energy flow. By reusing the ambient heat, the heat pump is an energy-efficient and environmentally friendly alternative to conventional fossil fuel-based heating systems. A typical vapour compression heat pump configuration can be seen in Figure 3.1.

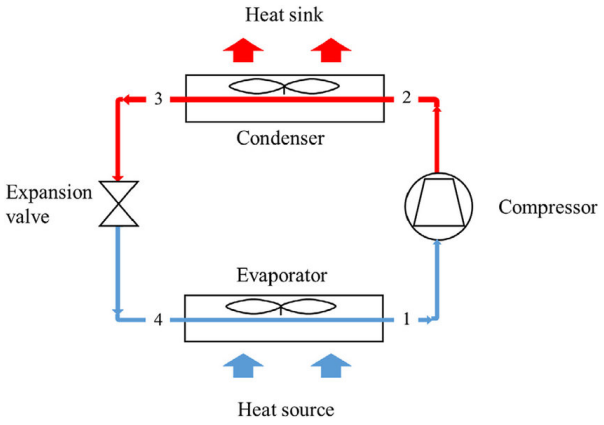

Figure 3.1: A standard vapour compression heat pump cycle. [21]

The basic process of a heat pump can be separated into four different main steps: evaporation, compression, condensation and expansion. Between state 1 and 2, as can be seen in Figure 3.1, the refrigerant is compressed by the compressor to a high pressure vapour. Subsequently, the refrigerant is condensed by rejecting its heat to the heat sink, which turns the refrigerant in a saturated liquid. The expansion valve will cause the refrigerant to go from a high pressure to low pressure. Lastly, the evaporator heats and vaporizes the refrigerant with the use of a heat source. When heat pumps deliver temperatures higher than $100\,^{\circ}\mathrm{C}$, they are defined by Annex 58 of IEA as high temperature heat pumps (HTHP) [22].

In the heat pump cycle there will be changes in the thermodynamic properties of the refrigerant. These

changes can be seen in the P-h and T-s diagrams of a standard heat pump cycle in Figure 3.2, which state numbers corresponding to Figure 3.1. Important factors that can be seen in the graphs are a constant entropy during the compression process, constant pressure in the condenser and evaporator, and constant enthalpy in the valve between state 3 and 4. These diagrams describe an ideal cycle, not a realistic cycle. In reality there will be losses.

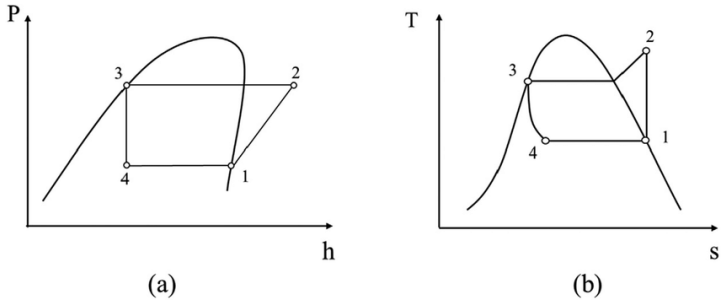

Figure 3.2: P-h diagram and T-s diagram of a standard heat pump cycle with the following components: compressor (1-2), condenser (2-3), expansion valve (3-4), evaporator (4-1) [21].

Heat pumps can be classified into two different types: subcritical and transcritical. This distinction depends on the thermodynamic conditions under which the refrigerant operates, relative to its critical point. This difference is of great importance when designing a heat pump cycle. The difference between the p-h diagrams a subcritical and transcritical cycle can be seen in Figure 3.3.

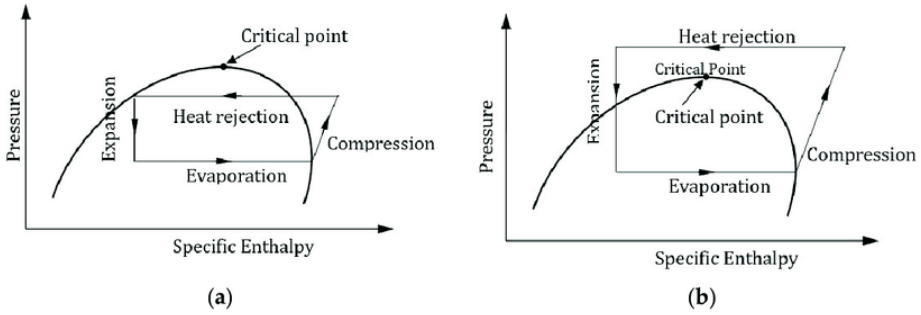

Figure 3.3: The p-h diagrams of (a) a subcritical cycle and (b) a transcritical cycle. [23]

In a traditional, subcritical cycle, the refrigerant remains below its critical temperature and pressure throughout the entire process. As a result, it is always clearly distinguishable whether the refrigerant is in the liquid phase or the gas phase. Refrigerants that are used in this cycle typically have a high critical temperature. This type of cycle is commonly applied in traditional heat pumps that are using refrigerants such as R-134a.

In a transcritical cycle, the refrigerant exceeds its critical temperature during the process, causing it to enter a supercritical state. In this state, the refrigerant no longer behaves distinctly as a liquid or a gas, and has its unique properties. Consequently, the term condenser is no longer used. Instead, this component is referred to as a gas cooler. An example of a transcritical cycle is when CO_2 is being used as working fluid. CO_2 has a relatively low critical temperature of $31.1\,^{\circ}\mathrm{C}$, making it simple for the refrigerant to pass its critical temperature in a heat pump cycle. Although this type of cycle is generally more complex than the sub-critical cycle, it can achieve high efficiencies with an appropriate design [23].

Several studies use the first and second law of thermodynamics to analyse the heat pump cycle [24] [25] [26]. The first law of thermodynamics states that energy can only change forms or be transmitted, but it cannot be created or destroyed. This results in the coefficient of performance (COP) being defined as the ratio of the discharged energy of the system Q_{out}, to the new work delivered to the heat pump W_{cycle}. This can be represented with the following equation [18]:

$$COP = \frac{Q_{out}}{W_{cycle}} = \frac{h_2 - h_3}{h_2 - h_1} \tag{3.1}$$

The second law of thermodynamics states it is impossible for any system to operate in a way that entropy is destroyed [18]. A fundamental concept in the second law thermodynamic analysis of the heat pump is exergy. Exergy represents the maximum possible work that can be extracted from a systems as it interacts with its environment until both reach a state of equilibrium, known as zero state [18]. An exergy analysis can be used to identify points where the thermodynamic losses can be reduced, to be able to develop more sustainable solutions [27]. The exergy of a system at a specific state can be determined by using the following equation:

$$E = (U - U_0) + p_0 (V - V_0) - T_0 (S - S_0) + KE + PE \tag{3.2}$$

where U, KE, PE, V and S denote the internal energy, kinetic energy, potential energy, volume and entropy, respectively. U_0, p_0, V_0, T_0 and S_0 are at the dead state of the system. The exergy balance for a closed system between state 1 and 2 is given by:

$$E_2 - E_1 = \int_1^2 \left(1 - \frac{T_0}{T_b}\right) \delta Q - [W - p_0 (V_2 - V_1)] - T_0 \sigma \tag{3.3}$$

where $E_2 - E_1$ is the exergy change and $\int_1^2 (1 - (T_0/T_b))\, \delta Q - [W - p_0 (V_2 - V_1)]$ the exergy transfers. $T_o\sigma$ is the exergy destruction E_d, which is zero when the system is reversible. When E_d is above zero, there are irreversibilities present within the system. Reducing exergy destruction ensures that less useful energy is lost. σ in this equation is the entropy production.

A cycle that is an example of an ideal cycle is a Carnot cycle, in which the entropy is not increasing. The Carnot cycle of a heat pump is a heat pump cycle undergoing a series of four internally reversible processes, resulting in a cycle with the theoretical maximum efficiency. This Carnot efficiency for a heat pump is described as:

$$COP_{Carnot} = \frac{T_H}{T_H - T_C} \tag{3.4}$$

where T_c is the temperature of the cold reservoir and T_H is the temperature of the hot reservoir. The compression and expansion are assumed to be isentropic. This cycle often differs from a real cycle since a constant temperature is used for the cold and the hot reservoir.

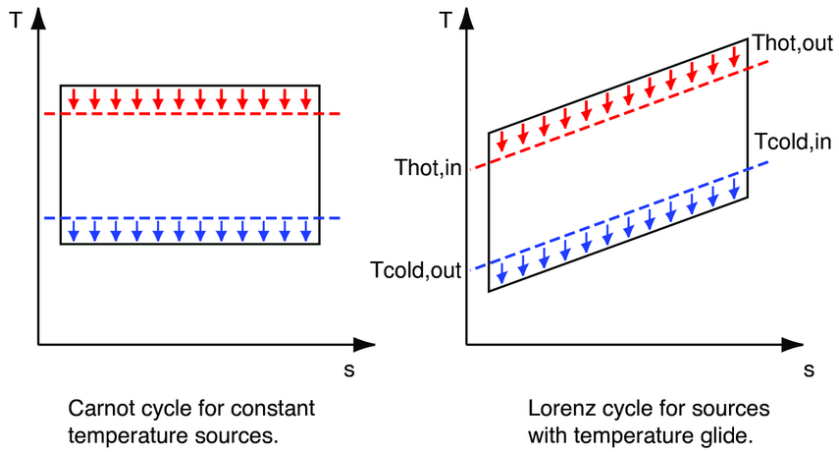

Figure 3.4: Comparison of the Carnot cycle and the Lorenz cycle. A constant temperature can be seen in the Carnot cycle, while the Lorenz cycle has a temperature glide. [28]

A model that is closer to reality for many cycles such as a transcritical or inverse Brayton cycle, is the Lorenz efficiency. Here temperature differences and irreversibilities are kept into account. A T-s diagram for the Carnot cycle and Lorenz cycle can be seen in Figure 3.4. As can be seen, the temperature in the sink and source are not constant for the Lorenz cycle in the T-s diagram. The COP for a Lorenz cycle is given by [29]:

$$COP_{Lorenz} = \frac{T_{lm,H}}{T_{lm,H} - T_{lm,C}} \tag{3.5}$$

where $T_{lm,H}$ and $T_{lm,C}$ are the logarithmic mean temperatures of the sink and source, respectively.

As a result, the second law efficiency of the heat pump can be determined. This is an expected COP of a real system, which can be used to put the cycle losses in perspective [24] [29]. The equation for the second law efficiency is given below, determined by dividing the real COP of the cycle by the COP of an ideal cycle. This ideal COP can be determined with for example the use of the Carnot or Lorenz efficiency.

$$\eta = \frac{COP}{COP_{ideal}} \tag{3.6}$$

3.2. Optimisation of the heat pump cycle

The performance of a vapour compression heat pump system cannot only be enhanced by the improvement of the separate components, but also by adding components. Three options to significantly improve the performance of the heat pump cycle by adding devices will be discussed, under which intercoolers, economizers and cascade cycles. Bertsch et al shows a relative efficiency for a two-stage cycle with intercooler, a two-stage cycle with economizer and a cascade cycle of 130%, 130% and 140% respectively, when compared to a one stage cycle [30].

One way of increasing the performance is by adding an intercooler. An intercooler is an extra heat exchanger which can be placed between two compressors, to reduce the temperature of the refrigerant after the first compression stage. The placement of this component can be seen in Figure 3.5(a). Lowering this temperature means less work needs to be done by the compressor, while compressing to the same pressure. Placing an intercooler between the first and second compressions stages in high-temperature heat pump cycles improves energy efficiency and eventually causes a decrease in CO_2 emissions [31].

Another way of optimizing the heat pump cycle is by integrating an economizer. An economizer is a component which is used to reduce energy losses, by recycling energy which is produced within the system. Thereby it reduces the entropy generation by optimizing compression and expansion steps. A diagram of a heat pump cycle with an economizer can be seen in Figure 3.5(b). A part of the refrigerant is moved to the compressor without going through another expansion valve. Studies by Maddah et al and Bertsch et al have shown an increase in efficiency of the heat pump cycle while using an economizer [30][32] .

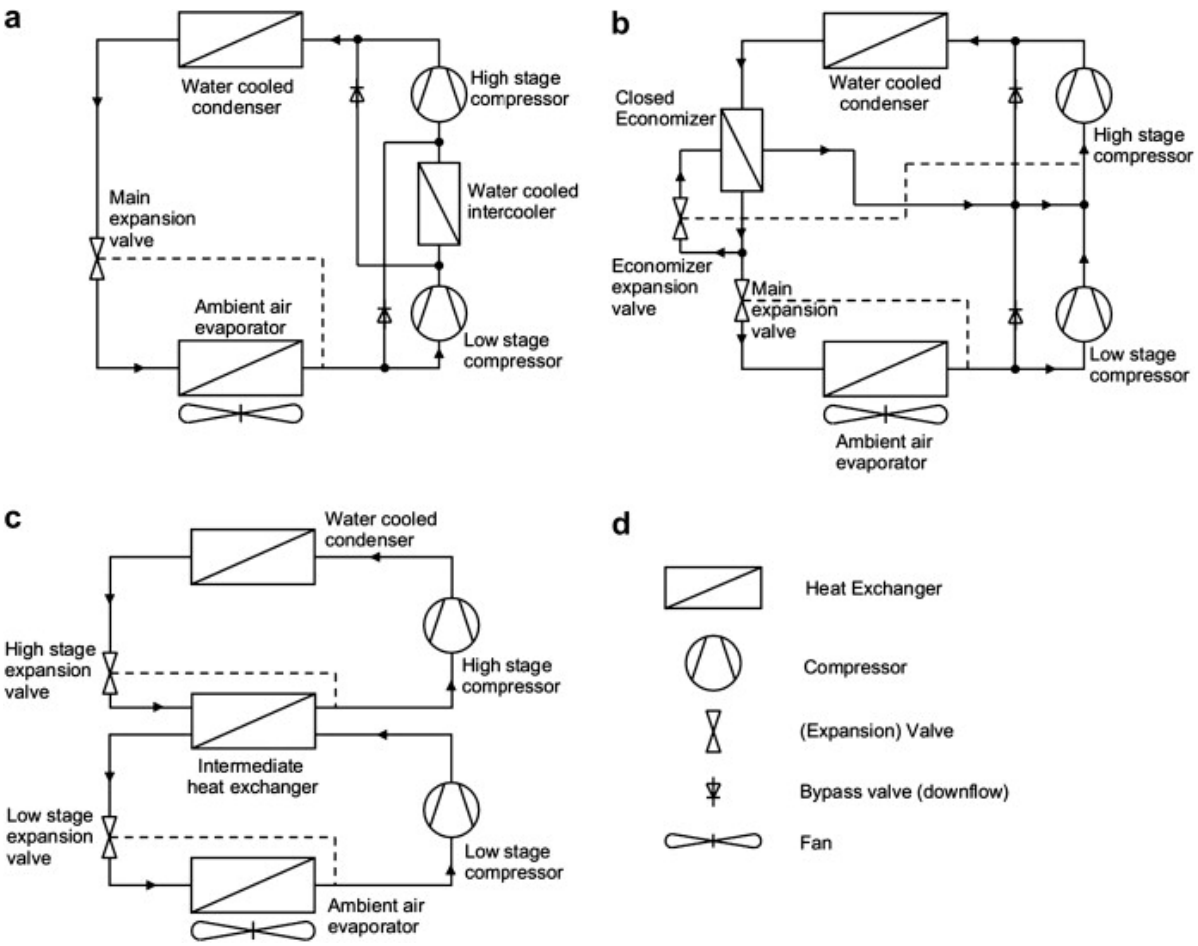

Figure 3.5: Schematics of (a) two-stage cycle with intercooler, (b) two-stage cycle with closed economizer, (c) cascade cycle and (d) legend [30]

One more option to increase the performance of a cycle is to combine two or more heat pump (or refrigerant) cycles, with the intermediate heat exchangers as connection between the two cycles. An overview of this cycle, known as cascade cycle, can be seen in Figure 3.5(c). In this way, the part of the system with the higher temperature can operate at a higher evaporation temperature, and the part with the lower temperature at a lower evaporating temperature. Through this different refrigerants can be used, which can both operate at its optimum range of operating conditions. This results in a design with high temperature differences where the compression ratios can remain low, leading to higher compression efficiency than a heat pump with one cycle [33]. Wang et al demonstrated that coupling two heat pump cycles together can increase the energy efficiency ratio of the system by 20%, compared to the single-stage mode [34].

3.3. Heat exchangers

In a heat exchanger heat is being exchanged between two process streams. A lot of different heat exchangers are used in engineering which vary in geometric flow configuration, material choice and type of heat transfer surface. This section will cover the heat transfer rate, fouling, the analysis of heat exchangers, an overview of different types and the selection criteria for heat exchangers.

3.3.1. Heat transfer rate

In most heat exchangers heat transfer occurs between two flows through a wall. In many cases, the wall is a plate or a tube. A diagram of this can be seen in Figure 3.6. The associated heat transfer rate then is:

$$\dot{Q} = UA\,(T_H - T_C) \tag{3.7}$$

Here is U the overall heat transfer coefficient in $\mathrm{W\,m^{-2}\,K^{-1}}$, A the surface area of the heat exchanger where heat transfer takes place in $\mathrm{m^2}$, and T_H and T_C the temperatures of the hot and the cold stream in K. The overall heat transfer coefficient can be calculated with the following equation:

$$\frac{1}{UA} = \frac{1}{h_1 A} + \frac{\Delta x}{kA} + \frac{1}{h_2 A} \tag{3.8}$$

The overall heat transfer coefficient is an important part of the heat exchanger analysis. When looking at Figure 3.6, h_1 is the heat transfer coefficient of the cold fluid in $\mathrm{W\,m^{-2}\,K^{-1}}$, and h_2 the heat transfer coefficient of the warm fluid in $\mathrm{W\,m^{-2}\,K^{-1}}$. Δx is the thickness of the metal wall in m and k is the thermal conductivity of the wall in $\mathrm{W\,m^{-1}\,K^{-1}}$.

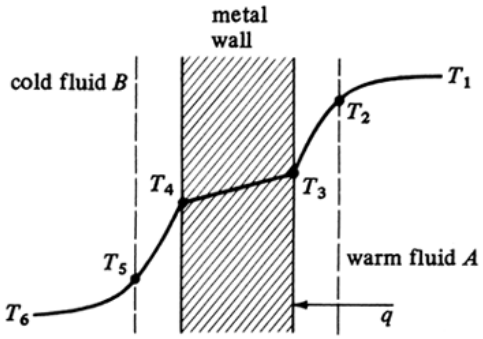

Figure 3.6: Figure of heat transfer between two flows through a wall. [35]

3.3.2. Fouling

When a heat exchanger is being used for some time, fouling may occur. Deposits may form on the surfaces of the heat exchanger and influence the heat transfer resistance. If the average thickness (δ_f) and the thermal conductivity (k_f) of the foul are known, an additional resistance can be determined as $R_f = \delta_f / k_f$. This is per unit area. The overall heat transfer coefficient can then be written as:

$$\frac{1}{U_f \mathcal{P}} = \frac{1}{U\mathcal{P}} + \frac{R_{fH}}{\mathcal{P}_{\mathcal{H}}} + \frac{R_{fC}}{\mathcal{P}_C} \tag{3.9}$$

where U_f is the overall heat transfer coefficient for the fouled heat exchanger and $\mathcal{P}$ is the perimeter. R_{fH} and R_{fC} are the fouling resistances of the hot and the cold stream. Mills et al (2015) gives a recommended value of $0.35 \times 10^3 \mathrm{m^2K/W}$ for the fouling resistance for refrigerant vapours, and $0.2 \times 10^3 \mathrm{m^2K/W}$ for refrigerant liquids [19]. For comparison, the range of a fouling resistance for river water is 0.2-$0.7 \times 10^3 \mathrm{m^2K/W}$. Figure 3.7 illustrates the temperature distribution of a heat exchanger where fouling occurred, where T_1 is the temperature of the hot fluid and T_2 the temperature of the cold fluid.

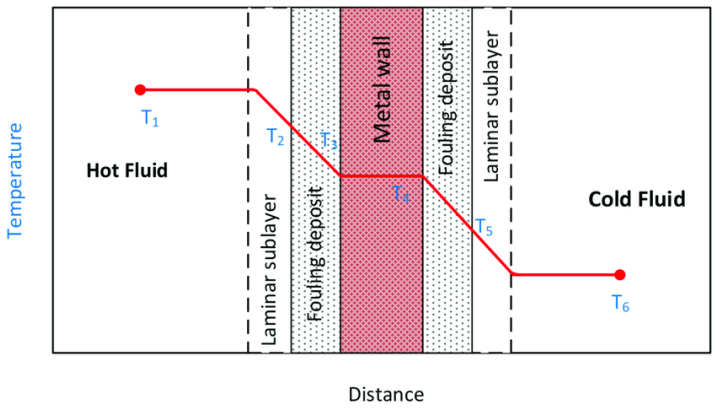

Figure 3.7: Temperature distribution across fouled heat exchanger surfaces. [36]

The most common mechanisms of fouling are the following [37]:

- Scaling/precipitation: salts in the fluid will form crystals due to temperature change. This is the most common type of fouling and typically found in water.
- Sedimentation: occurs when particles in the fluid, such as sand or dirt, move across the surface of the heat exchanger.
- Corrosion: can occur due to a chemical reaction with the heat exchanger surface.
- Chemical fouling: happens due to chemical reactions in the process stream, resulting in a decomposition of the heat transfer surface.
- Freezing fouling: occurs when the temperature of the component decreases near the freezing point.
- Biological fouling: biological organisms, including algae or other microbes, grow in the heat exchanger surface.

Despite many studies on the analysis of fouling, it remains a major problem in reality [37]. Current heat exchangers are designed in such a way that they can tolerate a certain amount of fouling. The most common way to tackle fouling in the industry is by mechanical cleaning [37]. When designing a heat exchanger, it must be taken into account that it should be possible to clean the exchanger.

3.3.3. Analysis of heat exchangers

Two methods to analyse heat exchangers will be described: the logarithmic mean temperature method and the effectiveness-number of transfer units method. In both methods, it is assumed that the overall heat transfer coefficient is constant through the entire heat exchanger.

An important factor to consider in this analysis is the geometric flow configuration. The two most common configurations are parallel-flow and counter flow. As the name suggests, in a parallel flow the flows run parallel to each other in the same direction, while with counterflow they run in the opposite direction. The configurations together with their temperature profiles can be seen in Figure 3.8 and Figure 3.9.

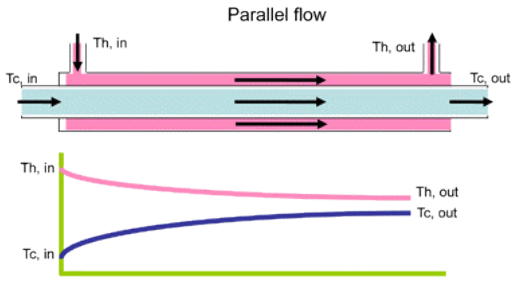

Figure 3.8: Parallel flow in a heat exchanger, with associated temperature profile. [38]

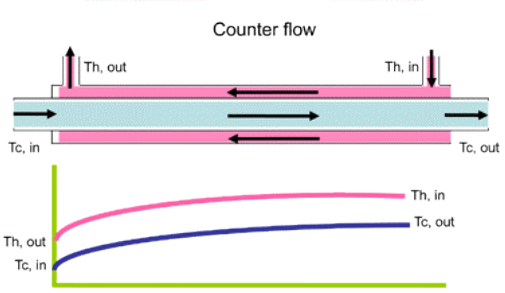

Figure 3.9: Counterflow in a heat exchanger, with associated temperature profile. [38]

First of all, the logarithmic mean temperature difference method (LMTD) is discussed. In this case the total heat transfer in the exchanger is written as

$$\dot{Q} = UA\Delta T_{lm} \tag{3.10}$$

where UA is the overall heat transfer coefficient times the heat transfer area, as calculated in Equation 3.8 and Equation 3.9. L is the length of the heat exchanger and ΔT_{lm} is the log mean temperature difference. For a parallel-flow and counterflow exchanger, this can be determined with the following equation:

$$\Delta T_{lm} = \frac{(T_H - T_C)_L - (T_H - T_C)_0}{\ln\left[(T_H - T_C)_L / (T_H - T_C)_0\right]} \tag{3.11}$$

in which 0 is referring to the inlet of the exchanger and L to the outlet. When the heat exchanger differs from a ideal coaxial type of exchanger, a correction factor F can be used [19] to keep the deviation into account. When F is low, and therefore the total heat transfer is low, the design needs to be revised for better thermal performance.

The LMTD method is useful when inlet and outlet temperatures are known. When this is not the case, the effectiveness and number of transfer units can be used. The effectiveness of a heat exchanger is described as the actual heat transfer divided by the maximum possible heat transfer. This can be written as

$$\epsilon = \frac{C_H\left(T_{H,in} - T_{H,out}\right)}{C_{min}\left(T_{H,in} - T_{C,in}\right)} = \frac{C_C\left(T_{C,out} - T_{C,in}\right)}{C_{min}\left(T_{H,in} - T_{C,in}\right)} \tag{3.12}$$

where C is the flow thermal capacity ($\dot{m}c_p$) of the stream. Note that for parallel-flow and for counterflow heat exchangers the flow thermal capacity of the cold flow needs to be smaller than the thermal capacity of the hot flow. The number of transfer units (N_{tu}) and the capacity ratio (R_C) are defined as

$$N_{tu} = \frac{UPL}{C_{min}} \tag{3.13}$$

$$R_C = \frac{C_{min}}{C_{max}} \tag{3.14}$$

Using these equations, Equation 3.12 can be converted into another formula so it can be used without knowing all temperatures. The effectiveness for a parallel-flow exchanger can be rewritten as

$$\epsilon = \frac{1 - e^{-N_{tu}(1+R_C)}}{1 + R_C} \tag{3.15}$$

For a counterflow heat exchanger, the effectiveness can be rewritten as

$$\epsilon = \frac{1 - e^{-N_{tu}(1-R_C)}}{1 - R_C e^{-N_{tu}(1-R_C)}} \tag{3.16}$$

When $R_C = 0$, there is no temperature change in the exchanger. This satisfies the definition of a exchanger with a single stream.

3.3.4. Pinch technology

The pinch technology was developed by Linhoff et al (1982) and is used to optimize heat exchanger networks. The term pinch refers to the pinch which usually occurs in a plot of the temperatures and the transferred heat, between the curves of the hot and the cold stream. The point in the graph where this temperature difference is the smallest, is the place where the minimum amount of energy is required [39]. This method can be used to determine under which circumstances the energy requirements are at their minimum. In Figure 3.10 the T-Q graph of an evaporator is shown. Ni et al uses a pinch point temperature difference of 5K [10]. When the temperature difference increases, the exergy destruction will also increase. When the temperature difference decreases, the heat transfer rate will also be lower [10].

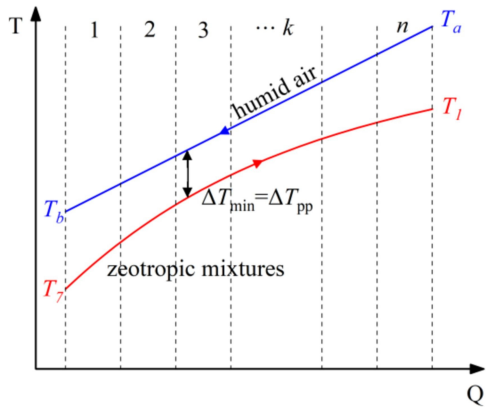

Figure 3.10: Schematic diagram of a pinch point in the heat transfer process of an evaporator. [10]

3.3.5. Different types of heat exchangers

An overview of different types of heat exchangers is given by Wang et al. [40]. Table 3.1 gives an overview of the heat exchangers with their typical values for the heat transfer coefficient, media, maximum pressure, temperature range and areas of application. The heat exchanger with the most simple design is the Double Pipe Heat Exchanger (DPHE) and can be seen in Figure 3.11. This type is based on two concentric pipes, usually formed in a U-turn to minimize the required space and maximize the heat transfer area per volume. One flow is going through the inner tube and the other flow through the outer tube. The dominant heat transfer in this heat exchanger takes place through the wall of the inner pipe, between the two flows. Due to the relative simple design, this type of heat exchanger is suitable for conditions with high-fouling or high-viscosity. Typically the DPHE is used in application with small duties, since expanding it causes higher pressure drops, material and operating costs. Originally the pipes are smooth, but fins can be added to improve the effectiveness of the heat exchanger.

Another type of heat exchanger to discuss is the finned tube heat exchanger (FTHE). This type of HEX is characterized by the fins, which are placed along the sides of tubes. Typically, finned tube heat exchangers are being used in systems where convection is the primary heat transfer method. This is being done because the fins increase the heat transfer surface, which makes the heat exchanger suitable for heat transfer between liquid and gas. Therefore finned tube heat exchangers can be found in industries such as automotive [41] and waste heat utilization [42]. By using different types of fins and orientation, the efficiency of the exchangers can be influenced. Standard wavy and rectangular fins can provide better heat transfer than other geometries, but causes an increase in pressure drop [43].

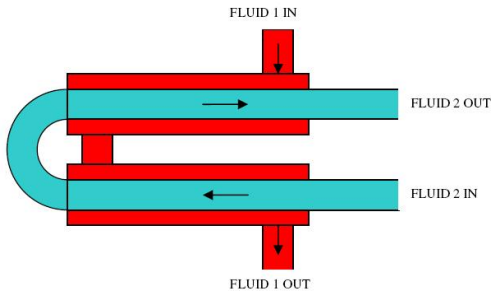

Figure 3.11: Figure of the double pipe heat exchanger (DPHE). [44]

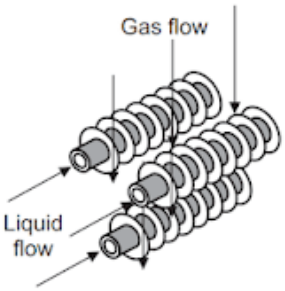

Figure 3.12: Figure of a finned tube heat exchanger. [45]

The most widely used heat exchanger in the industry is the shell-and-tube (STHE) [46] and can be seen in Figure 3.13. One flow is going through the tube and the other in the opposite direction through the shell. The baffles force the fluid on the shell side to flow across the tubes instead of in a straight line, which increases the amount heat transfer. Most working fluids can be used in this type of heat exchanger, which results in a wide range of applications. The disadvantage of this heat exchanger is that it is relatively large and expensive compared to other types.

Another type of heat exchanger is the coiled tube heat exchanger (CTHE), where a tube is wrapped around a core. Usually, the diameter of this tube is very narrow. The most common version of the CTHE is where a shell is placed around the coiled tube. This can be seen in Figure 3.14. The small diameter of the coiled tube does make the cleaning of this heat exchanger complicated, since mechanical cleaning is not possible. This makes the heat exchanger unsuitable to use in combination with fluids that have a high viscosity or high fouling. On the contrary, the CTHE is simple to produce and has a compact design.

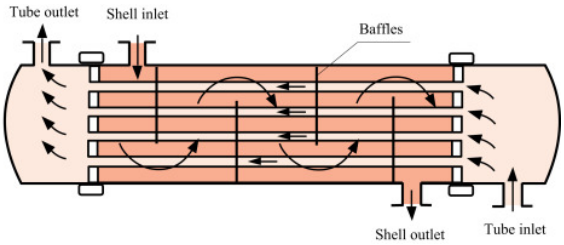

Figure 3.13: Figure of the shell-and-tube heat exchanger (STHE). [47]

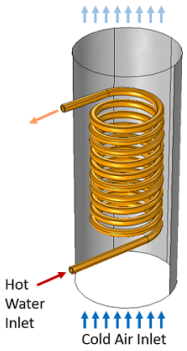

Figure 3.14: Figure of the coiled tube heat exchanger (CTHE). [48]

Plate heat exchangers (PHE) are being used in many different applications. They were less popular than tubular heat exchangers, but are becoming more popular nowadays. Due to their specific structure, their applicability is highly dependent on the particular field of use. The operation of this heat exchanger can be seen in Figure 3.15. Several heat transfer plated are clamped tightly to each other with the use of a frame. Fluid channels are created in the plates to increase the heat transfer between the flows. A disadvantage of a PHE is that it is susceptible to fouling. However, they can be easily disassembled for cleaning purposes.

A variation of the plate heat exchanger is the pillow-plate heat exchanger (PPHE). With this type of heat exchanger, two thin plates are welded together in a pattern, that is similar to the structure of a pillow. Within this structure, shown in Figure 3.16, a fluid can flow to induce heat transfer. Due to the turbulent flow caused by the channels, the HEX has a high efficiency. Nowadays, this application this being used

more frequently in the industry, as the PPHE is smaller in size and simpler to install compared to the commonly used shell and tube heat exchanger [49]. It is applied in wide variety of industries, including the food industry [50] and the pulp and paper industry [51].

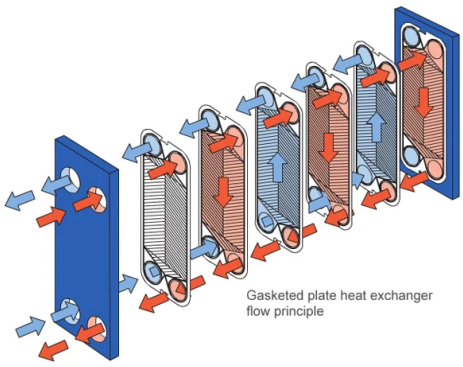

Figure 3.15: Figure of the plate heat exchanger (PHE). [52]

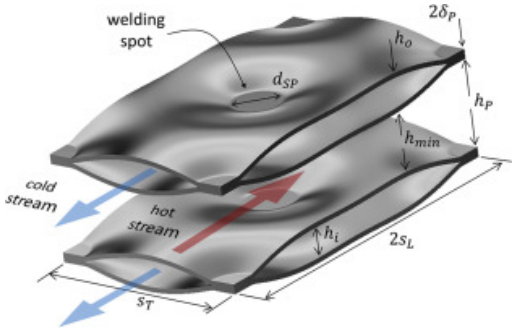

Figure 3.16: Figure of the pillow plate heat exchanger (PPHE). [53]

Another variation of the plate heat exchanger is the spiral plate heat exchanger (SPHE), which can be seen in Figure 3.17. This heat exchanger differs from traditional plate heat exchangers by the use of spiral plates. The spiral plates together form the flow channels in which the heat transfer takes place. As with other heat exchangers, the heat transfer takes place via the walls of the plates. The primary advantage of a spiral heat exchanger is its ability to efficiently process highly viscous and dirty fluids with minimized fouling. Key industries where spiral heat exchangers are being used are for example oil refining, petrochemicals, edible oils, pharmaceuticals and biotech. [54]

The last type of heat exchanger to discuss is the printed circuit heat exchanger(PCHE). A PCHE consists of thin sheet of metal that are stacked on top of each other and fused together. These sheets contain small channels, as can be seen in Figure 3.18. A flow passes through these channels, allowing heat to be exchanged. Since the sheets are connected by diffusion bonding, this ensures the heat exchanger to be strong, compact and efficient. This makes them resistant to high pressure and temperatures. These heat exchangers are therefore often used under extreme conditions.

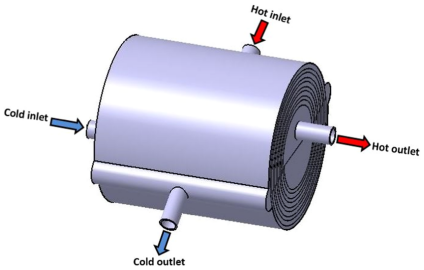

Figure 3.17: Figure of a spiral plate heat exchanger (SPHE). [55]

Figure 3.18: Figure of the printed circuit heat exchanger (PCHE). [56]

Table 3.1: Overview of typical heat exchangers with associating U-values, media, maximum pressure, temperature range and areas of application. [57]

Type	**Typical U-value** $\mathrm{W\,m^{-2}\,K}$	**Liquid/Gas**	**Maximum pressure** bar	**Temperature range** $^{\circ}\mathrm{C}$	**Application**
Double pipe	50 - 500	L-L	300 (shell), 1400(tube)	-100 to 600	Cooling/heating fluids in chemical plants
Finned tube	100 - 1.500	G–L	300 (shell), 1400(tube)	-100 to 600	Radiators, aerospace
Shell-and-tube	200 - 2.500	L-L / L–G	300 (shell), 1400(tube)	-25 to 600	Power plants, oil refineries
Coiled tube	500 - 2.000	L-L	100	-100 to 500	Refrigerators, air-conditioning an cryogenic applications
Plate	1.000 - 4.000	L-L	60 (higher in shells)	in excess of 650	HVAC, food processing
Pillow plate	500 - 3.000	L-L / L–G	60	-50 to 200	Paper & pulp industry, food industry
Spiral plate	500 - 3.000	L-L / L-G	18	up to 400	HVAC, industrial (chemical, food) and power generation
Printed circuit	5.000 - 15.000	G–G / G–L	1000	800	Marine, energy and oil & gas applications

3.3.6. Selection criteria for heat exchangers

When selecting a heat exchanger, a number of factors have to be taken into account. Some of these are application-specific, so no general rules can be defined for all the types of heat exchangers. An overview of the factors that need to be considered is presented in Table 3.2. These criteria make it possible to select a suitable heat exchanger.

Table 3.2: Selection criteria for heat exchangers. [40] [58] [57]

Selection criteria	Explanation
Thermal and hydraulic requirements	One of the most important are the thermal and hydraulic requirements. The heat exchanger should be able to meet the required heat transfer rate, fluid inlet and outlet temperatures, and the possible pressure drop.
Compatibility with fluids and operating conditions	The appearance of corrosion between the working fluid and the construction material needs to be kept into account. In addition, the heat exchanger needs withstand the stresses which are created by the operating pressure and temperature.
Maintenance	For maintenance, it is important to consider how often the exchanger needs to be cleaned, as well as when components need to be replaced. With some heat exchangers this can be done more easily than with others. Factors that have influence on this are the possibility to disassembly the exchanger and the diameter of the passages.
Availability	The timescales of project may have influence on the availability of designs or design methods. For example the time it takes for parts to be delivered can be effecting the selection.
Economic factors	The costs are a very important factor when selecting a type of heat exchanger. The total costs should be considered here, thus the capital and installation costs, but also the operation and maintenance costs for when the heat exchanger is in operation. Hewitt et al describes costing methods, under which the use of the C value method [59]. In the selection of the heat exchanger there will be a balance between the performance of the heat exchanger and the costs.
Space and weight	In some applications, like the aerospace industry, weight is really important since everything needs to be light, to reduce the required power to keep the vehicles in the air. Another application where space can be important is offshore structures, where the reduction of the size and loading of platforms is required.
Fouling	When the heat exchanger is being used some period of time, fouling can occur. The fouling of an exchanger should be kept into account during the selection process, since it may have a significant effect on the amount of heat transfer. Fouling can increase the heat transfer resistance of the heat exchanger.

3.4. Compressors

The compressor is an important part of the heat pump cycle, since it is driving the working fluid by increasing the temperature and pressure. The choice of compressor type has a major influence on the efficiency and overall performance of the heat pump [60], and the most suitable type of compressor strongly depends on the specific application. In this section the thermodynamics of the compressor will be discussed, together with different types of compressor and the selection criteria.

3.4.1. Thermodynamics

When designing a cycle with a compressor, it is important to understand the underlying thermodynamics. In this section key thermodynamic principles will be outlined, that are essential for selecting a compressor. In Figure 3.19 three types of compression processes can be seen: isentropic, actual, and isothermal compression.

With an isentropic compression, there is no heat added or removed from the gas during compression. Additionally, the process is frictionless. With these assumptions it can be assumed that the entropy of the gas is not changing in this process. During this compression, the following relation can be used for the temperature and pressure ratio:

$$\frac{T_2}{T_1} = \left(\frac{p_2}{p_1}\right)^{\frac{k-1}{k}} \tag{3.17}$$

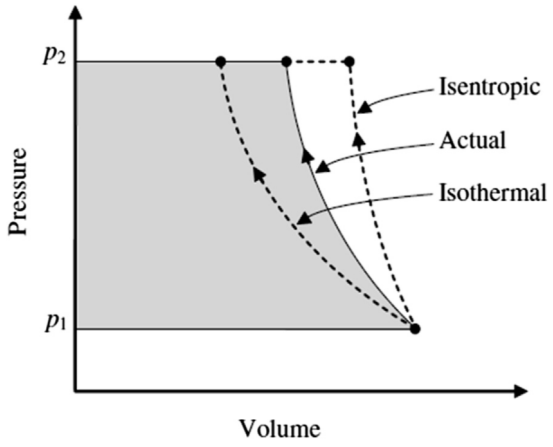

Figure 3.19: Pressure-volume diagrams for three types of compression [61].

where k is the ratio of heat capacities of gas at a constant pressure and temperature ($k = C_p/C_v$). p_1 is the pressure at the inlet (suction pressure) and p_2 the pressure at the outlet (discharge pressure). In this situation, the isentropic efficiency of the compressor can be determined. With this efficiency it is possible to indicate how closely the actual compressor approaches an ideal, frictionless compression process. The isentropic efficiency (η_s) can be determined with the following equation:

$$\eta_s = \frac{h_{2s} - h_1}{h_2 - h_1} \tag{3.18}$$

where h_1 is the enthalpy at the inlet, h_2 the enthalpy at the outlet and h_{2s} the enthalpy at the outlet under isentropic conditions. In a heat pump, the compressor often consumes the most energy, making a higher isentropic efficiency more desirable.

With the isothermal compression, there is no change in temperature during the compression process. This is not an adiabatic process, since heat needs to be removed during the compression to keep the temperature constant. This means that (T_2/T_1) is equal to zero.

The actual or polytropic compression can be compared to the isentropic compression, except it is not adiabatic. The relation between the temperature ratio and the pressure ratio for a polytropic compression can be given by:

$$\frac{T_2}{T_1} = \left(\frac{p_2}{p_1}\right)^{\frac{k-1}{k\eta_p}} \tag{3.19}$$

This equation is almost the same as the equation for the isentropic process, except for the included polytropic efficiency (η_p). This efficiency is often supplied by a compressor manufacturer.

The power required by the compressor to provide the necessary pressure depends on the mass flow rate and the enthalpy difference. This can be calculated using the following equation:

$$W_{comp} = \dot{m}\,(h_2 - h_1) \tag{3.20}$$

where the mass flow $\dot{m}$ is in $\mathrm{kg\,s^{-1}}$. h_1 is the enthalpy at the inlet of the compressor and h_2 the enthalpy at the outlet of the compressor, both in $\mathrm{kJ\,kg^{-1}}$. This gives the required work in kW.

Lastly, the pressure ratio can be related to the efficiency of the compressor, and therefore related to the overall efficiency. This ratio is defined as the pressure in the condensation section to the pressure in the evaporation section:

$$PR = \frac{P_{cond}}{P_{evap}} \tag{3.21}$$

When the pressure ratio increases, the compression efficiency will decrease.

3.4.2. Types of compressors

The goal of the compressor is to increase the pressure. This can be executes in two different ways: by decreasing the volume (displacement) or increasing velocity which is converted in pressure by the use of a diffuser (dynamic). The different types of compressors and the categorization of those can be found in Figure 3.20.

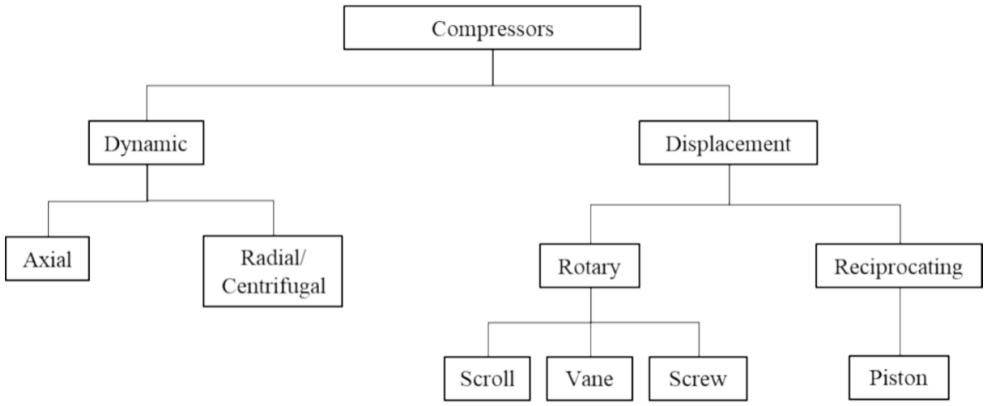

Figure 3.20: Classification of general compressors [60]

In Figure 3.21 the compressor options can be seen for different heating capacities. The axial compressor is not relevant for heat pumps, since this type is used in applications with large volume flows such as gas turbines or jet engines [62]. This can also be seen in Figure 3.22. These high volume flow rates are not achieved with heat pump applications. Another type of compressor that is not being used in industrial heat pumps are rotary vane compressors. They are only used in small applications due to their simplicity and compactness [60][63].

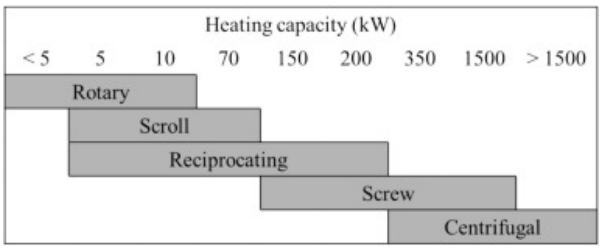

Figure 3.21: Compressor options for heat pumps. [60]

A dynamic compressor that is being used in heat pump applications is the centrifugal compressor. It differs from the axial compressor by the orientation of the flow. Centrifugal compressors compress with the use of centrifugal force, with the use of high-speeds impellers. The best application for this type of compressor is where large-capacity with continuous operation is required, and with a high efficiency. They are not often being used in household applications since they can be complex, large and have high initial costs. An industry where they are used is in industrial heat pump applications where higher capacity and efficiency are required for large-scale drying. In heat pump applications where the screw compressor cannot achieve the capacity that is required, turbo-compressors are used [60]. This is a type of centrifugal compressor.

In the other category of compressors, displacement compressors, the pressure of a fluid is increased by containing it within the compressor. After this the volume is reduced and then released via an exit valve. The displacement compressors can be divided into rotary and reciprocating. Positive displacement compressors, mainly piston and screw compressors, are most common in heat pump application, with piston compressors mostly covering the lower capacity applications [60].

The reciprocating compressor operate using a piston-cylinder mechanism. Here a piston moves up and down to compress the working fluid. This type of compressor is suitable for small-scale applications due to the high compressions ratio, and it is efficient in handling varying loads. Figure 3.22 shows this heating capacity range of the compressor. Compared to other types of compressor is the reciprocating type less efficient and noisier. This results in more maintenance, due to the mechanical wear and tear.

The other type of positive displacement compressors are the rotary compressors. The continuous rotary motion results in a smoother operation with fewer moving parts, causing better reliability and reduced vibration. Generally the efficiency is lower compared to reciprocating compressors due to the absence of a valve at the outlet. This type of compressor can be divided in separate categories by the type of device that is rotating.

The scroll compressor is typically used in heating, ventilation and air conditioning units. It operates with the use of a spiral shaped rotating part. The working fluid enters in the outer part of the spiral, and is moved to the central region by a rotating and a stationary spiral. When this compressor is being compared to the reciprocating compressor, it has a higher volumetric efficiency at single speeds. The popularity of this type of compressor in modern heat pumps is increasing due to its energy efficiency, which is a result of reduced leakage and a smooth operation with minimal frictional losses [60]. Scroll compressors are less prevalent in literature for high temperature industrial applications, where screw and turbo compressors are often preferred [60].

Another rotary compressor is the screw compressor, consisting of two meshing helical screws. Compression is applied continuously by the screws, with minimal pulsation. This type of compressor is being applied in large-scale and industrial application, since it can deliver at high capacity and operates stable. It is able to deliver a high efficiency, but this is accompanied by precise manufacturing, lubrication and regular maintenance. When this is not happening, wear will occur together with efficiency loss. Due to these advantages and disadvantages this type of compressor is generally not being used in small-scale heat pump dryers.

3.4.3. Selection of compressors

The selection of the compressor depends on several factors. Khan et al presents factors that are influencing the compressor selection [64]. The selection and design of the compressor depend on the selected refrigerant, cycle configuration, operating parameters and temperature rise. In addition, the choices are also influenced by materials, lubricants, size/heating capacity and ancillary components [60].

- First and foremost, the compressor must meet the required capacity specifications for the heat pump. The compressor must be able to provide the required volume flow at specific operating conditions. In Figure 3.22 the ranges of volume flow rates are shown which can be achieved by the associating compressor. Figure 3.21 illustrates the ranges in kW for the different types of compressors.

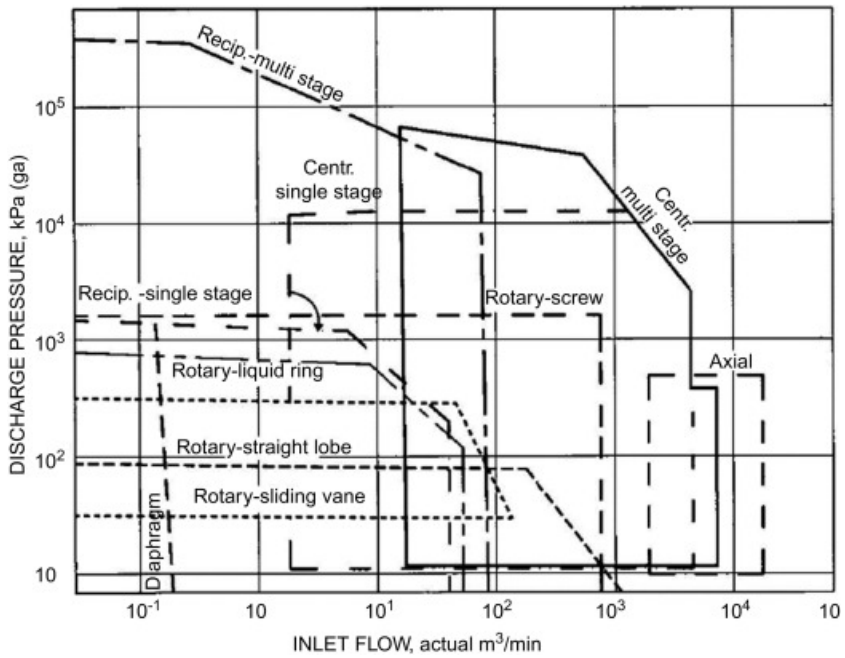

Figure 3.22: Compressor selection chart. [65]

- The temperatures at the sink and source of the heat pump determine the necessary pressure ratio across the compressor. Each type of compressor has a specific efficiency range at certain pressure ratios. Extreme pressure ratios can lead to low efficiency and may result in a shorter compressor lifespan. The general performance curve for dynamic and positive displacement compressors can be found in Figure 3.23, where characteristic curves are compared.

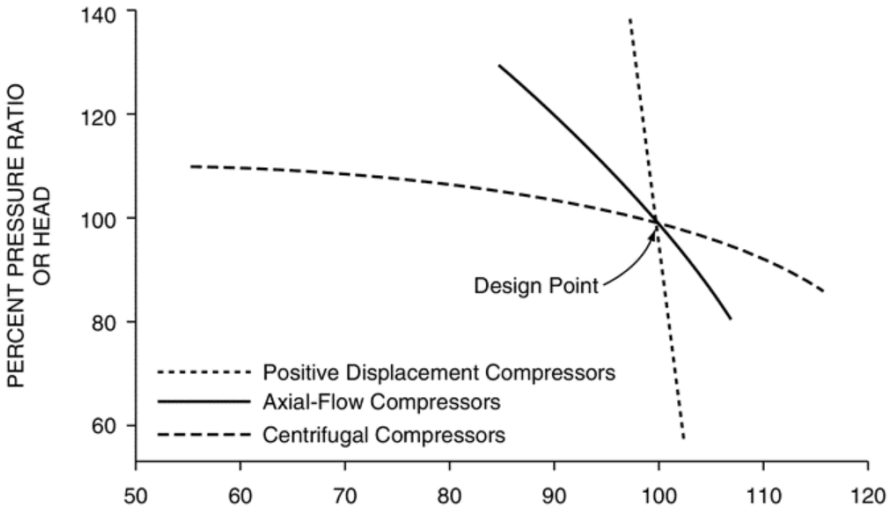

Figure 3.23: General performance curve for axial-flow, centrifugal, and positive displacement compressors. [66]

- In addition, the efficiency of the compressor is critical. A key indicator of this is the COP of the heat pump. The more efficient the compressor, the lower the energy cost and environmental impact.
- When selecting the compressor for a heat pump system, it is important to keep in mind the interaction between the refrigerant and the compressor. Research have shown that the isentropic efficiency of the compressor may be highly dependent of the refrigerant, and the main driver of the differences in refrigerant performance is the compressor [67].

- The reliability and lifespan of a compressor also influence the selection process. When this requirements are not met, this can result in additional costs and may cause the heat pump to stop functioning. Maintenance requirements also play a crucial role in the selection and must be taken into account. It is also important to consider the lubrication of the compressor, as this can improve the lifespan and performance.

Literature shows that the reciprocating piston and scroll compressors are most often chosen for a high temperature heat pump application. For the higher end of heating capacity the choice often falls on a screw or turbo compressor [60].

3.5. Pressure reduction component

In a heat pump cycle it is essential to reduce the pressure and close the cycle between the evaporator and the condenser to make heat transfer possible. Several methods are used to regulate and optimize the pressure difference and thereby improve the overall performance. In a conventional vapour compression system a capillary tube or an expansion valve is used. This part reduces the pressure level of the refrigerant to the level of the evaporator and is often assumed to be an isenthalpic process [18].

Since there is in reality still entropy production in this part, there are developments to improve this component. One of the options to reduce the expansion work loss in the heat pump system is by using an ejector. An ejector is a component that uses a nozzle to increase the velocity of a flow using the Venturi effect. Because of this the component has three different functions: changing the pressure, mixing and causing entrainment. An ejector has the following advantages: there is a limited amount of maintenance required, low costs, and there are no restrictions regarding working fluids [68]. On the contrary, making the design and predict the performance of the ejector can be challenging due the complex fluid dynamics. When an ejector is added to a heat pump, the expansion losses can be reduced and the pressure of the refrigerant can be raised without using additional electrical energy. A considerable amount of literature has been published on the addition of an ejector to a heat pump system. In Figure 3.24 a layout can be seen of a research by Elbel et al on prototype ejector in a transcritical R744 system. The effect of the nozzle can be seen in Figure 3.25. Instead of reducing the pressure in a valve, the flow is separated in two streams. A study by Xiaolong et al showed an increase of 21.4%-29.0% in COP while comparing an ejector-boosted solar-assisted flash tank vapour injection cycle for air source heat pump applications [69]. The result of another research by Elakhdar et al showed an improvement of 23% while performing a thermodynamic analysis of a novel ejector enhanced vapour compression refrigeration cycle and comparing this to a conventional vapour compression refrigeration cycle [70].

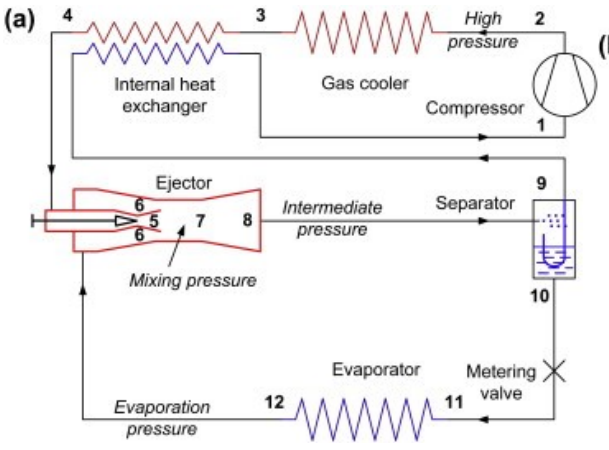

Figure 3.24: Component layout of a transcritical R744 ejector system. [71]

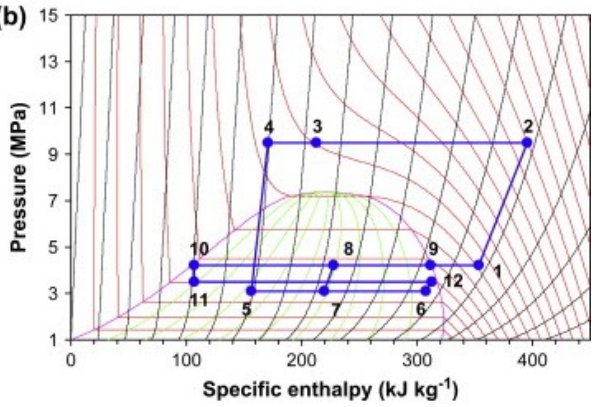

Figure 3.25: P-h diagram of the transcritical R744 ejector system from Figure 3.24 [71]

3.6. Refrigerants

As told in the introduction of heat pump cycles, refrigerant is the working fluid of the heat pump. It absorbs the heat from one location and increases the temperature level of another stream. Refriger-

ants play an important role in the heat pump, since they are crucial in the design of an optimal cycle, predicting the discharge temperature, determining the energetic and exergetic efficiency and with the selection of the components [72]. The primary refrigerants can be classified in five different main groups: halocarbons, hydrocarbons, inorganic compounds, azeotropic mixtures and zeotropic mixtures.

3.6.1. Selection Criteria of Refrigerants

Several studies give the selection criteria for an appropriate refrigerant for a heat pump system to ensure efficiency, safety and environmental sustainability [73] [74]. An overview of these requirements is given in Table 3.3.

Table 3.3: Selection criteria of refrigerants for application in HTHPs. [74]

Category	Required properties
Thermal suitability	• High critical temperature (> 150 °C) allowing subcritical heat pump cycles • Low critical pressure (< 30 bar) • Pressure at standstill > 1 atm • Low pressure ratio
Environmental compatibility	• ODP - 0 (no ozone depletion) • GWP < 10 (low global warming) • Future-proof according to regulations
Safety	• Non - toxicity • No or only low flammability
Efficiency	• High efficiency (COP) at high temperature lifts • Minimal superheat to prevent liquid compression • High volumetric heating capacity (VHC)
Availability	• Available on the market • Low price
Other factors	• Satisfactory solubility in oil • Thermal stability of the refrigerant - oil mixture • Lubricating properties at high temperatures • Material compatibility with aluminum, steel and copper

According to recent research by Sulaiman et al (2022), the typical characteristics a refrigerant of a heat pump dryer system has are the following: [72]

- The thermodynamic properties of the refrigerant must be outstanding and should not have a negative effect on the environment.
- Considering the safety, especially in household applications, the flammability should be low.
- Considering only subcritical heat pump cycles, the critical temperature must be higher than the condensation temperature.
- When analysing the temperature glides of zeotropic mixtures in the heat exchangers of the heat pump, they should be as close as possible to the air side temperature change. In research by Ni et al this temperature difference is set to $5\,\mathrm{K}$ [10].

3.6.2. Developments of refrigerants

In the past few years there have been several developments around refrigerants. The different developments in refrigerants can be divided into four separate generations, with their associated characteristics and environmental impacts [75] [76]. The changes in substances are mainly driven by legislation and the necessity to limit environmental damage.

First of all, the first generation refrigerants, which were used between 1830 and 1930. These are mainly natural substances such as ammonia, carbon dioxide, propane and sulphur dioxide, which were

used in the very first systems. The choice for these substances was mainly because it worked in the system, and choices with regard to for example the environment were not kept in mind. Because of this, accidents happened often, because refrigerants were toxic, combustible and poisonous [76].

These dangerous situations led to the development of new refrigerants: the second generation (1931-1990). The first synthetic refrigerants were introduced, known as CFCs. As safety and durability were increasingly considered, these refrigerants were safer to use, as they were not flammable or toxic. However, over time it was discovered that CFCs contribute to the depletion of the ozone layer. This led to the Montreal Protocol in 1987, which severely limited their use [77].

This led to new developments, which led to the third generation of refrigerants (1990-2010). Here, more attention was paid to the ozone depletion potential (ODP) of substances. Hydrochlorofluorocarbons (HCFCs) and hydrofluorocarbons (HFCs) were introduced to replace CFCs. Later, it turned out that these refrigerants have a high Global Warming Potential (GWP), and therefore have a major negative effect on the environment and are contributing to climate change.

The current generation, the fourth generation, started around 2010. There is now a main focus on refrigerants with zero/low ODP, low GWP and high efficiency. As a result, more natural refrigerants are used again, such as CO_2, but also less risky mixtures of synthetic refrigerants. Since 2016, the use of current HFCs is reduced with the Kigali Amendment, because of their greenhouse effect [78].

One of the developments that is currently receiving a large part of the attention is the impact of per- and polyfluoroalkyl substances, also known as PFAS. This includes any substance that contains at least one fully fluorinated methyl or methylene carbon atom, without any H/Cl/Br/I attached to it [79]. These are substances that do not occur naturally in the environment and have a negative effect on health and climate [80]. The European Chemicals Agency is currently working on a PFAS restriction [81]. The restriction is on the manufacture, placing on the market, and use of PFAS.

3.6.3. Zeotropic mixtures

Several studies, including the ones executed by Liu et al (2023), Kristensen et al (2023) and Ni et al (2024), show a positive effect on the performance of heat pump cycles by using a zeotropic mixture [82] [83] [10]. This is in the case when there is also a temperature glide on the air side of the heat exchanger. A zeotropic mixture, also known as a nonazeotropic mixture, is a mixture of two or more substances of different volatiles. Since it is a mixture, there is no constant boiling temperature but a range. The interest in this type of refrigerants is increasing, especially for heat pumps, as it introduces a new perspective on the layout and design of vapour compression systems [73]. The key characteristics of zeotropic mixtures that makes them attractive for vapour compressions heat pumps system are the performance improvement, energy-saving potential, easy capacity control and easy adaptation of hardware components regarding capacity and applications limits.

Due to the composition change during evaporation and condensation of the zeotropic mixture, the mixtures evaporates and condenses between two temperatures. This is called a temperature glide. Mixtures where the temperature glide is significant, which means about $5\,^{\circ}\mathrm{C}$ or larger, present a theoretical possibility for enhancing the performance and energy efficiency of vapour compression systems [84]. This is achieved by matching the temperature profile of the refrigerant with the profile of the heat transfer fluid, also known as glide matching. Additionally, this also decreases the pressure range for the compressor which improves the COP. An example of a heat exchanger temperature profile is given in Figure 3.26. As can be seen, the overall temperature difference between the refrigerant and the heat transfer fluid is smaller for the zeotropic mixture (b) compared to the pure refrigerant (a). Zühlsdorf et al (2018) shows that selecting working fluids with appropriate temperature glides can effectively improve the temperature matching and system efficiency [85].

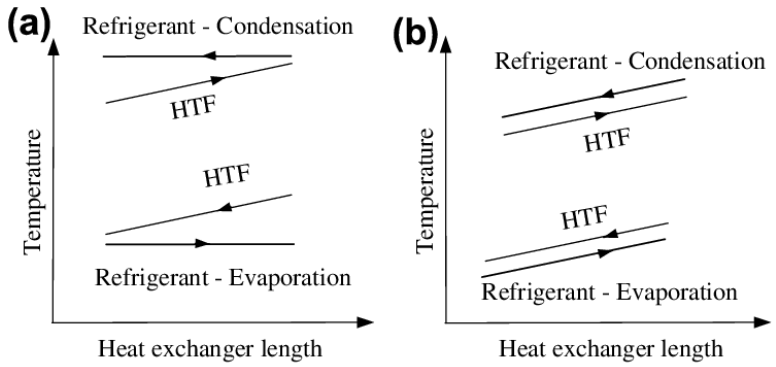

Figure 3.26: The temperature profiles of a heat exchanger with (a) a pure refrigerant and (b) a zeotropic refrigerant mixture with glide matching, during phase change. [84]

A study on the performance of a closed heat pump dryer by Ni et al (2024) showed an increase of the performance while using zeotropic mixtures, while working with temperatures variating between $12\,^{\circ}\mathrm{C}$ and $67\,^{\circ}\mathrm{C}$ [10]. The optimal working fluid was CO_2/R290 (mass fraction of 20/80). R290 is also known as propane. This refrigerant mixture caused an increase in, among other performance coefficients, the COP with 33.6% compared to the use of R134a. In several other studies, CO_2 also appears to be an attractive substitute [86] [82]. The advantages of CO_2 that makes it interesting to add is its environmental friendliness, low price, nonflammability, nontoxicity, zero ODP and low GWP.

A research on the performance increase on heat pumps due to future-proof binary zeotropic refrigerant mixtures is performed by Widdows [9]. Combinations were made of the following 13 natural refrigerants: water, ammonia, (iso)butane, (iso)pentane, methane, ethane, propane, carbon dioxide, propylene, ethylene and hexane. Based on calculations with different inlet and outlet temperatures, the mixtures with the highest COP were selected. These result can be found in Table 4.1. Here can be seen that 87.5$\%_{mol}$ Isobutane-Ethane and 87.5$\%_{mol}$ NH_3-Propane have the highest COP for the high dryer inlet temperature. 87.5$\%_{mol}$ CO_2-Isopentane and 90$\%_{mol}$ CO_2-Isobutane achieved the highest COP with the low inlet temperature. In Table A.1 which can be found in Appendix A, the properties of the 13 natural refrigerants used by Widdows together with common refrigerants can be found.

4

Methodology

This research focuses on the design of an experimental setup for a heat pump dryer. Heat pump dryers are increasingly recognized as an energy efficient alternative to conventional drying techniques. By recovering the heat from drying air, energy consumption can be reduced, while the quality of the drying process remains the same. In previous research, conducted by Widdows [9], several zeotropic refrigerant mixtures were identified that resulted in a high COP for a heat pump dryer. To validate these findings, an experimental test setup will be constructed. This chapter discusses the approach taken for designing the setup and explains how the results and insights from previous research work are incorporated into this design.

4.1. Outcome model study and choice of refrigerants

Recent research by Widdows [9] at Delft University of Technology demonstrated that the performance of vapour compression heat pump integrated dryers can be increased across all relevant temperature ranges by the use of future-proof binary zeotropic mixtures. This resulted in four high performing mixtures in terms of COP at different temperature conditions. An overview of these mixtures can be found in Table 4.1. The four mixtures that emerged from this study as the most promising options are: $87.5\%_{mol}$ Isobutane-Ethane, $87.5\%_{mol}$ NH_3-Propane, $87.5\%_{mol}$ CO_2-Isopentane and $90\%_{mol}$ CO_2-Isobutane.

Table 4.1: Overview of best performing mixtures for each studied drying condition by Widdows. [9]

Dryer inlet temperature	Dryer outlet temperature: 80 °C			Dryer outlet temperature: 50 °C		
	Mixture	COP	PR	Mixture	COP	PR
180 °C	87.5%$_{mol}$ Isobutane–Ethane	3.38	16.53	87.5%$_{mol}$ NH_3–Propane	3.44	6.84
120 °C	87.5%$_{mol}$ CO_2–Isopentane	3.96	3.58	90%$_{mol}$ CO_2–Isobutane	4.02	3.18

Since the different temperature levels and refrigerant mixtures make it unrealistic to construct a single setup capable of testing all four mixtures under their optimal conditions, a selection must be made. During the selection process, the focus was mainly on safety for in the laboratory and on the similarities between the mixtures. An overview of the selection criteria can be seen in Table 4.2. It can be seen that the mixture containing ammonia scores particularly low. This is mainly due to the high toxicity of ammonia, which makes it undesirable to work with in a laboratory environment. In addition to this, the pressure and temperature of the situations with the lower dryer inlet temperature are easier to predict, which makes the system more controllable. Based on these considerations, $87.5\%_{mol}$ CO_2-Isopentane and $90\%_{mol}$ CO_2-Isobutane are selected as the most suitable mixtures to be used in the setup. In addition, both mixtures contain a large fraction of CO_2 and a small fraction of hydrocarbons, suggesting that these two mixtures are likely to have comparable thermodynamic behaviour when compared to the other options.

Table 4.2: Selection criteria for the refrigerant mixtures including associated assessment. With (1) 87.5%$_{mol}$ Isobutane–Ethane, (2) 87.5%$_{mol}$ NH_3–Propane, (3) 87.5%$_{mol}$ CO_2–Isopentane and (4) 90%$_{mol}$ CO_2–Isobutane

Selection criteria	(1)	(2)	(3)	(4)
Toxicity	+	-	+	+
Flammability	- -	- -	-	-
High temperature	-	-	+	+
High pressure	+	-	-	-

4.2. Description of the cycles

The refrigerants resulting from the study of Widdows [9], are obtained by maximising the coefficient of performance (COP) of the heat pump cycle. This is the ratio of heat released at the condenser to the amount of work used by the compressor [87] [88]:

$$COP = \frac{Q_{cond}}{W_{comp}} \tag{4.1}$$

Since the cycle operates above the critical points of both refrigerant mixtures, it is a transcritical cycle. Therefore, this is a basic heat pump cycle consisting of the four main components: the compressor, the gas cooler, the expansion valve, and the evaporator. For both selected refrigerants, 87.5$\%_{mol}$ CO_2-Isopentane and 90$\%_{mol}$ CO_2-Isobutane, a T-s and Q-T diagram is made. These diagrams of 90$\%_{mol}$ CO_2-Isobutane can be found in Figure 4.1 and Figure 4.2. This cycle will be reviewed with associated assumptions.

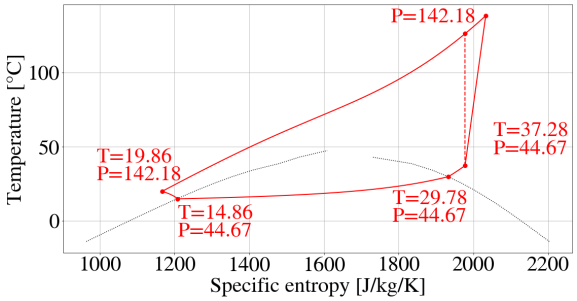

Figure 4.1: T-s diagram of the heat pump cycle of the refrigerant 90$\%_{mol}$ CO_2-Isobutane. With a dryer inlet temperature of $120\,^{\circ}\mathrm{C}$ and a dryer outlet temperature of $80\,^{\circ}\mathrm{C}$.

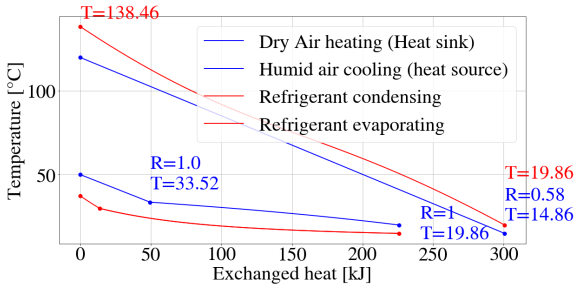

Figure 4.2: Q-T diagram of the heat pump cycle of the refrigerant 90$\%_{mol}$ CO_2-Isobutane. With a dryer inlet temperature of $120\,^{\circ}\mathrm{C}$ and a dryer outlet temperature of $80\,^{\circ}\mathrm{C}$

Starting at Figure 4.1, at the inlet of the compressor, where the temperature is $37.3\,^{\circ}\mathrm{C}$ and the pressure $44.47\,\mathrm{bar}$. The compressor increases the pressure and the temperature of the refrigerant mixture, delivering it to the gas cooler as a supercritical gas. It is assumed that the compression is adiabatic and the compressor is modelled using an isentropic efficiency:

$$\eta_c = \frac{h_{3,is} - h_2}{h_3 - h_2} \tag{4.2}$$

here h_i is the refrigerant mixture's specific enthalpy at state i and $h_{i,is}$ is the specific enthalpy at state i if the compression was performed isentropically. An initial assumption was made that the isentropic efficiency is equal to 0.7. Next, the refrigerants enters the gas cooler. The global pinch point temperature difference used here and also in the evaporator, is chosen to be $5\,^{\circ}\mathrm{C}$. In addition, the pressure losses in the heat exchangers have not been taken into account and the flows are assumed to be in opposite direction. In transcritical systems, such as with CO_2, the COP is highly dependent on the high-side pressure and the outlet temperature of the gas cooler. Therefore, optimisation of the high

pressure side is crucial for achieving maximum efficiency. The gas cooler, where the temperature of the refrigerant decreases, is followed by the expansion valve. The pressure of refrigerant is decreased here during an isenthalpic expansion. Since it is assumed there are no pressure losses, the expansion valve operates between the maximum pressure of the cycle and the minimum pressure of the cycle. After expansion, the refrigerant goes to the evaporator. Here the same assumptions are applied as the gas cooler. To prevent wet compression from taking place, a degree of superheating is applied. The degree of superheat in this cycle is $7.5\,^{\circ}\mathrm{C}$.

In Figure 4.3 and Figure 4.4, the diagrams of the $87.5\%_{mol}$ CO_2-Isopentane refrigerant mixture are shown. The same assumptions were made as mentioned above, and the cycle is again optimized based on its coefficient of performance.

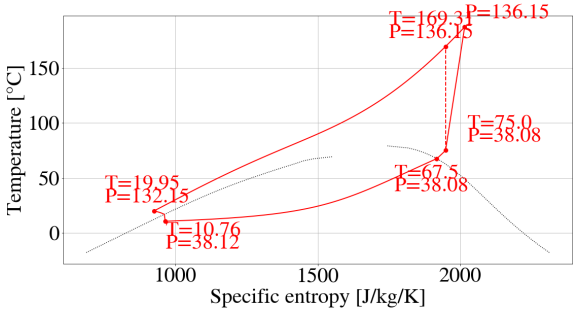

Figure 4.3: T-s diagram of the heat pump cycle of the refrigerant $87.5\%_{mol}$ CO_2-Isopentane. With a dryer inlet temperature of $120\,^{\circ}\mathrm{C}$ and a dryer outlet temperature of $80\,^{\circ}\mathrm{C}$.

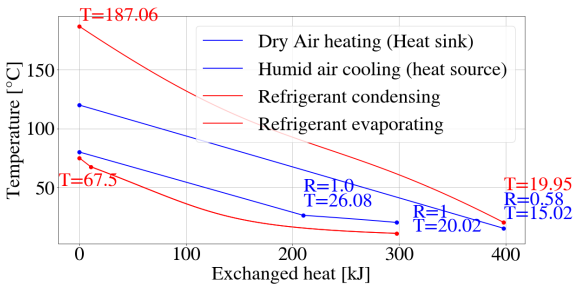

Figure 4.4: Q-T diagram of the heat pump cycle of the refrigerant $87.5\%_{mol}$ CO_2-Isopentane. With a dryer inlet temperature of $120\,^{\circ}\mathrm{C}$ and a dryer outlet temperature of $80\,^{\circ}\mathrm{C}$.

4.3. Design of the experimental setup

To be able to validate the refrigerant mixtures found in previous research, an experimental setup is designed. In this section, the foundation for the development of the design will be shown. First, the basic cycle on which the design is based will be described. Then, the approach to the design process will be explained. Finally, the main components of the cycle will be discussed in more detail, including how they will be selected and designed.

4.3.1. Process flow diagram

The flow chart of the basis heat pump cycle is shown in Figure 4.5. This cycle is based on the previous research that has been done.

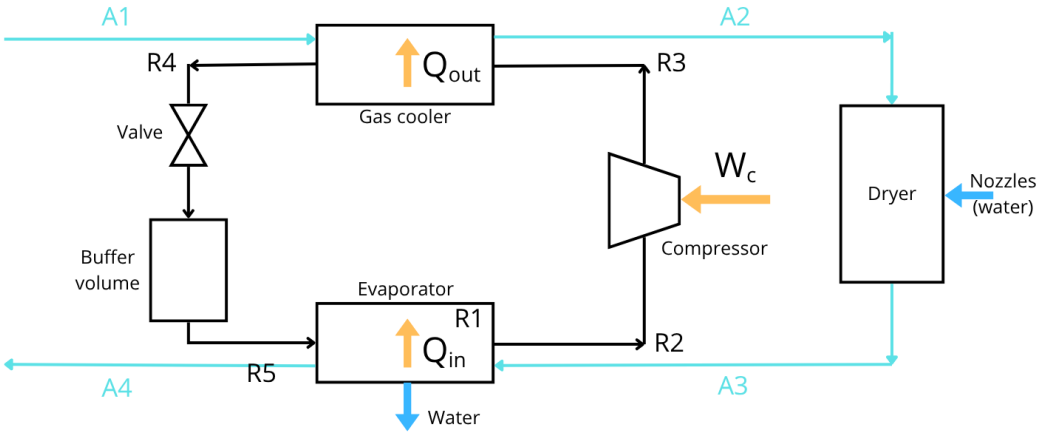

Figure 4.5: Process flow diagram of the basic heat pump cycle.

The air stream A1 enters the gas cooler at a relatively low temperature, since it is taken from the environment. It is assumed the temperature is $10\,^{\circ}\mathrm{C}$, the pressure 1 atm and the relative humidity 80% [16] [9]. In the gas cooler, the refrigerant mixture releases heat Q_{out} to the air, which brings the air to the required temperature for the dryer. With the chosen refrigerant mixtures this is $120\,^{\circ}\mathrm{C}$. The heated air will go the the dryer. This is not a commercial dryer, but an own dryer will be designed. A drying process will be simulated by injecting water into the air stream to increase the humidity and thereby reproduce the drying behaviour. This will also decrease the temperature of the air. Next, the moist air from the dryer will flow to the evaporator. here, the humid air will transfer heat to the refrigerant, causing the air to cool down and the water vapour contained within it to condense. Finally, the air will be released into the surrounding environment.

4.3.2. Design approach

An overview of the design process followed in this study, is presented in Figure 4.6. This approach is developed to ensure a clear overview of the design process. The process begins with gathering and reviewing all the available data on the thermodynamic cycle and system requirements. This includes data on operating conditions and component specifications, mostly based on the research results of previous research. Based on this information, the main components of the heat pump cycle will be selected and designed. This includes the compressor, the heat exchangers and the dryer. Since the heat exchangers can often be customized, it is important to first select a compressor. Here, the system is most dependent on what the availability is in the industry. The selection of the compressor will have an effect on the total cycle, for example on the maximum pressure. Therefore, an adjustment of the total cycle is required after the compressor selection. When the heat exchangers are designed, their pressure drop can be determined, which also results in small recalculation of the total cycle. After the design of the dryer is developed, all the system components are integrated into a complete design. This allows the effect of the components on each other to be seen, and important data like the total pressure drop can be calculated. In this way, the overall performance can be determined. Finally, a sensitivity analysis will be performed to test the robustness of the system under different conditions.

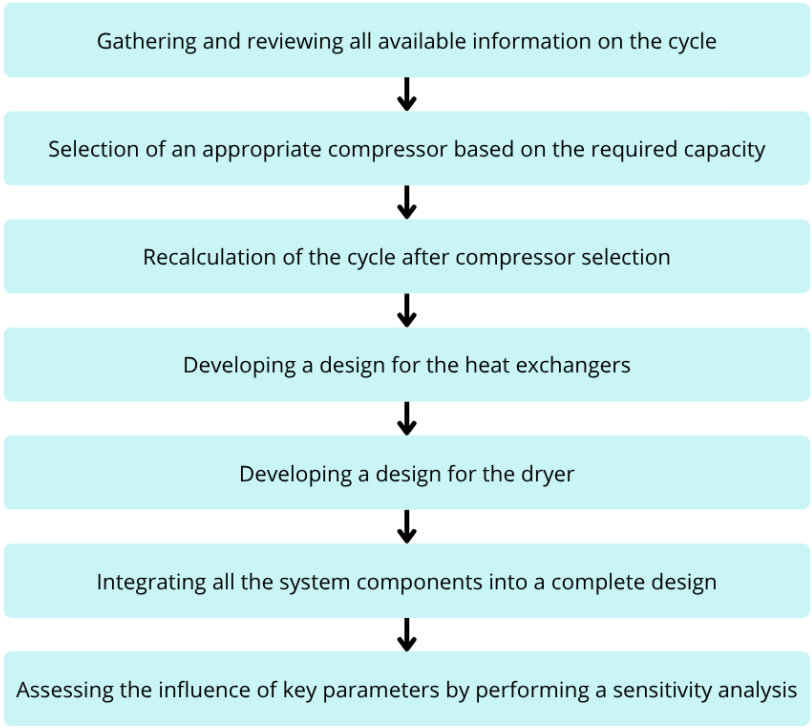

Figure 4.6: Diagram of the overall design process.

4.3.3. Heat exchanger design

One of the most crucial components in a heat pump are the heat exchangers. These can be custom made, and because they have a significant impact on the efficiency of the heat pump, it is essential to optimise them. This section will therefore describe the approach used for designing the heat exchangers.

Design approach

To be able to design the heat exchanger, a systematic and iterative approach is required. This is needed to ensure technical feasibility and efficiency. A model is developed in Excel to predict the behaviour and optimise the design of the heat exchanger. Within this model, both the heat transfer and expected pressure drop can be calculated. It is primarily based on the work of Pis'mennyi et al. [89], which serves as the starting point of the design. The flowchart representing this model is shown in Figure 4.7. Subsequently, the procedure for performing the heat exchanger calculations will be discussed.

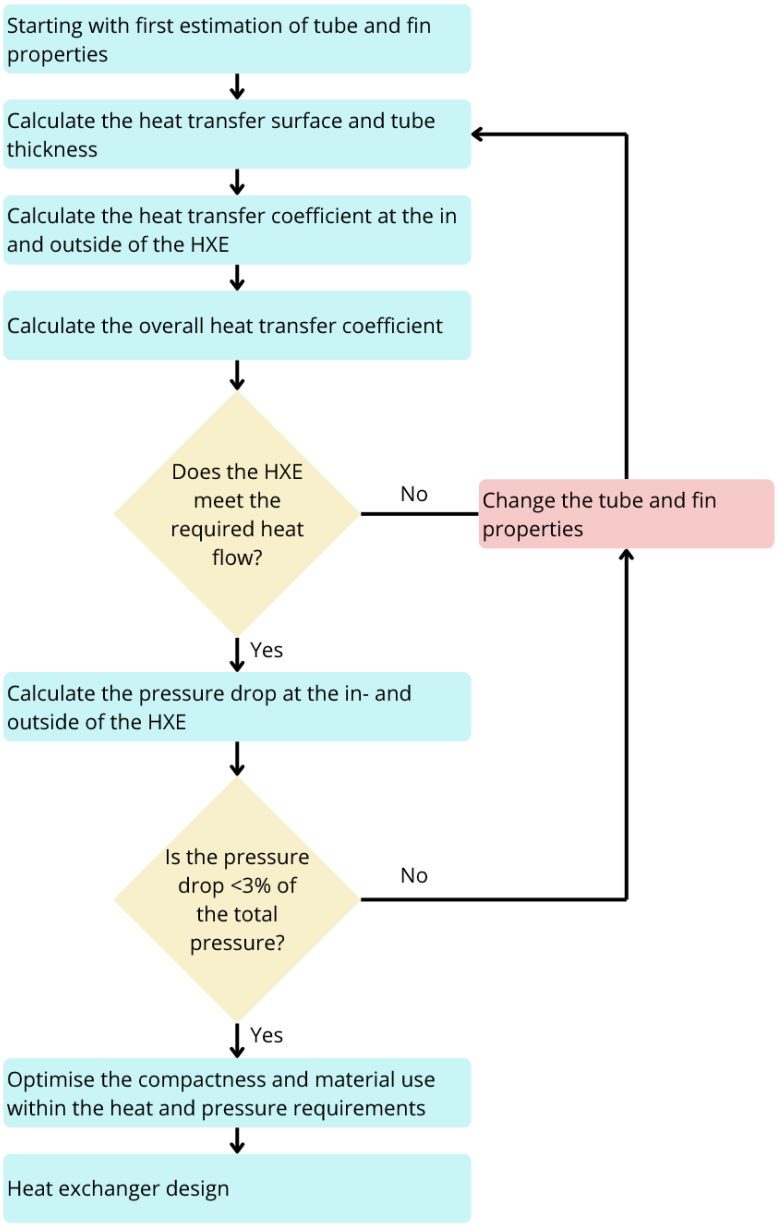

Figure 4.7: Flowchart of the model for finned tube heat exchanger design.

Heat exchanger configuration

First, the type of heat exchanger must be selected. The selection of the heat exchanger type is primarily determined by the fact that the external medium is air. Since air has a low thermal conductivity, a finned tube heat exchanger is selected to maximize the heat transfer efficiency.

Thereafter, different fin configurations can be selected for the finned tube heat exchanger [89]. The fins are positioned around the tube, were a distinction can be made between circular and rectangular fin geometries. Various studies have shown that a higher efficiency can be achieved with circular fins, since they have a greater heat transfer and lower pressure drop [90] [91]. This is due to the fact that circular fins have a higher fin efficiency: the heat conduction is uniformly distributed in all directions, whereas the corners of rectangular fins create longer conduction paths. Moreover, the effect of the 'additional' material in rectangular fins is negligible, meaning that the UA per unit mass of material is higher for the circular fins. Finally, circular fins are more aerodynamically streamlined, resulting in less flow separation and vortices at the corners, and therefore a lower air resistance and pressure drop. For these reasons, circular fins have been selected for this application.

Furthermore, a selection can be made between tubes in in-line and staggered arrangements. The spacing characteristics of these arrangements can be found in Figure 4.8. A staggered arrangement allows for a higher heat transfer rate [89]. An in-line arrangement is more attractive when the heat exchanger is prone to fouling. For the experimental test setup, heat transfer is more important than the ease of cleaning the HEX, so a staggered arrangement is chosen.

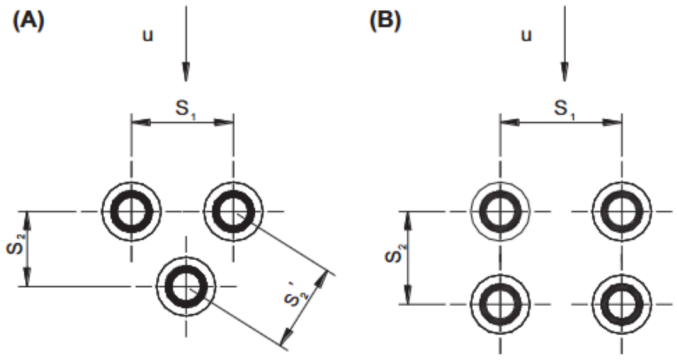

Figure 4.8: Spacing characteristics of finned tubes bundles. With (A) staggered arrangement and (B) in-line arrangement. [89]

Estimation of the surface area with the LMTD method

Since the inlet and outlet values of the heat exchangers are known due to the fact the optimal cycle is known, the LMTD method is used. Subsequently, an estimation of the required heat exchanger surface area can be obtained by using an approximate value of the overall heat transfer coefficient U. The total heat transfer in a HEX can be expressed as:

$$Q = UA\Delta T_{lm} \tag{4.3}$$

where ΔT_{lm} is the logarithmic mean temperature difference (LMTD), U the overall heat transfer coefficient in $\mathrm{W\,m^{-2}\,K^{-1}}$ and A the heat transfer surface in $\mathrm{m^2}$.

To be able to calculate the required surface area, first of all Q needs to be determined. This can be done with the following equation.

$$\dot{Q} = \dot{m} \cdot \Delta h \tag{4.4}$$

where $\dot{m}$ is the mass flow of the refrigerant in $\mathrm{kg\,s^{-1}}$ and Δh the enthalpy change in the heat exchanger in $\mathrm{J\,kg^{-1}}$. Then, ΔT_{lm} can be determined using the following equation:

$$LMTD = \frac{(T_{hi} - T_{co}) - (T_{ho} - T_{ci})}{\ln\left(\frac{(T_{hi} - T_{co})}{(T_{ho} - T_{ci})}\right)} \tag{4.5}$$

were the temperature are in K. Furthermore, the h subscript stands for the hot side, c for the cold side, i for the inlet and o for the outlet.

As can be seen in the QT diagram of the heat exchangers, the lines are not perfectly linear. To make a reliable estimation of the LMTD, the graph is separated in smaller parts. To verify the calculation of the LMTD across the different segments, the number of sections is increased. This resulted in converging values of LMTD, indicating that the method is valid. Using as assumed value of U, the expected required surface area of the HEX can be calculated. Based on values reported in literature discussed in chapter 3, an overall heat transfer coefficient of $200\,\mathrm{W\,m^{-2}\,K^{-1}}$ was used. These initial estimates for the heat exchanger can be used for the preliminary selection of the tube and fin geometry.

Structural and material considerations

The structural and material considerations are important aspects to keep into account when designing heat exchangers. They play a crucial role in achieving a high thermal efficiency and mechanical reliability, long and short term. While comparing various finned tube heat exchanger in similar operating conditions, the materials used in the constructions were also considered, as shown in Appendix B. This revealed that carbon steel, stainless steel and aluminium are the most commonly used materials for this type of heat exchanger. The most basic and cost effective option used is carbon steel for the tube and aluminium for the fins. Aluminium is used for the fins because of the high thermal conductivity, causing efficient heat transfer. While carbon steel is being used for the tube since it can withstand the higher pressures, which are typically present inside the tubes.

Tube and fin geometry

For the selection of the tube geometry, a combination of TEMA standards, the handbook of transversely finned tube heat exchangers and papers with comparable situations are being used [89] [92]. The geometric characteristics of circular finned tubes are shown in Figure 4.9.

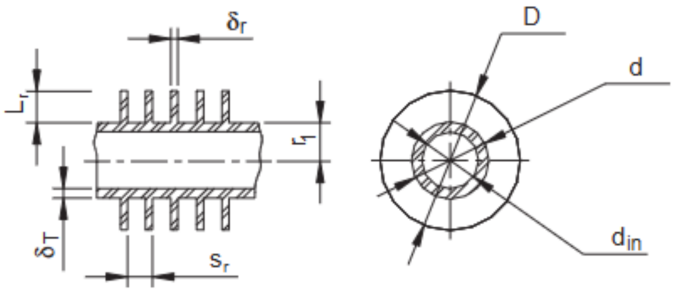

Figure 4.9: Geometric characteristics of circular finned tubes. [89]

The first approximation of the tube diameter is approximately 15 to $20\,\mathrm{mm}$. With the use of common tube diameters from TEMA [92], a first selection of $19.1\,\mathrm{mm}$ is made. Together with this, a range is given for the wall thickness. The wall thickness range for this diameter is between 0.889 and $2.769\,\mathrm{mm}$.

According Pis'mennyi et al. [89], the wall thickness of the tube can be determined with the following equation:

$$\delta_{calc} = \frac{P \cdot d}{2\varphi_w[\sigma] + P} \tag{4.6}$$

where d is the inside diameter of the tube in m, φ_w the strength coefficient and σ the allowable stress. The strength coefficient for finned tubes is generally 1 [89]. Lastly, P is the design pressure in Pa. This refers to the pressure of the working medium, and should be equal to or higher than the maximum pressure. An allowable stress of $145\,\mathrm{MPa}$ is selected from the table with nominal stresses by material and temperature by Pis'mennyi [89], which is based on a maximum temperature of $200\,^{\circ}\mathrm{C}$. The allowable wall thickness can be determined by multiplying the design wall thickness by 1.15 [89].

For the fin geometry, comparable cases involving finned tube heat exchangers were first examined. An overview of these cases can be found in Appendix B. Based on this review, an initial selection of the fin dimensions is made. Subsequently, the fin temperature distributions can be optimized using the model developed for the heat exchangers.

When the measurements of the heat exchanger are known, the surface areas can be calculated. The parameters can also be found in Figure 4.9. The total heating surface A is calculated by adding the heating surface of the fins A_r to the heating surface of the tubes A_t.

$$A = A_r + A_t \tag{4.7}$$

where all the heating surfaces are in m^2. The heating surface of circular fins is determined with the following equation:

$$A_r = \frac{\pi}{2}\left(D^2 - d^2 + 2 \cdot D \cdot \delta_r\right)\frac{L_{rs}}{S_r}z \tag{4.8}$$

In this equation D and d are the outer and the inner diameter, respectively, in m. L_{rs} is the length of the finned segments of the tubes in m. The heating surface of the tubes themself can be calculated from the equation:

$$A_t = \pi \cdot d\left[L_{rs}\left(1 - \frac{\delta_r}{S_r}\right)z + L_t\right] \tag{4.9}$$

Here, L_t is the total length of the heated unfinned tube segments in m. This includes the bends and junction regions.

Since the mass flow is known together with the diameter of the tube, the velocity of the fluid can be determined. This can be done by dividing the mass flow by the density and cross sectional area of the flow. Since the temperature in the flow is changing, the density is also changing. This results in a changing velocity of the flow. For the flow velocity in the heat exchanger the average of the density can be taken.

Detailed thermal analysis

A detailed thermal analysis of the heat exchanger is required to make a valid estimation of the heat transfer. These calculations are performed in Excel to make a model for the heat exchanger calculations, of which the flowchart is given in Figure 4.7

The main goal for this section is to determine the overall heat transfer coefficient of the finned tube heat exchanger. This coefficient indicates how well heat is transferred from one flow to the other, within the heat exchanger. It accounts for the combined thermal resistances, for this situation including the conduction through the wall material, convection on the external side and convection on the internal side. The equation for this is as follows:

$$U = \frac{\Psi}{\frac{A}{A_{in}} \cdot \frac{1}{h_2} + \frac{A}{A_{in}} \cdot R_t + \frac{1}{h_{1rdc}}} \tag{4.10}$$

where h_2 is the heat transfer coefficient from the tube wall to the internal medium in $\mathrm{W\,m^{-2}\,K^{-1}}$, h_{1rdc} the reduced heat transfer coefficient in $\mathrm{W\,m^{-2}\,K^{-1}}$ and R_t is the thermal resistance of the tube wall in $\mathrm{m^2\,K\,W^{-1}}$. Ψ is the thermal efficiency factor, which keeps into account the decrease in heat absorption

caused by the heating surface, by for example partial overflowing of gases past it and the formation of stagnations regions. A_{in} is the inside heat transfer surface of the tube in m^2. This inside heat transfer surface for a tube can be calculated by using:

$$A_{in} = \pi \cdot d_{int} \left(L_{rs} \cdot z + L_t \right) \tag{4.11}$$

In this equation, d_{int} is the internal diameter of the tube in m, z the amount of tubes in the heat exchanger, L_{rs} the total length of a finned tube in m and L_t the total length of heated unfinned tube segments in m.

At the bottom of the equation for the overall heat transfer coefficient, the three forms of heat transfer for this case are represented. The first part is the convection on the inside, the second part the conduction through the tube wall, and the last part is the convection at the outside of the tube. The resistances for the internal convection and the conduction through the wall are normalized to the total surface area. The difference types of heat transfer will be explained separately.

Conduction through tube

First, the conduction will be discussed. The thermal resistance R_t of the tube wall of ordinary uniform tubes can be determined using the following equation:

$$R_t = \frac{\delta_t}{k_t} \tag{4.12}$$

where δ_t is the thickness of the tube in m and k_t is the thermal conductivity of the tube in $\mathrm{W\,m^{-1}\,K^{-1}}$. This gives as a result the thermal resistance in $\mathrm{m^2\,K\,W^{-1}}$. For heat exchangers, materials with low thermal conductivity are mainly chosen, so that the heat can be transferred with a relatively low resistance.

Outside heat transfer coefficient

Subsequently, the convection on the outside of the HEX is determined. This can be summarized in the following equation:

$$h_{1rdc} = \left(\frac{A_r}{A} E \cdot \mu_r \cdot \psi_E + \frac{A_t}{A} \right) h_c \tag{4.13}$$

In this equation, h_{1rdc} is the reduced convective heat transfer coefficient from outside (gas) in $\mathrm{W\,m^{-2}\,K^{-1}}$, E is the theoretical efficiency of the fin, μ_r is the factor taking account of fin widening toward base, ψ_E is the correction factor to the theoretical efficiency and h_c is the convective heat transfer coefficient in $\mathrm{W\,m^{-2}\,K^{-1}}$. As can be seen, the equations consists of two separate parts: the convection at the fins and the convection at the parts of the tube without fins. The fins need some further explanation. First of all, the theoretical efficiency E for a circular fin with $\beta \cdot l_r \leq 2$ and $D/d \leq 3$ can be determined with the following equation:

$$E = \frac{\tanh\left(\beta l_r'\right)}{m l_r'} \tag{4.14}$$

β is a fin parameter in $\mathrm{m^{-1}}$, l_r' is the conventional fin height in m and m is another fin parameter which can be determined with the use of Equation 4.15. The equation show above, is the equation for a pin fin. Within the given boundaries, is gives the same fin efficiency as the more complex fin efficiency equation for a circular fin.

$$\tanh\left(m l_r'\right) = \frac{e^{2\beta l_r'} - 1}{e^{2\beta l_r'} + 1} \tag{4.15}$$

The conventional fin height keeps into account the effect of bending a fan around the tube. If the geometric fin height is used, the estimation of the heat resistance will be higher than in reality. The conventional fin height can be determined using the relation:

$$l'_r = l_r \left[1 + \left(0.191 + 0.054 \times \frac{D}{d}\right) \times \ln\left(\frac{D}{d}\right)\right] \tag{4.16}$$

where l_r is the geometric fin length in m, D is the fin diameter in m and d is the tube diameter in m. The last factor used to calculate the convection at the fins is the correction factor ψ_E. it keeps in account the non uniformity of heat transfer over the fin surface, and can be determined with the following equation:

$$\psi_E = 1 - 0.016\left(\frac{D}{d} - 1\right)\left[1 + \tanh\left(2 \cdot \beta l_r - 1\right)\right] \tag{4.17}$$

where l_r, D and d are the same parameters as above and all in m. Lastly β is the fin parameter in m^{-1}

Before the convection at the fins and the tubes can be determined, the convective heat transfer coefficient is required. At the gas side with a transverse flow around the tubes, this can be done with the following relation:

$$h_c = 1.13 \cdot C_z \cdot C_q \cdot \frac{k_g}{d} \cdot \left(\frac{u_g \cdot d}{v_g}\right)^n \cdot Pr_g^{0.33} \tag{4.18}$$

Here is k_g the thermal conductivity of the gas $\mathrm{W\,m^{-2}\,K^{-1}}$, d the diameter of the tube m, u_g the velocity of the gas $\mathrm{m\,s^{-1}}$, v_g the specific volume of the gas $\mathrm{m^3}$, Pr_g the Prandtl number of the gas and n, C_z and C_q are correction factors. C_z is the correction for number of tube rows in bundle in direction of gas flow (z_2). When z_2 is greater than 8, C_z is equal to 1 [89]. The exponent n characterizes the dependence on the Reynolds number. This means that n determines how strongly the convective heat transfer varies with the flow velocity and regime. Lastly, C_q is a correction factor taking into account the influence of the fins. n and C_q can be determined with the following equations:

$$n = 0.7 + 0.08 \cdot \tanh\left(X\right) + 0.005 \cdot \Psi_r \tag{4.19}$$

$$C_q = \left(1.36 - \tanh\left(X\right)\right) \cdot \left(\frac{1.1}{\Psi_r + 8} - 0.014\right) \tag{4.20}$$

where X is the shape parameter of the bundle and Ψ_r is the fin coefficient, which takes in to account the ratio of total outside surface of finning tubes to external surface of the tube not occupied by fins. The shape parameter X can be determined with:

$$X = \frac{\sigma_1}{\sigma_2} - \frac{1.26}{\Psi_r} - 2 \tag{4.21}$$

where σ_1 is the relative transverse spacing of tubes ($\sigma_1 = S_1/d$) and σ_2 is the relative longitudinal spacing of tubes ($\sigma_2 = S_2/d$). The fin coefficient Ψ_r, which is required in a few of the equations above, can be determined with the following relation:

$$\Psi_r = \frac{1}{2d \cdot S_r}\left(D^2 - d^2 + 2 \cdot D \cdot \delta_2\right) + 1 - \frac{\delta_1}{S_r} \tag{4.22}$$

where d diameter of the tube in m, S_r is the fin spacing in m, D is the fin diameter in m, δ_2 fin thickness at tip in m and δ_1 fin thickness at base m. In this situation the fin thickness is kept the same over the length of the fan, which means that δ_1 and δ_2 are similar.

The heat transfer coefficient on the outside of the evaporator differs from the gas cooler. At the evaporator, the transfer occurs with moist air instead of dry air. Due to the temperature change in the HEX, the water in the air will condense. This increases the heat transfer coefficient, which must be taken into account in the calculation. Consequently, the heat transfer on the outside of the evaporator consists of convective heat transfer (sensible) and heat transfer due to condensation (latent).

Additionally, for the evaporator, the heat transfer due to condensation therefore must be calculated. The Chilton-Colburn analogy is used to calculate the contribution of water condensation to the heat transfer coefficient [93] [94] [95] [96]. This approach links heat and mass transfer through the use of the Colburn factor j. The Colburn j factors j_H and j_M are the dimensionless heat and mass transfer coefficients, and can be expressed as follows:

$$j_H = StPr^{2/3}, \qquad \text{with} \quad St = \frac{h}{\rho V c_p} \tag{4.23}$$

$$j_M = \frac{k_m}{\rho V} Sc^{2/3}, \qquad \text{with} \quad Sc = \frac{\mu}{\rho D_{AB}} \tag{4.24}$$

Here, h is the expected heat transfer coefficient for convection, k_m is the mass transfer coefficient, and D_{AB} is the diffusion coefficient of humid air. The diffusion coefficient is assumed to be $2.4 \times 10^{-5}\,\mathrm{m^2\,s^{-1}}$ [97]. When j_M and j_H are set equal to each other, this relationship can be solved for k_m.

$$k_m = \frac{h}{c_p} \left(\frac{Pr}{Sc} \right)^{2/3} \tag{4.25}$$

Subsequently, using k_m, and the mass fractions of vapour (Equation 2.2), the mass flow density can be calculated, representing the condensation rate per $\mathrm{m^2}$.

$$\dot{m}'' = k_m \left(Y_{in} - Y_{surf} \right) \tag{4.26}$$

The latent heat flux q_{lat} of condensation can be calculated by multiplying the mass flow density by the latent enthalpy.

$$q_{lat} = \dot{m}'' \cdot h_{fg} \tag{4.27}$$

Finally, the effective heat transfer coefficient can be calculated by dividing q_{lat} by the temperature difference between the heat exchanger surface and the fluid.

Inside heat transfer coefficient gas cooler

Lastly, the heat transfer coefficient from the wall to the internal medium can be determined. Since no phase change occurs in the gas cooler but it does in the evaporator, they both require a different approach. First, the flow in the gas cooler is examined. Since there is no phase change in this part, the method proposed by Pis'mennyi et al. for a monophase turbulent flow can be applied [89]. The heat transfer coefficient over the inside surface at $Re_f = 4 \times 10^3 - 5 \times 10^6$ and $Pr_f = 0.1 - 2000$ is determined with the equation:

$$h_2 = \frac{k_f}{d_{in}} \cdot \left[\frac{0.125 \cdot \zeta \cdot Re_f \cdot Pr_f \cdot C_{tem}}{\lambda + 4.5 \cdot \zeta^{0.5} \left(Pr_f^{0.666} - 1 \right)} \right] \tag{4.28}$$

Here k_f is the thermal conductivity of the flow in $\mathrm{W\,m^{-1}\,K^{-1}}$, d the inner diameter of the tube in m, ζ and λ both are correction parameters, Re_f is the Reynolds number of the inside flow, Pr_f is the Prandtl number of the inside flow, C_{tem} is the correction of the tube temperature. In this case there is no correction of the tube temperature included, so $C_{tem} = 1$. The correction parameters ζ and λ can be determined with the following relations:

$$\lambda = 1 + \frac{900}{Re_f} \tag{4.29}$$

$$\zeta = (1.82 \cdot \log(Re_f) - 1.64)^{-2} \tag{4.30}$$

To verify these calculations, forced convection correlations from Mills [19] are used to calculate the heat transfer coefficient in the gas cooler. Essential in this calculation is the friction factor f. This is a dimensionless number that characterizes flow resistance due to friction. For forced convection in fully developed flow in round tubes, the friction factor f can be determined with:

$$f = (0.790 \ln (Re_D) - 1.64)^{-2} \tag{4.31}$$

$$Nu_D = \frac{(f/8)\,(Re_D - 1000)\,Pr}{1 + 12.7\,(f/8)^{1/2}\left(Pr^{2/3} - 1\right)} \tag{4.32}$$

where f is the friction factor, Re_D is the Reynolds number in the tube, Pr is the Prandtl number in the tube and Nu_D is the Nusselt number of the flow in the tube. With the Nusselt number, the heat transfer coefficient can be determined by:

$$h = \frac{Nu \cdot k_f}{d} \tag{4.33}$$

where d is the inside diameter of the tube in m and k_f the thermal conductivity of the flow in the tube in $\mathrm{W\,m^{-1}\,K^{-1}}$.

Inside heat transfer coefficient evaporator

The heat transfer coefficient in the evaporator cannot be determined in the same way as the gas cooler, since the refrigerant changes phase. General heat transfer correlation for flow boiling for zeotropic mixtures in horizontal plain tubes are given by Zhang et al. [98]. This study analyses a large number of existing correlations and derives two new heat transfer correlations. For this situation, the new physics based correlation will be used, since it does not match the boundary conditions of the regression based correlation. For the physics-based correlation the dimensionless number T^* needs to be determined first, in order to see if the process consists of nucleate and convective boiling, or if the process is dominated by convective boiling. The dimensionless number can be determined:

$$T^* = T_g / T_{sat} \tag{4.34}$$

where T_g is the temperature glide and T_{sat} the saturation temperature, both in K. In this situation the dimensionless number T^* is 0.05, which is lower than 0.06, which makes the process concomitant by nucleate and convective boiling. If the difference between the temperature glide and the saturation temperature was larger dan 0.06, the process would have been dominated by convective boiling. This results in the following relation for the heat transfer coefficient:

$$h_{tp} = \left[(F_c h_{Cooper\_nb})^2 + (h_{Mishra})^2\right]^{0.5} \tag{4.35}$$

The contribution of the convective boiling is based on the correlation by Mishra [99]. This correlation is developed based on experimental result with the use of multiple regression. The two phase heat transfer coefficient by Mishra can be determined with the following correlation:

$$\frac{h_{tp}}{h_l} = 21.75 \left(\frac{1}{X_{tt}}\right)^{0.29} Bo^{0.23} \tag{4.36}$$

where h_l is the non-boiling coefficient of total liquid flow calculation, from the Dittus-Boelter equation. This can be calculated with the following equation:

$$h_l = 0.023 Re_l^{0.8} Pr_l^{0.4} \frac{k_l}{D} \tag{4.37}$$

Furthermore, the Martinelli number X_{tt} and the boiling number Bo are required to determine the heat transfer coefficient. These parameters are defined as:

$$X_{tt} = \left(\frac{\rho_v}{\rho_l}\right)^{0.5} \left(\frac{\mu_l}{\mu_v}\right)^{0.1} \left(\frac{1-x}{x}\right)^{0.9} \tag{4.38}$$

$$Bo = \frac{q}{G h_{fg}} \tag{4.39}$$

For the Martinelli number, ρ is the density in $\mathrm{kg\,m^{-3}}$, μ the dynamic viscosity in $\mathrm{Pa\,s}$ and x is the vapour quality. The subscript l is for liquid and v for vapour. For the boiling number, q is the heat flux in $\mathrm{W\,m^{-2}}$, G is the mass velocity in $\mathrm{kg\,m^{-2}\,s^{-1}}$ and h_{fg} is the latent heat of vaporization in $\mathrm{J\,kg^{-1}}$.

The contribution of nucleate boiling is derived by a correlation of Cooper [98], with the following correlation:

$$h_{Cooper\_nb} = 35 M^{-0.5} q^{-0.67} P_r^{0.12} \left(-\log_{10} P_r\right)^{-0.55} \tag{4.40}$$

where M is the molecular weight in $\mathrm{kg\,mol^{-1}}$, P_r the reduced pressure ($= P/P_{critical}$) and q is the again the heat flux in $\mathrm{W\,m^{-2}}$.

This correlation is derived by modifying the pool boiling correlation with a factor 0.7 [98]. The equation is applied as the base pure working fluid correlation, which needs to be multiplied by the mixture correction factor since there is a mixture in this situation. For the mixture correction factor F_c, the mass transfer resistance on nucleate pool boiling in plain tubes is analytically modelled, and defined as:

$$F_c = \left(1 + \left(\frac{h_{id}}{q}\right)(T_d - T_b)\left[1 - \exp\left(-\frac{Bq}{\rho_l h_{fg} \beta_l}\right)\right]\right)^{-1} \tag{4.41}$$

where B is a scaling factor which is assumed to be 1.0, since it is assumed that all the heat which is transferred to the surface of the bubble is converted into latent heat. In addition, the liquid-phase mass transfer β_l is assumed to be $0.0003\,\mathrm{m\,s^{-1}}$, which is demonstrated as the most reliable option when predicting the performance for mixture flow boiling [98]. h_{id} is the ideal heat transfer coefficient, which can be calculated with Cooper's correlation, which is shown below. Lastly, T_d and T_b are the temperatures at the dew and bubble line, respectively, in K. The difference between these two is the temperature glide (T_g).

$$h_{Cooper} = 55 M^{-0.5} q^{-0.67} P_r^{0.12} \left(-\log_{10} P_r\right)^{-0.55} \tag{4.42}$$

This equation is almost similar to Equation 4.40, except for the first value. This is because the equation presented above represents the original correlation for pool boiling, whereas Equation 4.40 is the modified version which includes the correction factor of 0.7 to be able to obtain the equation for nucleate boiling.

Since this heat transfer coefficient is changing over the length of the heat exchanger, the heat exchanger tube is separated in different segments. The heat transfer coefficient is then calculated for each segment, after which the average is taken of all the different segments.

Estimation of the pressure drop

When designing the heat exchanger, not only the heat transfer must be calculated, but also the pressure drop. The pressure drop across the heat exchanger largely determines the energy consumption of the compressor or fan used in the system. Consequently, it has a significant impact on the overall efficiency of the heat pump cycle. Therefore the pressure drop needs to be determined on the inside and the outside of the heat exchangers.

To be able to calculate the pressure drop in the inside of the heat exchanger, it needs to be divided in tubes and bends. To determine the pressure drop in the tubes, the Fanning formula can be used:

$$\Delta P = 4f\frac{L}{D}\frac{1}{2}\rho v^2 \tag{4.43}$$

where L is the length of one tube in m, D the inside diameter of the tube in m and ρ is the density of the refrigerant in $\mathrm{kg\,m^{-3}}$. In a turbulent case the Blasius formula can be used to determine the friction factor, which is $f = 0.0781Re^{-1/4}$.

To calculate the pressure drop over a bend, the following equation can be used:

$$\Delta P = K_L\frac{1}{2}\rho v^2 \tag{4.44}$$

K_L is the loss coefficient, and can be found in Mills for different kind of bends [19]. The loss coefficient for a 180° bend is assumed to be 1.5.

The total pressure of a complex system can be determined by calculating the pressure drop for all the different parts and adding them together.

$$\Delta P = \sum 4f\frac{L}{D}\frac{1}{2}\rho v^2 + \sum K_L\frac{1}{2}\rho v^2 \tag{4.45}$$

The pressure drop on the external side of the heat exchanger, the air side, must be evaluated using a different approach. For this, the aerodynamic resistance on the outside of the finned tube needs to be determined. This can be done with the following equation:

$$\Delta P = C_{op}\cdot\zeta_0\cdot z_2\cdot\frac{\rho_g\cdot u_g^2}{2} \tag{4.46}$$

This is the equation for a bundles of finned tubes in cross flow. In this relation, C_op is the correction factor taking account of real operating conditions of the heat transfer surface, and is taken to be 1.1. ζ_0 is the resistance coefficient referred to a single transverse row of tubes, z_2 is the number of the tube rows in bundle in direction of gas flow, ρ_g is the density of the gas in $\mathrm{kg\,m^{-3}}$ and u_g is the velocity of the gas in $\mathrm{m\,s^{-1}}$.

The resistance coefficient ζ_0 depends on the geometric characteristics of the bundle of finned tube and the Reynolds number. This results in the following relation:

$$\zeta_0 = C_z'\cdot C_r\cdot\left(\frac{u_g\cdot d_{eq}}{v_g}\right)^{-n} \tag{4.47}$$

where C_z' and C_r are correction factors for the geometric characteristics and the remaining term represents the effect of the Reynolds number with exponent n. The exponent n and the coefficient C_r can be determined with the following equations:

$$n = 0.17\left(\frac{A_{total}}{F}\right)^{0.25}\left(\frac{S_1}{S_2}\right)^{0.57}\exp\left(-0.36\frac{S_1}{S_2}\right) \tag{4.48}$$

$$C_r = 2.8 \left(\frac{A_{total}}{F} \right)^{0.53} \left(\frac{S_1}{S_2} \right)^{1.30} \exp \left(-0.90 \frac{S_1}{S_2} \right) \tag{4.49}$$

where A_{total} is the total surface area of the outside of the tube in m^2, F is the frontal surface of the bundle which the air approaches, in m^2. S_1 is the transverse spacing of tubes in m and S_2 is the longitudinal spacing of tubes in m. To simplify the calculations presented above, the ratio A_{total}/F can be determined using the following equation:

$$\frac{A_{total}}{F} = \frac{\pi \left[d \cdot s_r + 2 \cdot l_r \cdot \delta_r + 2 \cdot l_r \cdot (l_r + d) \right]}{S_1 \cdot s_r - (d \cdot s_r + 2 \cdot l_r \cdot \delta_r)} \tag{4.50}$$

where d is the tube diameter in m, s_r is the fin spacing in m, l_r is fin height m, δ_r is the average fin thickness in m and S_1 is the transverse spacing of tubes in m. These parameters can also be found in Figure 4.9.

The diameter used for the Reynolds number in Equation 4.47 is the equivalent diameter of the most contracted cross-section of the bundle. It can be determined using the following equation:

$$d_{eq} = \frac{2 \left[s_r \left(S_1 - d \right) - 2 l_r \delta_r \right]}{2 l_r + s_r} \tag{4.51}$$

Lastly, the correction factor taking into account number of rows of the bundle needs to be determined. When the number of tubes in the direction of the gas flow (z_2) is smaller than 6, the following relation can be used:

$$C_z' = \exp \left(0.1 \left(\frac{6}{z_2} - 1 \right) \right) \tag{4.52}$$

When the the number of tubes in direction of the gas flow is larger dan 6, the correction factor taking into account the small number of rows in the bundle C_z' can be set to 1.

5

Component selection and design

A heat pump dryer consists of four major components: the compressor, the gas cooler, the evaporator and the dryer. To create a reliable and well-performing system, it is crucial that these components meet the thermodynamic requirements of the design. This chapter discusses the selection and design of the four main components of the cycle.

5.1. Compressor selection

The compressor is a crucial part of the heat pump cycle. Unlike heat exchangers, the compressor is not a component that can easily be customized. Therefore, the decision is made to first select the compressor for the system from existing compressors of suppliers. Based on this selection, the heat exchangers are designed. There are several important factors to consider when selecting a compressor. First of all, it must be compatible with the refrigerant. Furthermore, it must match the operating pressures and temperatures of the cycle. The mass flow rate must also be compatible with the rest of the cycle.

Section 3.4 shows that reciprocating and scroll compressors are most often used in high temperature heat pump application. Furthermore, the reciprocating compressor was identified as an appropriate choice for small-scale applications. After analysing various compressors in the required pressure and power range, Bitzer appeared to be a suitable supplier. The reciprocating compressor is chosen here, because besides the fact that Bitzer offers specific models for transcritical CO_2 cycles, this compressor is also a cheaper and more robust option for a relatively small installation. Additionally, it is more resistant to frequent starts and stops than the scroll compressor, and the scroll compressor is not able to achieve the required maximum pressure.

For the compressor, the reciprocating compressors of Bitzer are considered. These are categorized based on the type of refrigerant being used. Since the majority of the refrigerant consists of $\mathrm{CO_2}$ and the cycle is transcritical, compressors for transcritical $\mathrm{CO_2}$ were considered. The ECOLINE series has a maximum pressure of $160\,\mathrm{bar}$ on the high-pressure side and displacements ranging from $3.3\,\mathrm{m^3\,h^{-1}}$ to $38.2\,\mathrm{m^3\,h^{-1}}$, what makes this a suitable option for the application of the heat pump dryer [100].

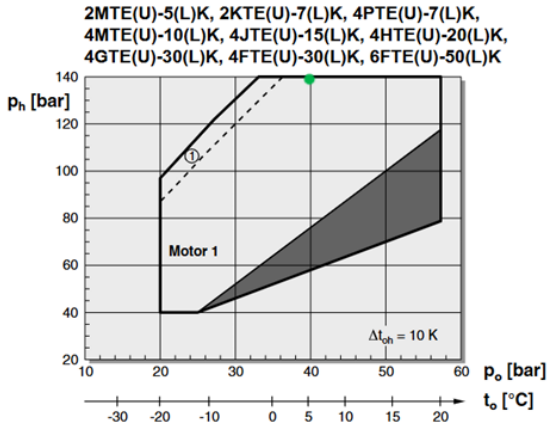

Figure 5.1: Application limit of the Bitzer compressors which can reach up to 140 bar. p_h is the high pressure, p_o the suction pressure, t_o the evaporating temperature in °C and ΔT_{oh} the suction superheat. The green dot is the operating point of the heat pump dryer application. [100]

In the ECOLINE series, there is only one group of compressors able to bring the pressure of the refrigerant up to $140\,\mathrm{bar}$. The application limit of this group of compressors can be found in Figure 5.1. This figure shows that the compressor is feasible to compress the refrigerant from 40 to $140\,\mathrm{bar}$. Based on similar experimental setups, discussed in chapter 3, the decision is made that the refrigerating capacity should be about the order of $10\,\mathrm{kW}$. Technical and performance data of the compressor is also given, which can be used to select a compressor from the list given in the graph. Subsequently, the 4PTE-7K proved to be the best match. This compressor has a displacement of $4.3\,\mathrm{m^3\,h^{-1}}$. An overview of the important performance data can be found in Table 5.1.

Table 5.1: Overview of technical and performance data of the 4PTE-7K compressor from Bitzer [100].

Compressor type	**4PTE-7K**
Maximum pressure	$140\,\mathrm{bar}$
Displacement at 50 Hz	$4.3\,\mathrm{m^3\,h^{-1}}$
Power consumption (t_o =5 °C)	$5.02\,\mathrm{kW}$

After selecting the compressor, several subsequent steps can be taken. First, the maximum pressure of both cycles is reduced to $130\,\mathrm{bar}$. This adjustment ensures that the compressor does not continuously operates at its maximum capacity and provides a margin to account for potential pressure drops within the system. The new T-s and Q-T diagram for this adjustment can be found in Figure 5.2 and Figure 5.3. In addition, the mass flow of the refrigerant mixture can be determined.

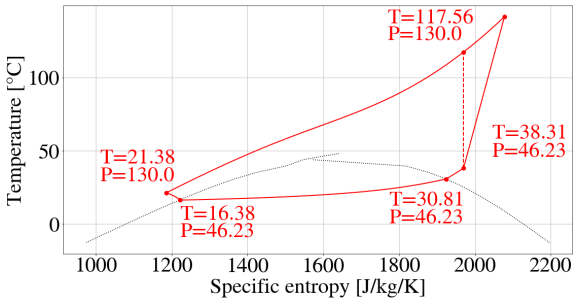

Figure 5.2: T-s diagram of the heat pump cycle of the refrigerant 90%$_{mol}$ CO_2-Isobutane. With the maximum pressure adjusted to $130\,\mathrm{bar}$

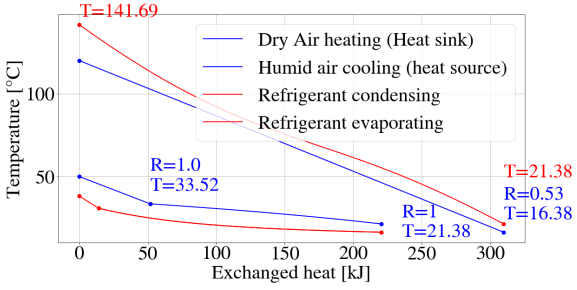

Figure 5.3: Q-T diagram of the heat pump cycle of the refrigerant 90%$_{mol}$ CO_2-Isobutane. With the maximum pressure adjusted to $130\,\mathrm{bar}$

5.2. Heat exchanger design

Once the compressor has been selected, the heat exchangers can be designed. Since the heat pump cycle is transcritical, there will be a gas cooler and an evaporator. Given that the heat exchangers are critical components in the heat pump cycle, as they determine the amount of heat transferred, special attention must be given to their geometry. This can then be used to give an estimation of the required heat transfer surface area, heat transfer and pressure drop. This section will start with the approach of the heat exchanger design. Subsequently, the design choices are explained, along with the model that was developed and applied for this purpose.

5.2.1. System requirements

Most of the initial specifications can be obtained from the optimal cycle, which is generated with the use of the python model. At this moment, there are two types of refrigerants that are considered to be tested in the setup. For the design of the heat exchangers it is practical to focus on one of these two. Since both mixtures must be capable of achieving the required heat transfer, the refrigerant mixture demanding the largest heat transfer surface area is selected for further analysis. When comparing the Q-T diagrams of both mixtures, it can be observed that the area between the lines of the refrigerant and the air is larger for the mixture containing isopentane, than for the mixture containing isobutane. This indicates, with support of LMTD calculations, that the 90$\%_{mol}$ CO_2-Isobutane mixture needs a higher surface area to achieve the required heat transfer. Therefore, the calculations for the heat exchanger designs will be executed using the properties of the 90$\%_{mol}$ CO_2-Isobutane mixture.

Table 5.2: System parameters of the gas cooler and evaporator for the 90$\%_{mol}$ CO_2-Isobutane refrigerant mixture.

	Gas cooler	**Evaporator**
Refrigerant		
Inlet temperature	$141.7\,^{\circ}\mathrm{C}$	$16.4\,^{\circ}\mathrm{C}$
Inlet pressure	$130.0\,\mathrm{bar}$	$46.23\,\mathrm{bar}$
Outlet temperature	$21.4\,^{\circ}\mathrm{C}$	$38.3\,^{\circ}\mathrm{C}$
Outlet pressure	$130.0\,\mathrm{bar}$	$46.23\,\mathrm{bar}$
Mass flow	$0.132\,\mathrm{kg\,s^{-1}}$	$0.132\,\mathrm{kg\,s^{-1}}$
Air		
Inlet temperature	$16.4\,^{\circ}\mathrm{C}$	$50.0\,^{\circ}\mathrm{C}$
Inlet pressure	$1.01\,\mathrm{bar}$	$1.01\,\mathrm{bar}$
Outlet temperature	$120.0\,^{\circ}\mathrm{C}$	$21.4\,^{\circ}\mathrm{C}$
Outlet pressure	$1.01\,\mathrm{bar}$	$1.01\,\mathrm{bar}$
Mass flow	$2.8\,\mathrm{kg\,s^{-1}}$	$2.8\,\mathrm{kg\,s^{-1}}$

5.2.2. Design choices

Based on the methods named in subsection 4.3.3 from chapter 4, choices were made for the design of the heat exchangers. First, a selection was made for the type of heat exchanger. An important factor in this decision is that heat needs to be exchanged with air, which is a challenging medium. For this primary reason, a finned tube heat exchanger was chosen. Additionally, this type is suitable for a relatively small system, has lower investment costs compared to other heat exchangers, and can be easily cleaned. The additional design choices made for the finned tube heat exchanger can be seen in Table 5.3. The measurements of the fin and tube parameters can be seen in Table 5.5.

Table 5.3: Choices made for the design of the finned tube heat exchanger.

Design choice	
Flow type	Cross-flow
Fin geometry	Circular
Fin thickness	Constant
Tube arrangement	Staggered

For the flow velocity in the heat exchanger the average of the density is taken, which results in an average flow velocity of $1.45\,\mathrm{m\,s^{-1}}$ for the gas cooler and $4.18\,\mathrm{m\,s^{-1}}$ for the evaporator.

In addition, a choice has been made for the materials. For similar heat pump applications, carbon steel and aluminium are often used. For the specific application of the heat pump dryer, however, carbon steel is not a feasible choice since is it susceptible to corrosion when exposed to oxygen and water. Therefore, stainless steel is a better option. The corrosion rate of stainless steel is approximately $0.0025\,\mu\mathrm{m\,y^{-1}}$, compared to the significantly higher rate of $1.3\,\mu\mathrm{m\,y^{-1}}$ to $25\,\mu\mathrm{m\,y^{-1}}$ of carbon steel [101] [102].

Although aluminium is also prone to corrosion, replacing it with another material would significantly reduce the fin efficiency. In Figure 5.4 the decrease of the overall heat transfer coefficient is shown when the conductivity of the fin material is decreased. The difference in conductivity of stainless steel and aluminium can be seen here. Therefore, the aluminium fins will be coated with a corrosion protection layer. In this way, the fins are keeping their thermal efficiency, while enhancing the corrosion resistance [103].

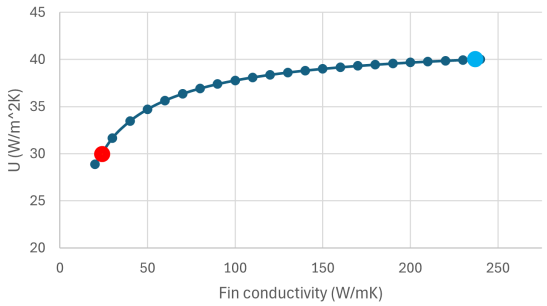

Figure 5.4: Effect of changing the fin conductivity on the overall heat transfer coefficient U. The red dot is the conductivity of stainless steel and the blue dot is the conductivity of aluminium.

5.2.3. Optimization of the final design

In the design of a heat exchanger, there are three key parameters that must be optimized: the overall heat transfer coefficient U, the total heat transfer surface area A and the pressure drop ΔP. In the design process, the objective is to achieve a high UA in combination with a low ΔP. In this way the heat transfer efficiency is maximized while minimizing the compressor's energy consumption. In Table 5.4, an overview is given of the geometry parameters that may be interesting while optimizing the heat exchangers. Here is taken into account that the air side is the primary limitation to the overall heat transfer. During the optimization process, the other parameters are kept constant. The air velocity is kept at $10\,\mathrm{m\,s^{-1}}$ and the properties of the air are kept constant at the values obtained form the optimised model.

Table 5.4: Geometry parameters that can be optimized.

Parameter	Optimisation
Fin height (l_r)	Higher fins means higher heat transfer surface area but also higher pressure drop on the air side. Higher pressure drop results in higher energy consumption of the fan.
Fin thickness (δ_r)	A thicker fin increases the conductivity, but can reduce the surface area per unit length.
Fin spacing (s_r)	Smaller distance between fins results in larger heat transfer surface area and a higher heat transfer coefficient, but also a significantly higher pressure drop. When the spacing is too small, this can also lead to fouling.
Tube diameter (d)	A smaller tube diameter increases the velocity of the medium within the tubes, which improves the heat transfer coefficient. However, this also increases the internal pressure drop and reduces the total heat transfer surface area.
Tube length (l_{rs})	A longer tube increases the surface area, but the pressure drop increases linearly with length.
Tube spacing (S_1, S_2)	A smaller distance results in a more compact design and greater heat transfer on the air side, but can also restrict airflow and increase pressure drop.
Air velocity (u_{air})	A higher air velocity leads to a higher heat transfer coefficient, but also an increase in the required power from the fan.
Refrigerant velocity (u_{ref})	An increase in refrigerant velocity leads to a higher pressure drop on the inside of the heat pump cycle. When the velocity is too low, this may lead to insufficient heat transfer.

For the parameters that showed a clear point of optimization, the results will be discussed. Starting with the tube spacing, S_1 and S_2. Since S_1 and S_2 have an effect on each other, a 3D graph is used to plot the effect of different dimensions. The results of this can be seen in Figure 5.5 and Figure 5.6. A clear peak can be seen at Figure 5.5 for a relatively small S_2 and a relatively larger S_1. Figure 5.6 shows that the variations in S_2 have a significantly smaller effect on the pressure drop compared to changes in S_1. When selecting the values for S_1 and S_2, values located at the peak were chosen.

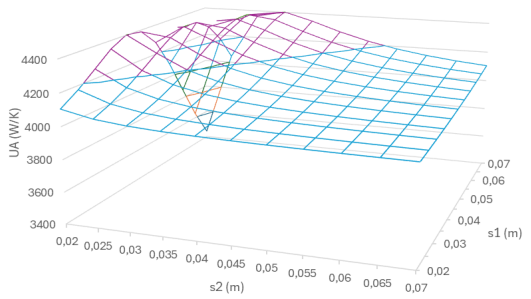

Figure 5.5: Representation of UA for different values of the tube spacings S_1 and S_2.

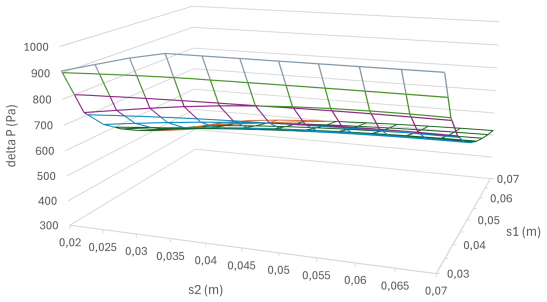

Figure 5.6: Representation of the outside pressure drop ΔP for different values of the tube spacings S_1 and S_2.

To clarify these graphs, an additional plot was created in which the results of the individual graphs are combined. This is shown in Figure 5.7. The optimum can be found in the upper left corner, where UA is maximized and ΔP is minimized.

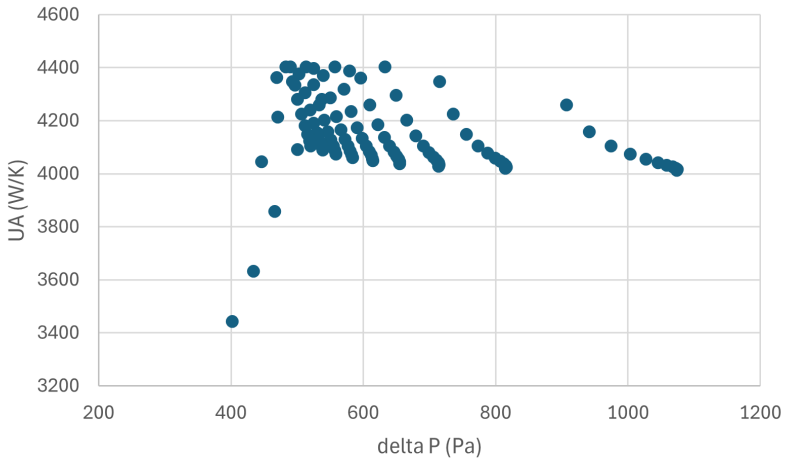

Figure 5.7: Combination of the values from Figure 5.5 and Figure 5.6, for different values of tube spacing.

In addition, the effect of fin spacing on heat transfer and pressure drop can be seen in Figure 5.8. Here it can be seen that there is optimization point in this graph. Therefore, UA is divided into the overall heat transfer coefficient and the heat transfer surface in Figure 5.9. In this graph, it can be seen that when fin spacing increases, the total surface area decreases, but the overall heat transfer coefficient increases. The decrease in A can be explained by the decrease in the number of fins per tube. In addition, several factors can play a role in the increase in U. The airflow is less disrupted between the fins, which, together with a drop in pressure, can ensure smoother airflow. Both result, up to a certain point, in an increase in the heat transfer coefficient of the air.

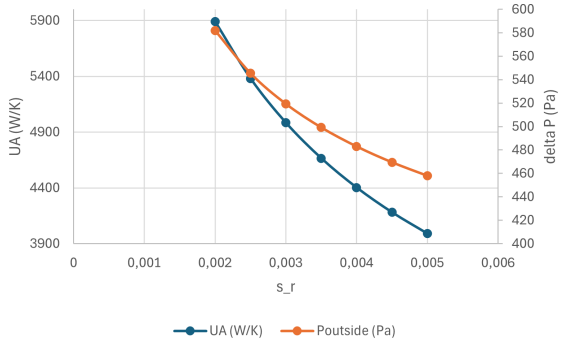

Figure 5.8: Representation of the outside pressure drop ΔP and UA for different values of the fin spacings S_r.

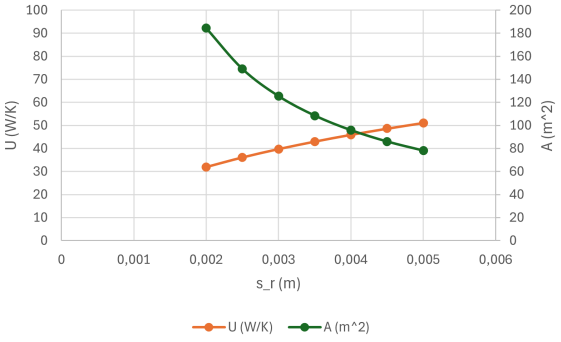

Figure 5.9: Representation of the overall heat transfer coefficient U and heat transfer surface A for different values of the fin spacings S_r.

Several steps were taken to arrive at the final design. Early in the process, it was observed that the refrigerant velocity in the evaporator was relatively low, falling below $1\,\mathrm{m\,s^{-1}}$. To increase this, the tube diameter was slightly reduced. However, this adjustment also required consideration of the resulting pressure drop, which increases as the tube diameter decreases. A greater challenge in optimizing the design is achieving the desired air velocity. Since the air mass flow is known and an optimal air velocity has been determined, the required maximum cross sectional surface area of the air duct can be calculated. This results in maximum dimensions in two directions for the heat exchanger, to be able to achieve the correct air velocity. This air velocity is selected by finding an optimum between the pressure drop and heat transfer coefficient. Since the gas cooler is the biggest challenge and is the component where the greatest amount of heat transfer occurs, the surface area was determined here first. With an air velocity of $10\,\mathrm{m\,s^{-1}}$, this resulted in a maximum surface area of $0.271\,\mathrm{m^2}$. The challenge here lies in keeping the heat exchanger compact and the pressure drop low. To avoid exceeding the maximum

surface area and to keep the heat exchanger compact, the tubes must be shortened. This requires more bends to achieve the required heat transfer, which increases the pressure drop.

5.2.4. Final design

Finally, both a gas cooler and evaporator were designed. Both are meeting the required heat transfer performance, the pressure drop remains within a few percent, and the required mass flow of the air can be achieved. An overview of the dimensions of these heat exchangers can be found in Table 5.5. In Solidworks, a simplified image is created for both heat exchangers, without the bends. These can be found in Figure 5.11 and Figure 5.12. In Figure 5.10, a representation is given of the path of the refrigerant and air flow.

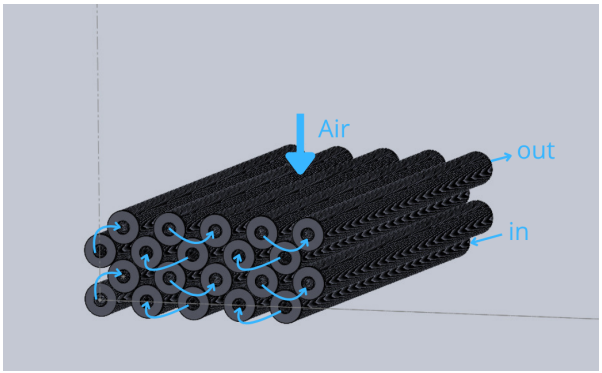

Figure 5.10: Representation of the refrigerant path inside the heat exchanger and of the airflow over the tube bundle.

Table 5.5: Geometry parameters of the gas cooler and evaporator.

		Gas cooler	**Evaporator**
d	Tube diameter	19.1 mm	19.1 mm
d_{int}	Tube inner diameter	17.1 mm	17.1 mm
D	Fin diameter	48.1 mm	48.1 mm
δ_t	Tube wall thickness	1.0 mm	1.0 mm
δ_r	Fin thickness	1.0 mm	1.0 mm
s_r	Fin spacing	3.0 mm	3.0 mm
L_r	Fin height	14.5 mm	14.5 mm
S_1	Tube spacing	70 mm	70 mm
S_2	Tube spacing	35 mm	35 mm
L_{rs}	Tube length	720 mm	720 mm
z	Number of tubes	160	40
z_1	Number of tubes	10	10
z_2	Number of tubes	16	4
W	Width	363 mm	363 mm
H	Height	573 mm	153 mm

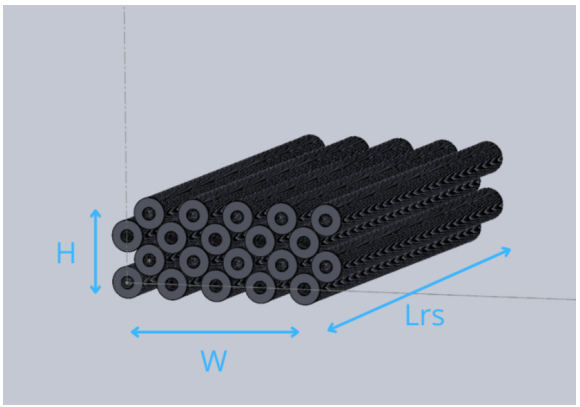

Figure 5.11: Visual representation of the design of the evaporator.

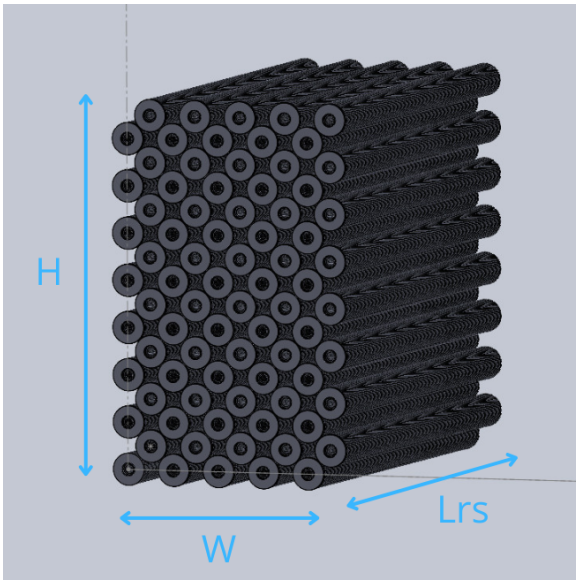

Figure 5.12: Visual representation of the design of the gas cooler.

5.3. Dryer section design

The main focus of the experimental heat pump dryer set up will be the heat pump cycle. Despite the absence of an actual dryer, a design for a dryer will be made to establish a representative setup. This will be achieved by creating an environment where the relative humidity of the air is increased and its temperature reduced, through the injection of water. To be able to develop a representative setup, it is essential to understand the evaporation process of water and make an estimation of the time required for the water to fully evaporate. In addition, the duct in which this process takes place will be designed, and a suitable method for adding water to the air will be selected. Lastly, a fan needs to be selected to ensure the supply of air.

5.3.1. Estimation of the dryer length

The evaporation of a water droplet in an air stream is described in Mills [19]. The droplet evaporates because water molecules at its surface transition into the vapour phase. Consequently, mass transfer occurs from the droplet surface to the surrounding air. This process requires energy in the form of latent heat of vaporization, which must be transported from the air to the droplet surface. An overview of this process can be seen in Figure 5.13. The time required for the droplet to evaporate therefore depends on the effects of mass and heat transfer combined.

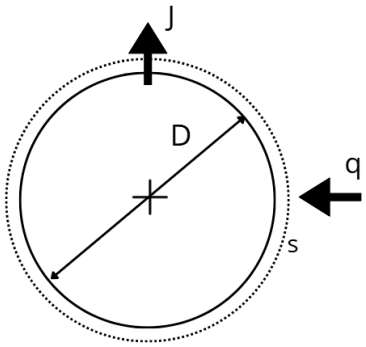

Figure 5.13: A visual representation of the evaporation of the droplet, where J is the diffusion, and q the heat transfer to the droplet. s is assumed to be a thin layer, representing the surface layer.

First, several assumptions are made, such as that the droplet reaches a constant surface temperature after a short transient period. In addition radiative heat transfer is neglected, and it is further assumed that the droplet is fully entrained in the airflow. With the use of the mass transfer process and Fick's law, the evaporation rate in $\mathrm{kg\,s^{-1}}$ can be determined with the use of the surface area of the sphere.

The analysis begins with the mass transfer process. Water vapour diffuses into the surrounding air with a flux $j_{1,s}$ in $\mathrm{kg\,m^{-2}\,s^{-1}}$. According to Fick's law, this is proportional to the concentration difference between the droplet surface and the surrounding air. This gives the following equation:

$$\dot{m} = j_{1,s}A = g_{m,1}\left(m_{1,s} - m_{1,e}\right)A \tag{5.1}$$

where g_{m1} is the locally averaged mass transfer conductance in $\mathrm{kg\,m^{-2}\,s^{-1}}$, $m_{1,s}$ the mass fraction of water vapour at the surface and $m_{1,e}$ the mass fraction of water vapour in the air stream. The surface area of the sphere is $A = \pi D^2$. The value of $g_{m,1}$ depends on the Sherwood number (Sh), which characterizes the diffusion and flow around the droplet. Given the assumption that the droplet is completely entrained in the airflow, the molecular diffusion around the sphere is purely laminar, and thus $Sh \approx 2$. Using this value gives the following expression:

$$Sh = \frac{g_{m1}D}{\rho\mathcal{D}_{12}} \approx 2 \rightarrow g_{m1} = \frac{2\rho\mathcal{D}_{12}}{D} \tag{5.2}$$

where D is the diameter of the droplet in m, ρ the density of water in $\mathrm{kg\,m^{-3}}$ and $\mathcal{D}_{12}$ the diffusion coefficient in $\mathrm{m^2\,s^{-1}}$. The total decrease in mass of the droplet due to evaporation will therefore look like the following:

$$\dot{m}_1 = \frac{2\rho\mathcal{D}_{12}A}{D}\left(m_{1,s} - m_{1,e}\right) \tag{5.3}$$

Next, the mass balance of the droplet can be calculated. The loss of the droplet's mass should be equal to the evaporation rate:

$$\frac{d}{dt}\left(\frac{1}{6}\pi D^3\rho_l\right) = -j_{1,s}A \tag{5.4}$$

By substituting the surface area A and applying differentiation, the expression can be rewritten as follows:

$$\frac{dD}{dt} = -\frac{4\rho\mathcal{D}_{12}\left(m_{1,s} - m_{1,e}\right)}{D\rho_l} \tag{5.5}$$

By applying integration, the droplet lifetime (τ) can be determined:

$$\tau = \frac{\rho_l D_0^2}{8\rho\mathcal{D}_{12}\left(m_{1,s} - m_{1,e}\right)} \tag{5.6}$$

The mass fractions in the equation above can be calculated with the equations given in subsection 2.2.1. The relation between the droplet diameter and its evaporation time is shown in Figure 5.14. The graph shows that the evaporation time increases sharply with diameter. This curvature of the graph indicates that evaporation time does not scale linearly with the diameter.

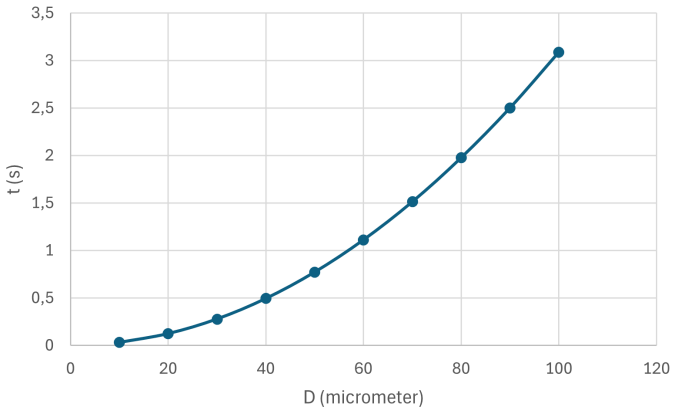

Figure 5.14: Relation between the droplet diameter and the evaporation time of the droplet.

Assuming the diameter of a water droplet is $30\,\mu\mathrm{m}$ with the use of Figure 5.15, this results in a lifetime of $0.278\,\mathrm{s}$. Together with the air velocity of $10\,\mathrm{m\,s^{-1}}$, this gives a minimum length of $2.78\,\mathrm{m}$. This length can be shortened by adjusted the frontal surface area of the air flow. In the duct, conservation of mass applies. For example, when the duct is brought to $0.8 \times 0.8\,\mathrm{m}$, the air velocity reduces to $4.2\,\mathrm{m\,s^{-1}}$ and therefore the length can be reduced to $1.2\,\mathrm{m}$.

5.3.2. Nozzle selection

The injection of water into the airflow is an essential part of the dryer. A nozzle is selected to inject the water into the airflow. Since a nozzle divides the water stream into droplets, it provides a larger contact surface are between the water and the airflow. Thereby, it reduces the time required for the water droplets to evaporate completely. Moreover, smaller droplets result in faster evaporation rates.

There are different types of nozzles, each producing different spray characteristics. They can be classified into two main categories: hydraulic nozzles and air atomising nozzles. Air-atomizing nozzles use pressurized air to break the liquid into a fine spray, whereas hydraulic nozzles rely on the internal energy of the fluid to generate the desired spray pattern. The hydraulic nozzle is considered the most suitable option for this application with the dryer, as it does not require an additional source of compressed air [104]. With compressed air, extra air is being added to the system.

Since the humidity of the air needs to increase in the dryer, it is important for the nozzle selection in this application for the droplets to have a small diameter. In this way the droplets evaporates faster and therefore increase the humidity of the air. In Figure 5.15 can be seen which droplet diameter is produced by which type of nozzle. The hydraulic nozzle with the smallest droplets is the misting nozzle, which therefore will be used in the dryer.

When the nozzle creates droplets, not every droplet will have exactly the same size. In spray technology, this distribution is often characterized using the Sauter Mean Diameter (SMD), which represents the statistical distribution of droplet diameters. Higher spraying pressures generally produce smaller droplets. For mists, the SMD typically ranges between 30 and $60\,\mu\mathrm{m}$. To determine the exact value, laboratory measurements can be performed, for example using laser diffraction or high speed imaging.

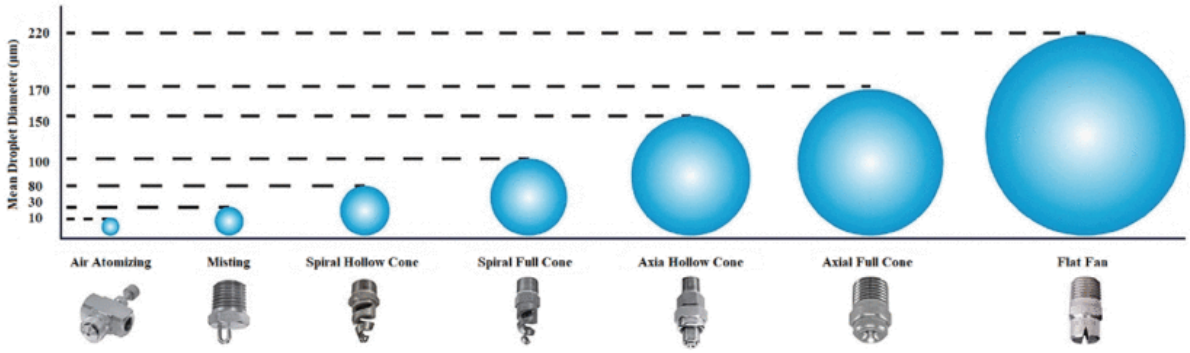

Figure 5.15: Overview of different types of nozzles with diameters of the generated droplets. [105]

Using the given heat pump cycle, the required mass flow of the water can be determined. The humidity ratio of the air is known at the inlet and the outlet of the dryer. With use of conservation of mass, the following equation can be determined:

$$m_w = m_a \cdot (\omega_2 - \omega_1) \tag{5.7}$$

where m_v is the mass flow of the water and m_a the mass flow of the air, both in $\mathrm{kg\,s^{-1}}$. ω_1 and ω_2 are the humidity ratio's at the inlet and outlet of the dryer simulation, in kg_{water}/kg_{dryair}.

The results of the calculation of the mass flow of water are shown in Table 5.6. This resulted in a required volume flow of water of $4.78\,\mathrm{L\,min^{-1}}$ for the nozzle to supply.

Table 5.6: Overview of the calculation results for the dryer.

Quantity	Value
Humidity ratio inlet	$0.0061\,\mathrm{kg\,kg^{-1}}$
Humidity ratio outlet	$0.0337\,\mathrm{kg\,kg^{-1}}$
Mass flow water	$0.0276\,\mathrm{kg\,s^{-1}}$
Volume flow water	$4.78\,\mathrm{L\,min^{-1}}$

5.3.3. Fan selection

To be able to achieve the required air velocity by the heat exchangers and in the dryer, a fan is required. First, the type of fan needs to be selected. A chart as shown in Figure 5.16 can be utilized to support this decision.

With the use of the head coefficient (ψ) and the flow coefficient (ϕ), it can be determined whether a radial or an axial fan is most appropriate for the design. Axial fans are generally more suitable for flow conditions characterized by high volumetric flow rates and low pressure drops. In contrast, a radial fan is the preferred option when the pressure differences are relatively high. The transition between the operating ranges of axial and radial fans generally occurs at the pressure difference of around $450\,\mathrm{Pa}$ [106]. The pressure difference in the application of the dryer will be around $1000\,\mathrm{Pa}$. This consists of the pressure drop along the length of the air duct, across the heat exchangers, and through the bends that are introduced due to the use of the radial fan.

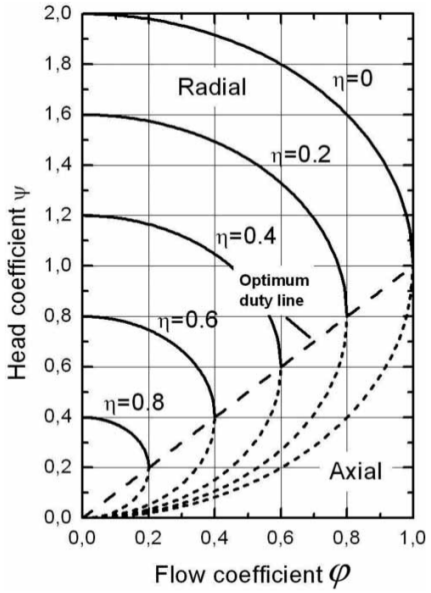

Figure 5.16: Graph showing the relationship between the flow coefficient and the head coefficient for turbomachinery. [107]

Table 5.7: An overview of the parameters required for the selection of a suitable fan.

Quantity	Value
Surface area air ($Lrs \times W$)	0.363×0.740 m = $0.269\,\mathrm{m}^2$
Air velocity	$10\,\mathrm{m\,s^{-1}}$
Mass flow air	$2.8\,\mathrm{kg\,s^{-1}}$
Air density	$1.034\,\mathrm{kg\,m^{-3}}$
Pressure drop over heat exchangers	$786\,\mathrm{Pa}$
Estimation total pressure drop	$1000\,\mathrm{Pa}$
Volume flow	$2.71\,\mathrm{m^3\,s^{-1}}$

Prior to making a selection, an estimation of the heat coefficient (ψ) and flow coefficient (ϕ) must be made using Equation 5.9 and Equation 5.10. The relevant data for this calculation, obtained from the heat pump dryer, are listed in Table 5.7. Furthermore, the pump head (H) can be determined from Equation 5.8. To maintain the efficiency of the cycle, a single fan is incorporated into the system, positioned downstream of the inlet of the duct, and upstream of the gas cooler. Due to this placement, there is more control over the incoming air, since not everything is drawn in. Additionally, fewer losses occur along the suction length. In this configuration, an overpressure is generated inside the duct. This expected pressure drop can be found in the equations as Δp. Additionally, N is the rotational speed and D the diameter of the fan.

$$H = \frac{\Delta p}{\rho \cdot g} \tag{5.8}$$

$$\psi = \frac{gH}{N^2 D^2} \tag{5.9}$$

$$\phi = \frac{Q}{N D^3} \tag{5.10}$$

The pressure drop presented in Table 5.7 represents the contribution of both the heat exchangers located in the air duct. However, as additional components in the duct are expected to cause further

pressure losses, the total pressure drop is estimated to be $1000\,\mathrm{Pa}$. Based on this assumption, the head coefficient and flow coefficient are calculated as 1.18 and 0.72, respectively. When these values are compared with Figure 5.16, while also taking into account the pressure boundary of Pa, it can be concluded that a radial fan appears to be the most appropriate choice for this situation. The required shaft power of the fan can then be determined as follows:

$$P_w = \frac{Q \cdot \Delta p}{\eta_w} \tag{5.11}$$

where Δp is the expected pressure drop in the system in Pa, Q is the volume flow in $\mathrm{m^3\,s^{-1}}$, the power P_w is in W and η is the efficiency of the fan. When the efficiency of the motor is also taken intro account, the expected electrical power consumption can be estimated. The efficiency of the fan is assumed to be 0.5 and the efficiency of the motor is assumed to be 0.95. With the estimation of a pressure dorp of $1000\,\mathrm{Pa}$, this leads to an estimated electrical power demand of $5.71\,\mathrm{kW}$.

When this situation is compared with fans available on the market, the results show good agreement. For suppliers such as Reitz Group or Slingerland Techniek, the calculated operating conditions lie well within the range of products offered [108] [109]. For the remainder of the design process, the MXE 010-016018 fan supplied by Reitz Group will therefore be used, as it represents the most suitable choice for the given operating conditions.

6

Off design performance analysis

To evaluate the robustness and performance of the heat pump dryer setup, a sensitivity analysis was carried out. The aim of this analysis is to determine the extent to which variations in the process and design parameters affect the performance of the system. The primary focus lies on the coefficient of performance (COP) and the factors that influence it, such as the pressure drop and the heat transfer coefficients. The coefficient of performance says something about the entire system, since factors like the power of the fan is also included. In this analysis, four different aspects are varied:

- The relationship between the air velocity along the heat exchangers and the COP of the system.
- Variations in the inlet conditions of the air entering the gas cooler, including temperature and humidity.
- Variations in the outlet conditions of the air from the dryer, including temperature.
- The use of different refrigerants.

These parameters were selected based on their expected impact on the efficiency of the heat pump dryer. The results of the analyses are discussed individually in this chapter. During the analyses, all other parameters than those explicitly varied were kept constant at the previously assumed values.

6.1. Relationship between air velocity and COP

The air velocity on the external side of the heat exchangers influences the convective heat transfer coefficient of both the gas cooler and the evaporator. In this analysis, the air velocity is varied from 1 to $12\,\mathrm{m\,s^{-1}}$. The resulting effect on the heat transfer coefficient and the pressure drop of both heat exchangers is shown in Figure 6.1. The corresponding impact on the COP of the entire system is presented in Figure 6.2.

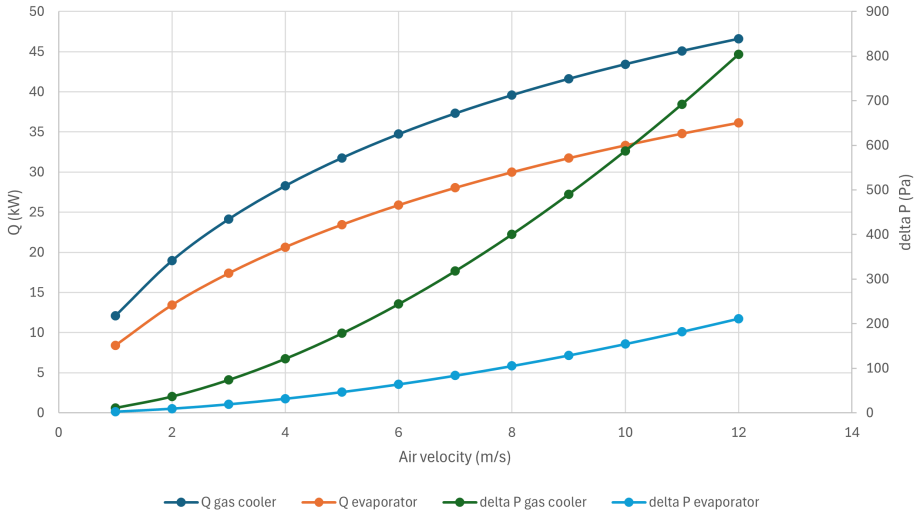

Figure 6.1: The effect of the change of in air velocity on the heat transfer and pressure drop in both heat exchangers.

At relatively lower air speeds, the heat transfer coefficient increases with increasing air speed, resulting in lower thermal resistance for both HEX in the heat pump cycle. As the air velocity increases, these improvements diminish. When air velocity increase, the pressure drop also increases. For the gas cooler, the larger increase in pressure drop can be explained by the fact that a significantly greater number of tubes are positioned in series relative to the airflow direction, resulting in a higher accumulated pressure drop.

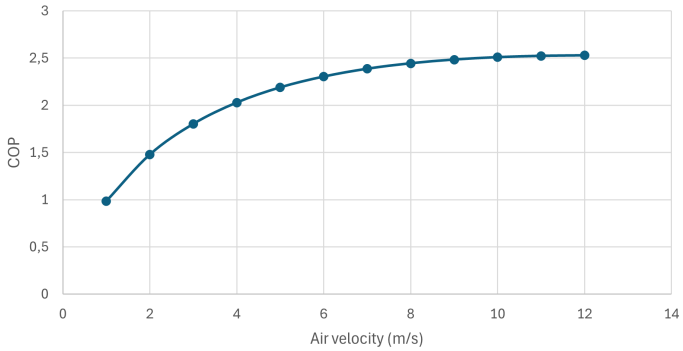

Figure 6.2: The effect of the change in air velocity at the heat exchangers on the COP of the total system.

The fan power increases quadratically with the air velocity, which in practice should result in an optimal operating point. A high velocity should result in a higher COP when considering only the heat pump cycle, but it does not result in higher efficiency of the overall system. Since the power of the fan is included in the COP in Figure 6.2, the increase of COP stagnates. The graph also shows that the COP is particularly sensitive at low air velocities, while the improvements diminishes as the air velocity increases.

In Figure 6.3 the impact of the power of the fan on the COP of the heat pump dryer can be seen. This figure shows a trend similar to Figure 6.2. In both graphs there can be seen that there is an optimal operating point for the fan. For the designed heat exchangers, this is in the range of 7 to $10\,\mathrm{m\,s^{-1}}$.

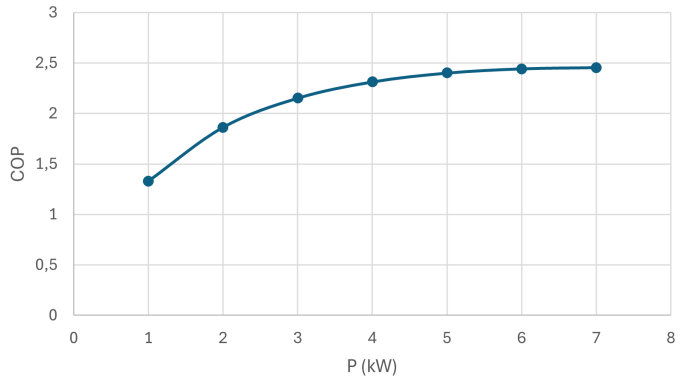

Figure 6.3: The effect of the change in fan power on the COP of the total system.

6.2. Variations in inlet air conditions

The inlet conditions of the air determine the amount of heat transfer required to bring the air to the correct conditions for the dryer. Variations in these conditions can therefore primarily affect the heat transfer of the gas cooler and also the compressor. For this reason, the inlet air conditions are expected to influence the COP of the heat pump dryer.

Changes in humidity

The relative humidity of the air entering the system is variated from 60% to 90%. A lower humidity than this is not possible while keeping the air inlet temperature constant at $10\,^{\circ}\mathrm{C}$. The results are shown in Figure 6.4. In the graph it can be seen that a higher humidity is resulting in a lower heat transfer in the gas cooler. This is because the properties of the air mixture change due to the higher vapour content, which can negatively impact the heat transfer coefficient. This results in lower heat transfer, and therefore a lower COP. The impact of the change in humidity is less significant than that of the temperature, but an effect is still visible.

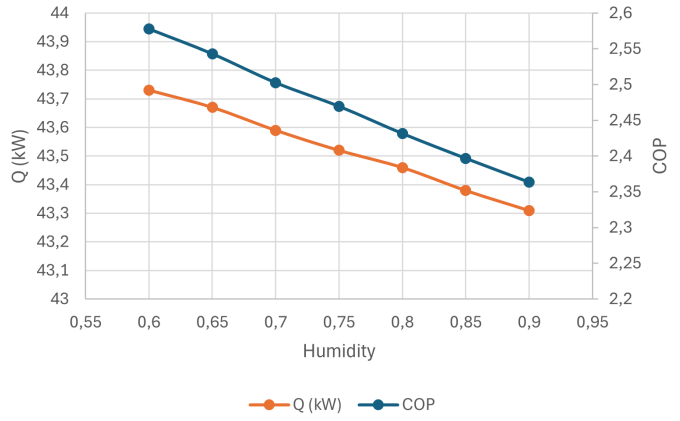

Figure 6.4: Effect of the variation of the inlet air humidity on the heat transfer in the gas cooler and the COP of the heat pump dryer.

Changes in temperature

The inlet air temperature was varied from $5\,^{\circ}\mathrm{C}$ to $25\,^{\circ}\mathrm{C}$, representing possible ambient conditions. The model produced errors when this variation was performed at a relative humidity of 0.8%, so the analysis was carried out at a slightly lower humidity of 0.7%. The errors occurred because REFPROP was unable to provide results under those conditions, since the relative humidity was too high for especially the higher temperatures. The results are shown in Figure 6.5.

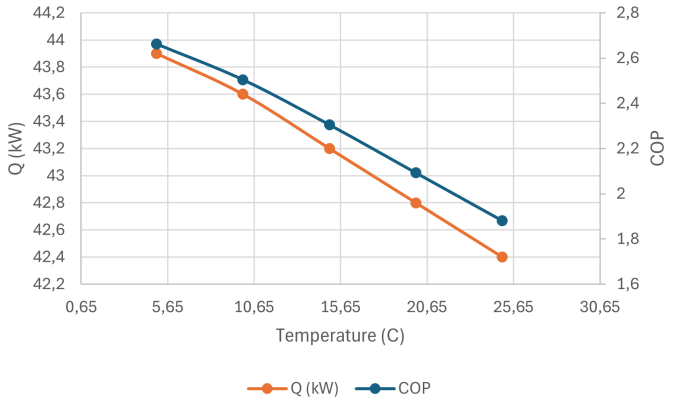

Figure 6.5: Effect of the variation of the inlet air temperature on the heat transfer in the gas cooler and the COP of the heat pump dryer.

The graphs shows that changes in temperature have a stronger effect on the efficiency of the system than changes in humidity. When the inlet air temperature is higher when entering the gas cooler, the temperature difference between the air and the refrigerant decreases, which reduces the heat transfer coefficient. As a result, the total heat transfer in the gas cooler decreases, leading to a reduction of the COP. In addition, the required compressor power increases due to the smaller temperature difference between the air and the refrigerant, which further contributes to the drop in COP. The increase in compressor power is caused by a decrease in the enthalpy at the inlet and an increase in the enthalpy at the outlet of the compressor, due to the temperature changes in the heat exchangers.

6.3. Variations in dryer outlet conditions

The conditions of the air exiting the dryer and heading towards the evaporator significantly affects the heat transfer in the evaporator. This air contains residual heat and moisture from the dryer, which influences the latent and sensible heat. In this analysis, the air temperature is varied so that the effect can be observed. The other conditions are kept constant.

The air temperature from the dryer outlet varies between 40 and $60\,^{\circ}\mathrm{C}$. The result of this can be seen in Figure 6.6. In general, the following applies to this situation: the higher the air temperature, the higher the heat transfer. On the left side of the graph, a deviant drop is visible. In Figure 6.7, it can be seen that this is due to the LMTD, which drops when increasing the temperature from $40\,^{\circ}\mathrm{C}$ to $45\,^{\circ}\mathrm{C}$.

The point at $40\,^{\circ}\mathrm{C}$ was expected to have a lower LMTD. This is caused by the shift in the dew point temperature. This point can be seen in the Q-T diagram in Figure 5.3, where it is represented by the blue point on the lower blue line. By changing the dryer outlet air temperature, this points shifts. At a dryer outlet temperature of $40\,^{\circ}\mathrm{C}$, this point is located far to the left. As a results, despite the graph being divided into different segments, the LMTD ends up being higher. When varying the outlet air temperature of the dryer, the COP remains nearly constant.

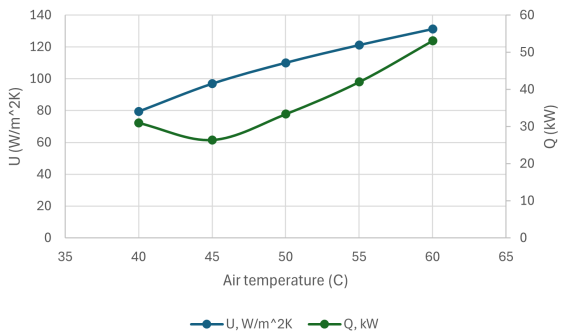

Figure 6.6: Effect of the variation of the air temperature from the dryer on the heat transfer in the evaporator.

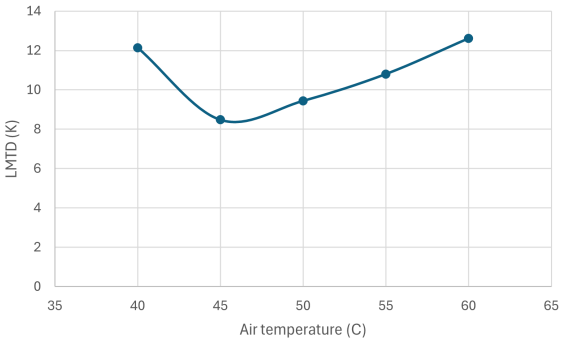

Figure 6.7: Effect of the variation of the air temperature from the dryer on the LMTD.

6.4. The use of different refrigerants

The refrigerant directly influences many different aspects of the heat pump cycle. When changing the refrigerant mixture, this has significant impact on, among other things, the critical properties, the gliding temperature, and the pressure levels, and thus the overall safety of the heat pump.

While designing the setup, the refrigerant mixture of $90\%_{mol}$ CO_2-Isobutane is used for the calculations, as it required the largest heat exchanger surface area. Since the plan was to be able to test multiple refrigerants in the setup, in this analysis the refrigerant mixture is changed to $87.5\%_{mol}$ CO_2-Isopentane. This allows for the examination of how the performance indicators of the system change when the refrigerant is altered. For this purpose, the model was updated with the refrigerant $87.5\%_{mol}$ CO_2-Isopentane and the dryer outlet temperature was set to $80\,^{\circ}\mathrm{C}$.

The optimized cycle from the previous study was used in the model, while the heat exchangers in the designed setup have a much larger surface area than required according to the optimum cycle. This combination leads to an unreliable result for the compressor power of the $87.5\%_{mol}$ CO_2-Isopentane mixture, and consequently an unrealistically high COP of 9.16. To obtain a more realistic estimate of the COP, a separate energy balance was created for the cycle with $87.5\%_{mol}$ CO_2-Isopentane. The results of this analysis are presented in Table 6.1. To be able to obtain a more reliable COP value, a new model must be developed in which the complete cycle for the $87.5\%_{mol}$ CO_2-Isopentane mixture is calculated.

Table 6.1: Overview the analysis of 87.5$\%_{mol}$ CO_2-Isopentane in the heat pump dryer setup.

	87.5$\%_{mol}$ CO_2-Isopentane	**90$\%_{mol}$ CO_2-Isobutane**
Gas cooler		
$T_{\text{inlet air}}$	$15.0\,^{\circ}\text{C}$	$15.0\,^{\circ}\text{C}$
$T_{\text{outlet air}}$	$120.0\,^{\circ}\text{C}$	$120.0\,^{\circ}\text{C}$
$T_{\text{inlet ref}}$	$187.1\,^{\circ}\text{C}$	$141.7\,^{\circ}\text{C}$
$T_{\text{outlet ref}}$	$20.0\,^{\circ}\text{C}$	$21.2\,^{\circ}\text{C}$
$LMTD$	$29.6\,\text{K}$	$8.6\,\text{K}$
U	$35.39\,\text{W}\,\text{m}^{-2}\,\text{K}^{-1}$	$39.22\,\text{W}\,\text{m}^{-2}\,\text{K}^{-1}$
Q	$134.4\,\text{kW}$	$43.45\,\text{kW}$
$\Delta P_{\text{outside}}$	$588\,\text{Pa}$	$588\,\text{Pa}$
ΔP_{inside}	$213\,452\,\text{Pa}$	$399\,862\,\text{Pa}$
Evaporator		
$T_{\text{inlet air}}$	$80.0\,^{\circ}\text{C}$	$50.0\,^{\circ}\text{C}$
$T_{\text{outlet air}}$	$20.0\,^{\circ}\text{C}$	$21.4\,^{\circ}\text{C}$
$T_{\text{inlet ref}}$	$10.8\,^{\circ}\text{C}$	$16.4\,^{\circ}\text{C}$
$T_{\text{outlet ref}}$	$75.0\,^{\circ}\text{C}$	$38.3\,^{\circ}\text{C}$
$LMTD$	$13.8\,\text{K}$	$9.4\,\text{K}$
U	$131.69\,\text{W}\,\text{m}^{-2}\,\text{K}^{-1}$	$110.04\,\text{W}\,\text{m}^{-2}\,\text{K}^{-1}$
Q	$58.3\,\text{kW}$	$33.33\,\text{kW}$
$\Delta P_{\text{outside}}$	$151\,\text{Pa}$	$155\,\text{Pa}$
ΔP_{inside}	$2517\,\text{Pa}$	$3437\,\text{Pa}$
Compressor		
W_{in}	$76.1\,\text{kW}$	$12.27\,\text{kW}$
Overall		
P_{fan}	$5.61\,\text{kW}$	$5.61\,\text{kW}$
COP_{hp}	1.77	3.55
COP_{dryer}	1.65	2.43

The results in the table show that changing the refrigerant has a significant impact on the behaviour of the heat pump cycle. In the gas cooler, a significant increase in heat transfer can be observed, which is associated with the higher LMTD. The temperature difference between the refrigerant and the air is larger, resulting in more efficient heat transfer. Another notable change is the decrease in pressure on the refrigerant side. This occurs due to the decrease in velocity of the isopentane mixture, because of the reduced mass flow rate. The volumetric flow rate is fixed by the compressor, and therefore this is a consequence of the change in refrigerant density. The pressure drop on the air side remains nearly the same, as the air velocity and the heat exchanger geometry remain unchanged.

In the evaporator, similar increases and decreases can be observed. However, the relative increase in heat transfer is smaller, which already indicated that the COP will decrease. This can also be seen at the compressor power. For the 87.5$\%_{mol}$ CO_2-Isopentane mixture, the compressor must deliver significantly more power. As a result, a different compressor may be required when testing the mixture containing isopentane.

The power consumption of the fan remains unchanged, as the air velocity is kept constant and the changes in pressure drop on the air side of the heat exchangers are negligibly small. Considering the decrease in COP of the entire dryer system from 2.43 to 1.65 when switching from the 90$\%_{mol}$ CO_2-Isobutane mixture to the 87.5$\%_{mol}$ CO_2-Isopentane mixture, it can be concluded that using the isobutane mixture results in the most efficient cycle. To optimize the cycle for the isopentane mixture, attention must therefore be directed toward the compressor.

7

Final design

In this chapter, the final design of the experimental heat pump dryer setup is presented. In addition to integrating all the main components, this section also addresses other important aspects such as safety considerations, instrumentation and the procedure for changing the refrigerant.

7.1. Total design

The systems consists of a heat pump cycle connected to a dryer. A piping and instrumentation diagram (P&ID) of the system can be found in Figure 7.1. A P&ID is a commonly used in the engineering field and show the piping and related components of the physical process flow. It differs from a process flow diagram in that it provides greater detail, including for example instrumentation and safety requirements.

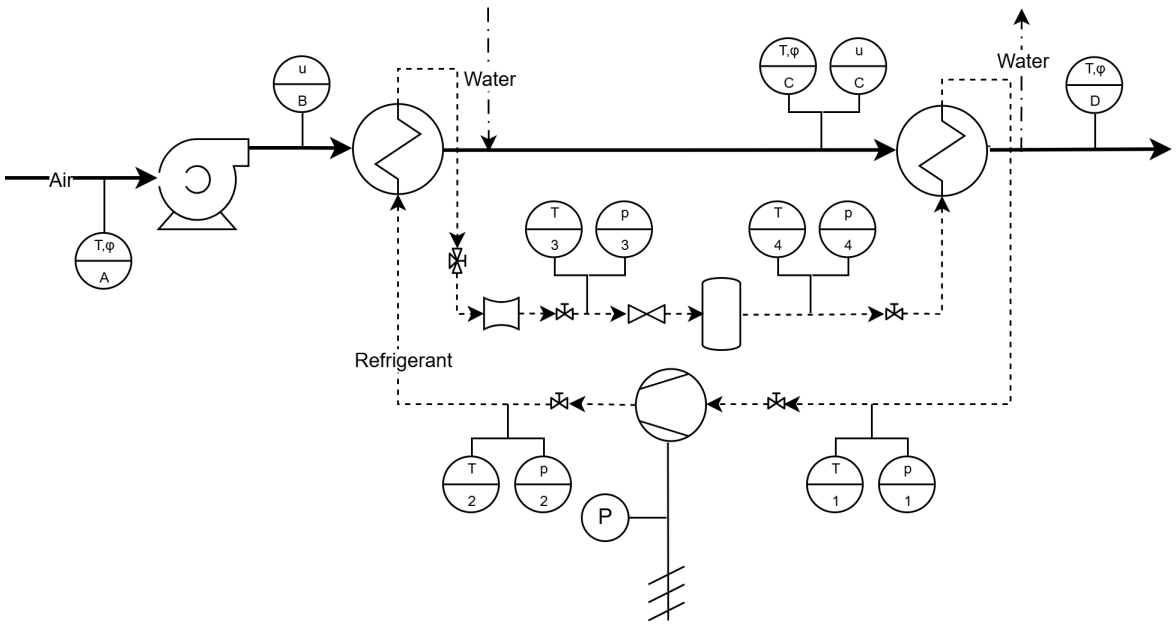

Figure 7.1: Piping and Instrumentation Diagram of the heat pump dryer set up.

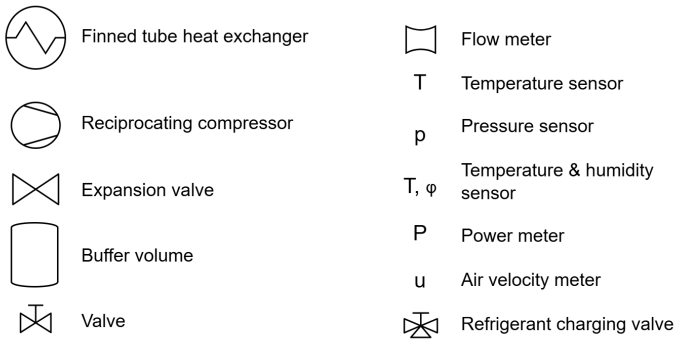

Figure 7.2: Legend of the Piping and Instrumentation Diagram.

All the main components are added in the cycle as they were discussed in chapter 5. First, the heat pump cycle is considered. To complete the cycle, a component is required to reduce the pressure of the refrigerant, after the gas cooler. As discussed in section 3.5, this is typically done with the use of a capillary tube or an expansion valve. While the capillary tube is the most cost effective and simplest option, it is not optimal in this application. Capillary tubes are specifically designed for the behaviour of a refrigerant, and since multiple refrigerants will be tested in this setup, this option lacks flexibility. Consequently, the choice must be made between a thermostatic or an electronic expansion valve. The electronic expansion valve is the most suitable option for this applications, since it offers a high regulation accuracy, a large flow rate adjustment range and a high generality. The only disadvantage is that electronic expansion valves are more expensive than thermostatic expansion valves. Additionally, a buffer volume is added to the cycle, between the expansion valve and the evaporator. This is often added to cycles to dampen pressure and temperature fluctuations within the cycle, which results form variations in load and dynamic conditions [110]. In experimental applications, such fluctuations are common, so it is beneficial to include a buffer volume to protect the cycle. This allows gas from the outlet of the evaporator to flow into the buffer.

Table 7.1: Overview of the required main equipment of the heat pump dryer.

Device	**Specifications**
Compressor	Reciprocating compressor Bitzer transcritical Ecoline series (4PTE-7K) Maximum pressure: $140\,\mathrm{bar}$ Displacement: $4.3\,\mathrm{m^3\,h^{-1}}$
Expansion valve	Electronic expansion valve High pressure: $130\,\mathrm{bar}$ Low pressure: $40\,\mathrm{bar}$
Fan	Radial fan Reitz Group MXE 010-016018 Mass flow: $2.8\,\mathrm{kg\,s^{-1}}$
Heat exchangers	Finned tube heat exchangers Measurements: Table 5.5 Materials: stainless steel tube with treated aluminium fins
Nozzles	Misting nozzle

In Table 7.1 an overview is provided of all the main components used in the design, including the required specifications. In addition to these components, an air duct is needed to construct the dryer system, and piping is required to connect all heat pump components to each other.

7.2. Instrumentation

To ensure that the heat pump cycle operates as expected, to guarantee safety and to determine the efficiency, sensors are required within the cycle to monitor key parameters such as the pressure and temperature. To be able to make a selection of suitable instrumentation for this application, comparable applications of heat pumps are compared and the specific values required for determining system efficiency are considered. This is followed by Table 7.2 in which all the required measurement equipment is presented, along with the necessary operating range.

The temperature within the heat pump is commonly measured using thermocouples (T- or K-type) [111][112][113], or with platinum resistance temperature detectors [114]. The platinum resistance temperature detectors are only used in exceptional circumstances because they are very expensive. In this setup, the thermocouples are a suitable option due to their lower costs, robustness and ability to withstand the relatively high temperatures present in the heat pump.

For measuring the pressure, typically used measurement tools are piezoelectric sensors [111], pressure gauges [112] [115] or pressure transducers [116]. From a safety perspective, a pressure transducer is the preferred choice, as it allows for the implementation of a maximum pressure limit within the heat pump, which can be further controlled in combination with a valve,

The relative humidity of the is often measured using capacitive sensors, with variations primarily in sensor design. In many cases, the humidity sensor is combined in the same housing with a temperature sensor [113] [116].

The volumetric flow rate in a tube can be determined using several methods. In comparable heat pump systems, ultrasonic flow meters [111] [114], Venturi flow meters [117], Coriolis mass flow meters [113], or electromagnetic flow meters [114] are commonly employed. The electromagnetic flow meter can not be applied in this situation, since it is not compatible with the used refrigerants. The most appropriate choice is the Venturi flow meter. However, careful consideration is required for the flow meter to make sure it is compatible with the operating pressure. Furthermore, the meter performs at its best when the tube is filled with a single liquid phase. Consequently, it is placed downstream of the gas cooler and before the expansion valve, where the refrigerant is in a single phase and the temperature is not at its maximum.

To be able to determine the COP of the cycle, the electrical power of both the fan and the compressor must be measured. This can be achieved using a power meter or an energy meter [113] [116]. Both operate on the same principle, although the energy meter integrates power over time. In laboratory environments, the power meter is more commonly used.

Finally, it is important to measure the air velocity of the air in the dryer. In similar drying systems, this is typically done using an anemometer, a hot-wire anemometer [115] [116], or a Venturi flow meter. The Venturi flow meter is used here due to its simplicity.

Table 7.2: Overview of the required measurement devices.

Parameter	Measurement Device	Minimum Range
Pressure	Pressure sensor	0 - $150\,\mathrm{bar}$
Temperature	Type T thermocouple	0 - $200\,^{\circ}\mathrm{C}$
Mass flow rate (refrigerant)	Venturi flow meter	0 - $3.0\,\mathrm{kg\,s^{-1}}$
Mass flow rate (air)	Venturi flow meter	0 - $0.5\,\mathrm{kg\,s^{-1}}$
Air humidity and temperature	Combined temperature and humidity sensor	0 - 100% RH, 0 - $130\,^{\circ}\mathrm{C}$
Electrical input power	Power meter	0 - kW

Sensors can be used for various purposes. Some instruments are required to keep the system operational, while others are used to perform measurements for scientific research. Of the sensors shown in Figure 7.1, most of those located within the heat pump cycle are essential for maintaining system operation. When the minimum and maximum pressure and temperature of the refrigerant, as well as mass flow rate are known, the heat pump cycle can be controlled to operate under the correct conditions. The rest of the instrumentation, mainly the ones in the air duct, are for scientific research.

7.3. Safety measures

To ensure that the experiments with the heat pump dryer can be conducted safely, several precautions must be taken due to the presence of high pressures, hazardous working fluids and possible system failures.

First, it is important to consider the refrigerant used and evaluate whether it has, for example, high flammability or toxicity. Depending on the severity of these, there are special, strict safety regulations or additional attention must be given to containment and leak management measures. In this application, a combination of CO_2 and hydrocarbons is used. Both hydrocarbons, isobutane and isopentane, fall under safety group A3 according to the ASHRAE safety group classifications [118]. This means they have low toxicity but high flammability and therefore require additional safety measures. When at least 60% of a non-flammable fluid (A1) is mixed with a highly flammable fluid (A3), the classification of the resulting refrigerant mixture shifts to mildly flammable (A2L) [119]. By adding CO_2, which is an A1 refrigerant, the flammability of the refrigerant mixture is therefore effectively reduced. Additionally, CO_2 itself is not very flammable, but if it leaks, it can cause asphyxiation if the space is not properly ventilated. Therefore, it is important to check the setup for leaks beforehand and to properly ventilate the space. This means that the safety design must contain the combined risks associated with flammability, high pressure, and potential oxygen displacement.

In addition, several other safety elements have been added to the cycle. Pressure also plays a significant role in safety. When designing a heat pump, it is important to consider worst-case scenarios and implement measures to prevent overpressure. Therefore, a valve was placed at the compressor outlet in this system. A valve was also placed between all the main components. This allows for isolation of all parts of the system, which is beneficial during maintenance or in possible emergency situations. Additionally, this is also beneficial during the replacement of the refrigerant.

7.4. Changing the refrigerant

Replacing the refrigerant mixture is a process that requires precision and careful attention for safety. When this is not performed correctly, damage may occur to the compressor, for example due to liquid slugging. For many refrigerants, this procedure must therefore be carried out by a certified professional. Before the mixture can be removed form the system, is must be switched off and completely cooled down. In addition, it important to check the system for leaks both before and after the refrigerant replacement. The mixture present in the system can be extracted by using a recovery or evacuation pump. The system is then often cleaned to remove any residues. Before the new mixture can be injected into the system, the heat pump system is typically brought to a high vacuum to prevent air and moisture from affecting the cycle. To replace the refrigerant, a charging valve is required. The optimal location for this valve is in the liquid phase of the refrigerant [120]. Therefore, for this cycle this will be the section after the gas cooler. After adding the mixture and performing all necessary safety checks, the system can be put back into operation. When different compositions of a refrigerant mixture need to be tested, an additional cycle can be used in which the composition can be adjusted [121]. Additionally, valves are placed at both sides of the buffer volume, since it then can be used as a temporary storage when for example changing the refrigerant.

7.5. Performance indicators

Using the generated models, the expected coefficient of performance of the heat pump dryer can be calculated. This also takes into account the required fan power. Using the refrigerant mixture 90$\%_{mol}$ CO_2-Isobutane results in the data shown in Table 7.3.

Table 7.3: An overview of the performance indicators of the final design.

Gas cooler	
Heat transfer	$43.45\,\mathrm{kW}$
Pressure drop refrigerant side	$4.00\,\mathrm{bar}$
Pressure drop air side	$587\,\mathrm{Pa}$
Evaporator	
Heat transfer	$33.33\,\mathrm{kW}$
Pressure drop inside	$2517\,\mathrm{Pa}$
Pressure drop outside	$154\,\mathrm{Pa}$
General	
COP heat pump	3.54
COP heat pump dryer	2.43

In this table an overview is given of the most important performance indicators of the final design of the heat pump dryer. It shows that both the gas cooler and the evaporator meet the required heat transfer rates necessary to achieve the optimal cycle conditions. In addition, the pressure drops remain within a few percent of the operating pressures, ensuring that the additional power required to keep the system running is kept to a minimum. At system level, this results in a COP of 3.54 for the heat pump itself. When considering the complete heat pump dryer, so including the power consumption of the fan, the COP becomes 2.43. This value is within the expected range for heat pump dryer systems and does not represent an unusual deviation [122][123].

8

Conclusion and Recommendations

In this chapter, the conclusions drawn from this research will be presented. In addition, recommendations will be provided for future work within this research field.

8.1. Conclusion

The goal of this research was to develop an experimental setup for a heat pump drying system, enabling the testing of various refrigerant mixtures. Based on the final design and the process followed throughout this project, the main research question can now be discussed, which was formulated as follows: *How can an experimental test setup be designed to evaluate the (thermodynamic) performance of a laboratory-scale convective industrial heat pump dryer with zeotropic mixtures?* In addition, the sub questions formulated will be discussed individually, after which the main research question will be discussed.

The first sub question is: What is the impact of zeotropic mixtures on the performance of the heat pump dryer at different operating conditions? This was seen as the motivation for building the test setup. Literature shows that zeotropic mixtures generally improve heat pump dryer performance, as their temperature glides enhances heat transfer in the heat exchangers. A sensitivity analysis revealed that fluctuations in temperature affect the COP much more than changes in relative humidity. The use of the refrigerant mixture 87.5$\%_{mol}$ CO_2-Isopentane was also examined, while the system was primarily designed using 90$\%_{mol}$ CO_2-Isobutane. This comparison confirmed that there is a large difference in heat transfer and required compressor power between the various refrigerant mixtures.

The next sub question was: What does the design of a test setup look like that is representative of industrial applications? For the temperature levels and the selection of zeotropic mixtures, previous research is used as a basis. After evaluating the options, it was decided, primarily for safety reasons, to test the refrigerant mixtures that were most promising at the lowest of the two considered dryer temperatures. These mixtures are 87.5$\%_{mol}$ CO_2-Isopentane and 90$\%_{mol}$ CO_2-Isobutane. In designing the setup, the original optimal temperature levels associated with these mixtures were retained. To determine the appropriate scale of the setup, existing systems were reviewed and the limitations of the laboratory were taken into account. Based on this, a setup in the order of $10\,\mathrm{kW}$ was selected.

The third sub question was: Which types of heat exchangers and compressors are the most suitable for a scaled-down test setup in a lab of an industrial dryer? The literature study examined various types of heat exchangers and compressors. The best option for the heat exchanger for this application is the finned tube heat exchanger, primarily because this type performs well when operating with air. These heat exchangers can also be scaled up effectively for industrial applications. For compressors, scaling is more critical because volumetric flow rate becomes a limiting factor. Although operating pressures remain similar at industrial scale, the volumetric capacity of reciprocating compressors restricts their applicability due to their maximum allowable volumetric flow rate.

The last sub question is: What zeotropic mixtures of refrigerant can be applied in the laboratory setup?

When selecting refrigerants, many different aspects must be considered. In selecting the zeotropic mixtures for this study, the main considerations were which mixtures performed best in the previous research and their associated safety aspects. This led to a focus on 7.5$\%_{mol}$ CO_2-Isopentane and 90$\%_{mol}$ CO_2-Isobutane as potential refrigerant mixtures.

This research provides an example of how a design can be developed for a laboratory-scale convective industrial heat pump dryer. In this, a setup was designed in which 87.5$\%_{mol}$ CO_2-Isopentane and 90$\%_{mol}$ CO_2-Isobutane can be tested, providing a basis for the experimental validation of the promising performance of these mixtures identified in previous research. During the design process, a key consideration was the need for a flexible test setup that can handle different refrigerant mixtures. This requires heat exchangers sized for the mixture with the largest required surface area, and the compressor must be capable of handling different pressures and refrigerants. At the location of the expansion device, neither a capillary tube nor often a thermostatic expansion valve can be used, as these are typically designed for a specific condition. Furthermore, the design must allows for relatively simple replacement of the refrigerant mixture. By ensuring this flexibility while also meeting the design requirements, safety considerations, and scalability, a representative experimental setup can be developed for a convective industrial heat pump dryer with zeotropic mixtures.

8.2. Recommendations

Based on the design process carried out and the answers to the research questions, several recommendations can be made for future research and further development of the heat pump dryer setup. First of all, a new model can be generated by making an adjustment of the combined Python model from previous research with the model created during this research in Excel. Hereby it is important that realistic calculations can also be made for the 87.5$\%_{mol}$ CO_2-Isopentane refrigerant mixture, since the current combination of the models gives an unrealistic coefficient of performance.

Once the setup has been constructed, it is recommended to perform measurements under controlled conditions in order to validate the models and assumptions used in this research. in particular, special attention should be given to the temperature glide, heat transfer coefficients, and pressure drop in the heat exchangers.

Although a selection of suitable zeotropic refrigerant mixtures has already been made, it may be valuable to test additional mixtures, especially blends with a low GWP, considering future environmental regulations. Furthermore, for the dryers it is important to consider their temperature glide characteristics. This will expand the range of mixtures that provide both high efficiency and sustainability.

Based on the experimental results, scale up to industrial capacities may be feasible. This can also include examining the extent to which trends observed on a laboratory scale also occur at an industrial level. This can include examining the components, mixtures, and controlling. This can be expanded with a study of economic feasibility and life cycle assessment (LCA). This can further substantiate the added value of using zeotropic mixtures in heat pump drying systems.

References

[1] Sunil Jayant Kulkarni and Ajaygiri Kamalgiri Goswami. “Application, Advancements and Research on Drying-A Review”. In: *International Journal For Research in Applied Science and Engineering Technology* (2015).

[2] International Energy Agency. *Energy system - Industry*. 2023. URL: https://www.iea.org/energy-system/industry.

[3] KJ Chua et al. “Batch drying of banana pieces—effect of stepwise change in drying air temperature on drying kinetics and product colour”. In: *Food Research International* 34.8 (2001), pp. 721–731.

[4] Hironao Ogura et al. “A control strategy for a chemical heat pump dryer”. In: *Drying Technology* 23.6 (2005), pp. 1189–1203.

[5] European Commission. *Climate strategies & targets - 2050 long-term strategy*. URL: https://climate.ec.europa.eu/eu-action/climate-strategies-targets/2050-long-term-strategy_en.

[6] Mahadi Hasan Masud et al. “Experimental investigation of a novel waste heat based food drying system”. In: *Journal of food engineering* 281 (2020), p. 110002.

[7] Li Jin Goh et al. “Review of heat pump systems for drying application”. In: *Renewable and Sustainable Energy Reviews* 15.9 (2011), pp. 4788–4796.

[8] Fakhreddin Salehi. “Recent applications of heat pump dryer for drying of fruit crops: A review”. In: *International Journal of Fruit Science* 21.1 (2021), pp. 546–555.

[9] P.I. Widdows. “Heat pump for industrial drying processes: Investigating zeotropic refrigerant mixtures for glide matching”. MA thesis. Delft University of Technology, 2024.

[10] Hui Ni, Peng Hu, and Yuchen Li. “Analysis and optimization of the performance of closed heat pump dryer based on zeotropic mixtures”. In: *Applied Thermal Engineering* (2024), p. 124916.

[11] IQS Directory. *Types of Industrial Dryers: Discover their Categories and Benefits*. URL: https://www.iqsdirectory.com/articles/dryer/types-of-dryers.html#what-is-an-industrial-dryer.

[12] CM van ’t Land. *Drying in the Process Industry*. John Wiley & Sons, 2011.

[13] Andreas BÜCK. “Drying in the Chemical Industry”. In: (2016).

[14] Arun S Mujumdar. *Handbook of industrial drying*. CRC press, 2006.

[15] Ajit K Ghosh. “Fundamentals of paper drying–theory and application from industrial perspective”. In: *Evaporation, Condensation and Heat Transfer*. IntechOpen, 2011.

[16] Jobien Laurijssen et al. “Optimizing the energy efficiency of conventional multi-cylinder dryers in the paper industry”. In: *Energy* 35.9 (2010), pp. 3738–3750.

[17] Samuel Ayofemi Olalekan Adeyeye, Tolulope Joshua Ashaolu, and Ayenampudi Surendra Babu. “Food drying: A review”. In: *Agricultural reviews* 1.8 (2022).

[18] Michael J Moran et al. “Moran’s principles of engineering thermodynamics”. In: *(No Title)* (2017).

[19] C.F.M. Mills A.F.; Coimbra. *Basic Heat and Mass Transfer*. 3th ed. Temporal Publishing, 2015.

[20] The Engineering ToolBox. *Moist Air - the Mollier Diagram*. 2003. URL: https://www.engineeringtoolbox.com/psychrometric-chart-mollier-d_27.html.

[21] Chan Oussa Suong and Attakorn Asanakham. “Evaluation of a single stage heat pump performance by figure of merit (FOM)”. In: *Energy Reports* 6 (2020), pp. 2735–2742.

[22] Benjamin Zühlsdorf. *High-Temperature Heat Pumps: Task 1–Technologies. Annex 58 about High-Temperature Heat Pump*. 2023.

[23] Rajib Uddin Rony et al. “Recent advances in transcritical CO2 (R744) heat pump system: A review”. In: *Energies* 12.3 (2019), p. 457.

[24] An Zhao, Rene Pecnik, and Jurriaan WR Peeters. “Thermodynamic analysis and heat exchanger calculations of transcritical high-temperature heat pumps”. In: *Energy Conversion and Management* 303 (2024), p. 118172.

[25] Mustafa Aktaş et al. “Performance analysis of heat pump and infrared–heat pump drying of grated carrot using energy-exergy methodology”. In: *Energy Conversion and Management* 132 (2017), pp. 327–338.

[26] Viorel Badescu. “First and second law analysis of a solar assisted heat pump based heating system”. In: *Energy conversion and Management* 43.18 (2002), pp. 2539–2552.

[27] Marc A Rosen, Ibrahim Dincer, and Mehmet Kanoglu. “Role of exergy in increasing efficiency and sustainability and reducing environmental impact”. In: *Energy policy* 36.1 (2008), pp. 128–137.

[28] Michele Zehnder. “Efficient air-water heat pumps for high temperature lift residential heating, including oil migration aspects”. PhD thesis. EPFL, 2004.

[29] Lars Reinholdt et al. “Heat pump COP, part 1: Generalized method for screening of system integration potentials”. In: *13th IIR Gustav Lorentzen Conference on Natural Refrigerants (GL2018)*. International Institute of Refrigeration. 2018, pp. 1097–1104.

[30] Stefan S Bertsch and Eckhard A Groll. “Two-stage air-source heat pump for residential heating and cooling applications in northern US climates”. In: *International journal of refrigeration* 31.7 (2008), pp. 1282–1292.

[31] Seon Tae Kim et al. “Performance analysis of multistage high-temperature heat pump cycle”. In: *Energy Science & Engineering* 11.10 (2023), pp. 3500–3511.

[32] Saeed Maddah, Marjan Goodarzi, and Mohammad Reza Safaei. “Comparative study of the performance of air and geothermal sources of heat pumps cycle operating with various refrigerants and vapor injection”. In: *Alexandria Engineering Journal* 59.6 (2020), pp. 4037–4047.

[33] Kian J Chua, Siaw K Chou, and WM Yang. “Advances in heat pump systems: A review”. In: *Applied energy* 87.12 (2010), pp. 3611–3624.

[34] W Wang et al. “Field test investigation of a double-stage coupled heat pumps heating system for cold regions”. In: *International Journal of Refrigeration* 28.5 (2005), pp. 672–679.

[35] *Temperature profile*. URL: `https://upload.wikimedia.org/wikipedia/commons/4/4f/Temperature_profile.gif`.

[36] Rached Ben-Mansour et al. “Experimental/Numerical Investigation and Prediction of Fouling in Multiphase Flow Heat Exchangers: A Review”. In: *Energies* 16.6 (2023), p. 2812.

[37] Oluseyi Ajayi and Stephen Ogbonnaya. “Fouling phenomenon and its effect on heat exchanger: A review”. In: *Frontiers in Heat and Mass Transfer (FHMT)* 9.1 (2017).

[38] Himanshu Dwivedi et al. “CFD Analysis of Fluid Flow in a Heat Exchanger Using ANSYS Software”. In: *Journal of Engineering and Technology, Sep* (2018).

[39] G.P. Towler and R.K. Sinnott. *Chemical Engineering Design: Principles, Practice and Economics of Plant and Process Design*. 2th ed. Elsevier, 2013.

[40] Bohong Wang et al. “Heat exchanger network retrofit with heat exchanger and material type selection: A review and a novel method”. In: *Renewable and Sustainable Energy Reviews* 138 (2021), p. 110479.

[41] Arafat A Bhuiyan and AKM Sadrul Islam. “Thermal and hydraulic performance of finned-tube heat exchangers under different flow ranges: A review on modeling and experiment”. In: *International Journal of Heat and Mass Transfer* 101 (2016), pp. 38–59.

[42] KPM Wipplinger, TM Harms, and AB Taylor. “Stainless steel finned tube heat exchanger design for waste heat recovery”. In: *Journal of Energy in Southern Africa* 17.2 (2006), pp. 47–56.

[43] S Basavarajappa, G Manavendra, and SB Prakash. “A review on performance study of finned tube heat exchanger”. In: *Journal of Physics: Conference Series*. Vol. 1473. 1. IOP Publishing. 2020, p. 012030.

[44] EnggCyclopedia. *Double pipe heat exchanger*. 2023. URL: https://enggcyclopedia.com/2023/01/double-pipe-heat-exchanger/.

[45] Mecanically. *Heat Exchangers: Types, Maintenance, Troubleshooting, and Calculations*. 2023. URL: https://www.mecanically.com/2023/12/heat-exchangers-types-maintenance-calculations.html.

[46] Jiří Jaromír Klemeš et al. “Heat transfer enhancement, intensification and optimisation in heat exchanger network retrofit and operation”. In: *Renewable and Sustainable Energy Reviews* 120 (2020), p. 109644.

[47] H Zheng. “Fundamental relationships of heat and mass transfer in solar seawater desalination systems”. In: *Solar Energy Desalination Technology* (2017), pp. 173–258.

[48] COMSOL Blog. *Modeling a Coil Heat Exchanger*. 2014. URL: https://www.comsol.com/blogs/modeling-coil-heat-exchanger.

[49] Mahmood Mastani Joybari et al. “Potentials and challenges for pillow-plate heat exchangers: State-of-the-art review”. In: *Applied Thermal Engineering* 214 (2022), p. 118739.

[50] Radia Eldeeb, Vikrant Aute, and Reinhard Radermacher. “Investigation of thermal-hydraulic characteristics of pillow plate heat exchangers using CFD”. In: (2016).

[51] A Zibart and EY Kenig. “Numerical investigation of conjugate heat transfer in a pillow-plate heat exchanger”. In: *International Journal of Heat and Mass Transfer* 165 (2021), p. 120567.

[52] East-Alliance. *East-Alliance Gasketed Plate Heat Exchangers*. n.d. URL: https://east-alliance.com/gasketed/.

[53] M Piper et al. “Determination of the geometric design parameters of pillow-plate heat exchangers”. In: *Applied Thermal Engineering* 91 (2015), pp. 1168–1175.

[54] Vedant Irabatti et al. “Comprehensive review of spiral heat exchanger for diverse applications”. In: *Materials Today: Proceedings* 72 (2023), pp. 1328–1334.

[55] Madhuri Charulatha Returi, Ramakrishna Konijeti, and Abhishek Dasore. “Heat transfer enhancement using hybrid nanofluids in spiral plate heat exchangers”. In: *Heat Transfer—Asian Research* 48.7 (2019), pp. 3128–3143.

[56] Chemical Processing. *Consider Printed Circuit Heat Exchangers*. 2021. URL: https://www.chemicalprocessing.com/processing-equipment/heat-exchangers/article/11291324/consider-printed-circuit-heat-exchangers-chemical-processing.

[57] ESDU. “Selection and Costing of Heat Exchangers”. In: *ESDU Data Items* (1994).

[58] Dusan P Sekulic and Ramesh K Shah. *Fundamentals of heat exchanger design*. John Wiley & Sons, 2023.

[59] Geoff F Hewitt and Simon J Pugh. “Approximate design and costing methods for heat exchangers”. In: *Heat transfer engineering* 28.2 (2007), pp. 76–86.

[60] Tala El Samad et al. “A review of compressors for high temperature heat pumps”. In: *Thermal Science and Engineering Progress* (2024), p. 102603.

[61] Saeid Mokhatab, William A Poe, and John Y Mak. *Handbook of natural gas transmission and processing: principles and practices*. Gulf professional publishing, 2018.

[62] Meherwan P Boyce. “Axial-flow compressors”. In: *Gas Turbine Engineering Handbook* (2012), pp. 303–355.

[63] YS Hu et al. “The theoretical and experimental research of a novel rotary cylinder compressor”. In: *IOP Conference Series: Materials Science and Engineering*. Vol. 604. 1. IOP Publishing. 2019, p. 012073.

[64] MO Khan. “Basic practices in compressors selection”. In: (1984).

[65] Klaus Brun and Timothy C Allison. *Machinery and energy systems for the Hydrogen Economy*. Elsevier, 2022.

[66] Royce N. Brown. *1.2 Compression Methods*. Elsevier, 2005. ISBN: 978-0-7506-7545-1. URL: https://app.knovel.com/hotlink/khtml/id:kt00C5FHU1/compressors-selection/compression-methods.

[67] Lisa Neumaier et al. “Refrigerant selection for heat pumps: the compressor makes the difference”. In: *Energy Technology* 11.4 (2023), p. 2201403.

[68] Giorgio Besagni. “Ejectors on the cutting edge: The past, the present and the perspective”. In: *Energy* 170 (2019), pp. 998–1003.

[69] Xiaolong Lv, Mengqi Yu, and Jianlin Yu. “Performance analysis of an ejector-boosted solar-assisted flash tank vapor injection cycle for ASHP applications”. In: *Solar Energy* 224 (2021), pp. 607–616.

[70] M Elakhdar et al. “Thermodynamic analysis of a novel ejector enhanced vapor compression refrigeration (EEVCR) cycle”. In: *Energy* 163 (2018), pp. 1217–1230.

[71] Stefan Elbel and Pega Hrnjak. “Experimental validation of a prototype ejector designed to reduce throttling losses encountered in transcritical R744 system operation”. In: *International Journal of Refrigeration* 31.3 (2008), pp. 411–422.

[72] Adam Y Sulaiman et al. “Thermodynamic analysis of subcritical High-Temperature heat pump using low GWP Refrigerants: A theoretical evaluation”. In: *Energy Conversion and Management* 268 (2022), p. 116034.

[73] Ibrahim Dincer. *Refrigeration systems and applications*. John Wiley & Sons, 2017.

[74] Cordin Arpagaus et al. “High temperature heat pumps: Market overview, state of the art, research status, refrigerants, and application potentials”. In: *Energy* 152 (2018), pp. 985–1010.

[75] M Sruthi Emani, R Roy, and B Kumar Mandal. “Development of refrigerants: a brief review”. In: *Indian J. Sci. Res* 14.2 (2017), pp. 175–181.

[76] Arun Krishna Vuppaladadiyam et al. “Progress in the development and use of refrigerants and unintended environmental consequences”. In: *Science of the Total Environment* 823 (2022), p. 153670.

[77] Guus JM Velders et al. “The importance of the Montreal Protocol in protecting climate”. In: *Proceedings of the National Academy of Sciences* 104.12 (2007), pp. 4814–4819.

[78] European Commission. *Fluorinated greenhouse gases - International*. URL: https://climate.ec.europa.eu/eu-action/fluorinated-greenhouse-gases/international_en#:~:text=The%20Kigali%20Amendment%20entails%20a,surface%20temperature%20over%20this%20century..

[79] European Chemicals Agency. *Registry of restriction intentions unitl outcome*. 2024. URL: https://echa.europa.eu/nl/registry-of-restriction-intentions/-/dislist/details/0b0236e18663449b.

[80] RIVM. *PFAS*. URL: https://www.rivm.nl/en/pfas.

[81] RIVM. *Voortangsupdate over het voorgenomen PFAS-verbod*. URL: https://www.rivm.nl/nieuws/voortgangsupdate-over-voorgenomen-pfas-verbod.

[82] Jian Liu et al. “Analysis of low GWP ternary zeotropic mixtures applied in high-temperature heat pump for waste heat recovery”. In: *Energy Conversion and Management* 292 (2023), p. 117381.

[83] Andreas Søgaard Kristensen et al. “Performance analysis of heat pumps with zeotropic mixtures at different load conditions”. In: *International Journal of Refrigeration* 145 (2023), pp. 264–275.

[84] Leelananda Rajapaksha. “Influence of special attributes of zeotropic refrigerant mixtures on design and operation of vapour compression refrigeration and heat pump systems”. In: *Energy conversion and Management* 48.2 (2007), pp. 539–545.

[85] Benjamin Zühlsdorf et al. “Analysis of temperature glide matching of heat pumps with zeotropic working fluid mixtures for different temperature glides”. In: *Energy* 153 (2018), pp. 650–660.

[86] Opeyemi Bamigbetan et al. “Review of vapour compression heat pumps for high temperature heating using natural working fluids”. In: *International journal of refrigeration* 80 (2017), pp. 197–211.

[87] S Prasertsan and P Saen-Saby. “Heat pump drying of agricultural materials”. In: *Drying technology* 16.1-2 (1998), pp. 235–250.

[88] Shane Clements, Xiguo Jia, and Peter Jolly. “Experimental verification of a heat pump assisted continuous dryer simulation model”. In: *International Journal of Energy Research* 17.1 (1993), pp. 19–28.

[89] Eugene Pis’ mennyi et al. *Handbook for transversely finned tube heat exchanger design*. Academic Press, 2016.

[90] H Nemati et al. “Shape optimisation of air-cooled finned-tube heat exchangers”. In: *International Journal of Thermal Sciences* 150 (2020), p. 106233.

[91] Han-Taw Chen and Jui-Che Chou. “Investigation of natural-convection heat transfer coefficient on a vertical square fin of finned-tube heat exchangers”. In: *International journal of heat and mass transfer* 49.17-18 (2006), pp. 3034–3044.

[92] Tubular Exchanger Manufacturers Association Inc. *Standards of the Tubular Exchanger Manufacturers Association*. Tubular Exchanger Manufacturers Association Inc, 2007.

[93] Thomas H Chilton and Allan Philip Colburn. “Mass transfer (absorption) coefficients prediction from data on heat transfer and fluid friction”. In: *Industrial & engineering chemistry* 26.11 (1934), pp. 1183–1187.

[94] James Welty, Gregory L Rorrer, and David G Foster. *Fundamentals of momentum, heat, and mass transfer*. John Wiley & Sons, 2014.

[95] Daniel Jonas Dezan, Leandro Oliveira Salviano, and Jurandir Itizo Yanagihara. “Interaction effects between parameters in a flat-tube louvered fin compact heat exchanger with delta-winglets vortex generators”. In: *Applied Thermal Engineering* 91 (2015), pp. 1092–1105.

[96] Dawid Taler. “Experimental determination of correlations for average heat transfer coefficients in heat exchangers on both fluid sides”. In: *Heat and Mass Transfer* 49.8 (2013), pp. 1125–1139.

[97] The Engineering Toolbox. *Air - Diffusion Coefficients of Gases in Excess of Air*. 2018. URL: `https://www.engineeringtoolbox.com/air-diffusion-coefficient-gas-mixture-temperature-d_2010.html`.

[98] Ji Zhang, Maria E Mondejar, and Fredrik Haglind. “General heat transfer correlations for flow boiling of zeotropic mixtures in horizontal plain tubes”. In: *Applied Thermal Engineering* 150 (2019), pp. 824–839.

[99] MP Mishra, HK Varma, and CP Sharma. “Heat transfer coefficients in forced convection evaporation of refrigerants mixtures”. In: *Letters in Heat and Mass Transfer* 8.2 (1981), pp. 127–136.

[100] BITZER Kühlmaschinenbau GmbH. *Semi-hermetic reciprocating compressors*. Tech. rep. BITZER Kühlmaschinenbau GmbH, 2022.

[101] Luca Paterlini et al. “Atmospheric Corrosion of Different Steel Types in Urban and Marine Exposure”. In: *Materials* 17.24 (2024), p. 6211.

[102] MACSTEEL. *Stainless Steel | Technical Data*. Tech. rep. MACSTEEL, 2022.

[103] Lorenzo Fedrizzi et al. “Heat exchangers corrosion protection by using organic coatings”. In: *Progress in Organic Coatings* 63.3 (2008), pp. 299–306.

[104] The Spray Nozzle People. *Humidification nozzle selection table*. Tech. rep. The Spray Nozzle People, 2024.

[105] Ali Kholghi Kalajahi and Payam Shams Ghahfarokhi. “High-Viscosity Spray Cooling System for High-Reliability Motor Drives in Electric Vehicles: A Review”. In: *IEEE Transactions on Transportation Electrification* (2024).

[106] Breuell & Hilgenfelt. *Axial fans*. Tech. rep. Breuell & Hilgenfelt, 2025.

[107] Ph Epple, Franz Durst, and Antonio Delgado. “A theoretical derivation of the Cordier diagram for turbomachines”. In: *Proceedings of the Institution of Mechanical Engineers, Part C: Journal of Mechanical Engineering Science* 225.2 (2011), pp. 354–368.

[108] Reitz Group. *Handbook Radial Fans*. Tech. rep. Reitz Group, 2015.

[109] Slingerland Techniek BV. *Centrifugal fans | BPR series*. Tech. rep. Slingerland Techniek BV, 2025.

[110] Mir Farooq Ali et al. “Impact of Buffer Sizing on Heat Pump Performances for Residential Applications”. In: *2025 26th International Carpathian Control Conference (ICCC)*. IEEE. 2025, pp. 1–6.

[111] Michael Uhlmann and Stefan Bertsch. “Measurement and simulation of startup and shut down of heat pumps”. In: (2010).

[112] Zhongchao Zhao et al. “Experimental research of a water-source heat pump water heater system”. In: *Energies* 11.5 (2018), p. 1205.

[113] Melanie Cop et al. “Experimental investigation of a heat pump tumble dryer with a zeotropic refrigerant mixture”. In: *International journal of refrigeration* 158 (2024), pp. 190–201.

[114] Valeriy Kharchenko et al. “Monitoring system of a heat pump installation for heating a rural house using low-grade heat from a surface watercourse”. In: *Journal of Sensor and Actuator Networks* 9.1 (2020), p. 11.

[115] Akhilesh Singh, Jahar Sarkar, and Rashmi Rekha Sahoo. “Comparative analyses on a batch-type heat pump dryer using low GWP refrigerants”. In: *Food and Bioproducts Processing* 117 (2019), pp. 1–13.

[116] Jia-Hao Cheng et al. “Evaluation of heat pump dryers from the perspective of energy efficiency and operational robustness”. In: *Applied Thermal Engineering* 215 (2022), p. 118995.

[117] Joo Hyun Park and Jae Eun Cha. “Measurements of the flow of supercritical pressure carbon dioxide through Venturi flow meter”. In: *Flow Measurement and Instrumentation* 91 (2023), p. 102364.

[118] ASHRAE. *Update on New Refrigerants Designations and Safety Classifications*. 2022. URL: `https://www.ashrae.org/file%20library/technical%20resources/bookstore/factsheet_ashrae_english_november2022.pdf`.

[119] Adrián Fernández-Moreno et al. “Optimal refrigerant mixture in single-stage high-temperature heat pumps based on a multiparameter evaluation”. In: *Sustainable Energy Technologies and Assessments* 52 (2022), p. 101989.

[120] Danfoss. *Inverter scroll compressors*. 2016. URL: `https://assets.danfoss.com/documents/latest/89803/AB196586423811en-020601.pdf`.

[121] Minsung Kim, Min Soo Kim, and Yongchan Kim. “Experimental study on the performance of a heat pump system with refrigerant mixtures’ composition change”. In: *Energy* 29.7 (2004), pp. 1053–1068.

[122] Trygve M Eikevik, I Strommen, and O Alves-Filho. “Heat pump fluidised bed dryer with CO2 as refrigerant–Measurements of COP and SMER”. In: *3rd Nordic Drying Conference, Karlstad, Sweden*. 2005.

[123] Peder Bengtsson, Jonas Berghel, and Roger Renström. “Performance study of a closed-type heat pump tumble dryer using a simulation model and an experimental set-up”. In: *Drying technology* 32.8 (2014), pp. 891–901.

[124] ASHRAE. *Fundamentals Handbook (SI)*. ASHRAE, 2001.

A

Refrigerant properties

Table A.1: Properties of several relevant refrigerants. [124]

Refrigerant	Refrigerant number	$T_{boiling}$ ($^\circ$C)	T_{crit}($^\circ$C)	P_{crit}(bar)
Ammonia	R-717	-33.3	133.0	114.17
Butane	R-600	-0.5	152.0	37.94
Carbon dioxide	R-744	-78.4	31.1	73.72
Ethane	R-170	-88.8	32.2	48.91
Ethylene	R-1150	-103.7	9.3	51.14
Hexane	-	68.71	234.67	30.34
Isobutane	R-600a	-11.73	135.0	36.45
Isopentane	R-601a	28.0	187.2	33.34
Methane	R-50	-161.5	-82.5	46.38
Pentane	R-601	36.1	196.6	33.7
Propane	R-290	-42.09	96.70	42.48
Propylene	R-1270	-47.7	91.8	46.18
Tetrafluoroethane	R-134a	-26.16	101.1	40.67
2,3,3,3-Tetrafluoro-propene	R-1234yf	-29.4	94.7	33.81
Water	R-718	100	373.99	220.64

Table A.2: Properties of several relevant refrigerants. [124][60]

Refrigerant	Safety	ODP	GWP	Molecular Mass($\mathrm{g/mol}$)
Ammonia	B2	0	0	17.03
Butane	A3	0	20	58.13
Carbon dioxide	A1	0	1	44.01
Ethane	A3	0	6	30.07
Ethylene	A3	0	4	28.05
Hexane	A3	0	3	86.18
Isobutane	A3	0	3	58.13
Isopentane	A3	0	5	72.15
Methane	A3	0	28	16.04
Pentane	A3	0	0	72.2
Propane	A3	0	3	44.10
Propylene	A3	0	2	42.09
Tetrafluoroethane	A1	0	1300	102.03
2,3,3,3-Tetrafluoro-propene	A2L	0	4	114.0
Water	A1	0	0	18.02

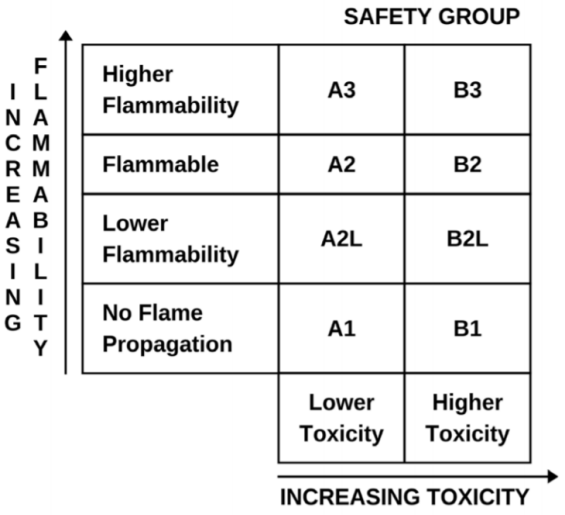

Figure A.1: Safety group classifications ASHRAE [118]

B

HXE properties comparison

Parameter	(1)	(2)	(3)	(4)	(5)
Tube diameter d_{in}	$0.028\,\mathrm{m}$	$0.0106\,\mathrm{m}$	$0.020\,\mathrm{m}$	$0.0092\,\mathrm{m}$	
Tube diameter D_{out}	$0.033\,\mathrm{m}$	$0.012\,\mathrm{m}$	$0.027\,\mathrm{m}$	$0.010\,\mathrm{m}$	$0.0095\,\mathrm{m}$
Nominal wall thickness Δt	$0.0025\,\mathrm{m}$	$0.0007\,\mathrm{m}$	$0.0035\,\mathrm{m}$	$0.0004\,\mathrm{m}$	
Number of tubes (z)	162	8 (5.5 passes)	50	36	
Number of rows in depth (z_2 or z_1)	$Z_2 = 18$, $Z_1 = 9$	(6 in depth)	5–6 tubes in row, 9 tube rows	12 tubes/row, 3 depth rows	16 tubes/row, 3 tube rows
Length of tube (L)	Total $81\,\mathrm{m}$	Total $46.2\,\mathrm{m}$ (1.4 × 6 × 5.5)	Total $34\,\mathrm{m}$	$0.5\,\mathrm{m}$	Total $19.2\,\mathrm{m}$
Arrangement	Staggered	Staggered	Staggered	Staggered	Staggered
Pitch (s_1, s_2)	$s_1 = 0.059\,\mathrm{m}$, $s_2 = 0.051\,\mathrm{m}$, $s_2' = 0.059\,\mathrm{m}$ (transverse, longitudinal, diagonal)	$s_1 = 50\,\mathrm{mm}$, $s_2 = 25\,\mathrm{mm}$, $s_3 = 35\,\mathrm{mm}$	Row pitch = $46.77\,\mathrm{mm}$, Tube pitch = $54\,\mathrm{mm}$	Tube spacing = $24.4\,\mathrm{mm}$, Row spacing = $22.2\,\mathrm{mm}$	Row pitch = $21.65\,\mathrm{mm}$, Tube pitch = $25\,\mathrm{mm}$
Thickness of fin (Δr)	$0.0008\,\mathrm{m}$	$0.0005\,\mathrm{m}$	$0.004\,\mathrm{m}$	$0.0002\,\mathrm{m}$	$0.000\,12\,\mathrm{m}$
Fin spacing (s_r)	$0.003\,\mathrm{m}$	$0.0024\,\mathrm{m}$	$0.02\,\mathrm{m}$	$0.002\,\mathrm{m}$	$0.002\,\mathrm{m}$
Fin height (l)	$0.0135\,\mathrm{m}$		$0.027\,\mathrm{m}$		

Table B.1: Comparison of the tube and fin parameters of various comparable finned tube heat exchangers.

Parameter	(1)	(2)	(3)	(4)	(5)
Material tube	Internal: carbon steel, external: aluminium	Stainless steel	Stainless steel	-	Copper
Material fins	Aluminium	Aluminium	Stainless steel	-	Aluminium

Table B.2: Comparison of the tube and fin materials of various comparable finned tube heat exchangers.